A comparison of Solar Sail actuation methods for parking in the circular restricted three body problem

Master of Science in Space Engineering

POLITECNICO
MILANO 1863

Supervisor
James Douglas Biggs

Alice Maria Piccirillo
mat. 879033

Department of Aerospace Sciences and Technologies
Politecnico di Milano
Accademic year
2018/2019

A comparison of Solar Sail actuation methods for parking in the circular restricted three body problem

Alice Maria Piccirillo

Supervisor

James Douglas Biggs

Abstract

Solar sails are spacecrafts that utilise the Solar Radiation Pressure, the force generated by impinging photons, for propulsion. In this thesis the solar sails motion is modelled as a circular restricted three-body problem (CRTBP) with the Earth and the Sun as the two primaries and the sail as the massless body. In this model the five Lagrangian points of the classical CRTBP are substituted by a continuum of new artificial points that form level surfaces as a function of attitude angles and lightness number. The dynamic stability of these stationary solutions is investigated and their instability established for both an ideal and non-ideal solar sail. Previous works in station-keeping of such points have used different actuation mechanisms such as variations in the sail's orientation, excess of thrust vector, and RCDs applications. In this work, new combinations of actuation mechanisms are investigated and their controllability, closed-loop stability and control performances are analysed. In particular, the actuator combinations considered are: (i) thrust vectoring through attitude control of a flat sail; (ii) attitude control of a heliogyro sail; (iii) thrust vectoring and a variable surface reflectivity distribution (RCD); (iv) RCD and a heliogyro. In each case an LQR controller is developed to compare and contrast each combination. Moreover, control performances, such as steady-state error, rate of convergence and feasibility of the actuation mechanisms are compared within a trade-off analysis. Additionally, a control approach that removes the need to linearise the control component in the LQR design is presented. This approach maps an ideal feed-back acceleration, determined by linear feedback, which is then mapped to the non-linear control variables by a Newton method within the closed-loop. The new mapping control is shown to be more effective than that applied to a system which is linearised with respect to the control variables.

Acknowledgements

First of all, I would like to thank my supervisor, Professor James Douglas Biggs. Thank you for your constant presence, your attention to my work and for all the precious advices, or rather, fundamental teachings that you gave me this year. Thank you because you knew how to make this hard and stressful time easier, bringing out my best.
Thanks to all the professors of the Politecnico, able to give everyone the push towards the achievement of our objectives.
Ringrazio Tata, zia con poteri eccezionali, senza il tuo prezioso aiuto non sarei qui, cosi come senza il supporto di Arturo e Maria, i miei dolcissimi nonni, insieme tutti e tre attenti a non farmi mai mancare nulla.
Ringrazio Giancarlo, la sua pazienza nel capire le mie assenze e le mie ansie, grazie di essere ancora e sempre qui, mi hai sostenuta quando ho avuto paura di non farcela, mi sei venuto incontro quando era troppo stanca per compiere un altro passo.
Ringrazio i miei colleghi amici dell'università per aver reso piu facile il cammino, perché insieme tutto è piu semplice. Grazie di avermi accolto e di avermi subito accettata, la vostra amicizia ha allontanato la solitudine. Un grazie speciale a Giulia e Valentina.
Grazie alle fantastiche quattro, mie amiche di sempre, un grazie particolare a Silvia che mi ha sostenuta con tutto il suo cuore fino a colmare i mille chilometri di distanza.
Grazie a Fabio e Martina che hanno fatto un po di posto per me nel loro nido, e grazie a Fabio e alla sua lucidità.
Grazie a Simone Benedetta e Mamma, grazie alle loro grida ai loro silenzi, alla loro allegria e alla loro dolcezza, alle parole dette e a quelle taciute, è grazie a voi se so di avere radici e braccia dove tornare.
Grazie a tutti voi, insieme siete stati i gradini e gli appligli di questa scalata, tanto faticosa quanto bellissima. Grazie per aver creduto in me piu di me.

Contents

List of Figures

List of Tables

Definitions, acronyms, and abbreviations

AU Astronimic Unit

CRTBP Circular Restricted Three Body Problem

ESA European Space Agency

ERTBP Elliptical Restricted Three Body Problem

IKAROS Interplanetary Kite-craft Accelerated by Radiation Of the Sun

JAXA Japan Aerospace Exploration Agency

LQR Linear Quadratic Regulator

LTI Linear Time Invariant

NASA National Aeronautics and Space Administration

RCD Reflective Control Device

SRP Solar Radiation Pressure

SSA Solar Sail Acceleration

SSCRTBP Solar Sail Circular Restricted Three Body Problem

SSE Steady State Error

Chapter 1

Introduction

The Solar sail is a unique form of propulsion, which is not associated with reaction mass. This singular system obtains momentum by the photons, quantum packets of energy that compose the solar radiations. Solar Sail must be large and light, to intercept a considerable quantity of photons and gain as much acceleration as possible from the momentum transported by them. This constant acceleration paves the way for a number of exciting missions and orbits that would not be otherwise possible. One such mission is the creation of artificial Lagrange points, to enable Solar Sail parking and about which generate possible Halo orbits. Control is crucial for a Solar Sail to maintain its planned trajectory due to the inhered link between the sail's attitude and the trajectory it will follow. The large inertias and long mission durations associated with Solar Sails make conventional actuators unsuitable for controlling the attitude of the latter. Many different control methods have been devised specifically for solar sails, and this research will contribute to broadening this area of Solar Sail technology, with a focus on Lagrangian points stabilization. Hereafter a brief exposition of Solar Sail history will be reported, followed by a fast overview of the current state of the art of Solar Sail control models, which constitute the basis of this thesis.

1.1 History of Solar Sail

James Clerck Maxwell in 1864 was the first person to theorise about the presence of solar radiation pressure in his paper "A Dynamical Theory of the Electromagnetic Field" [40]. After thirty years, in 1901 the Russian physicist Peter Lebedew proved it experimentally [37]. Surprisingly enough, though, it was not scientists that proposed the usage of solar radiation pressure as means of propulsion but science fiction writers such as Jules Verne in 1865 and B. Krasnogorskii in 1913. The first proposed concept of using light to propel ships by means of photonic engines was in 1920 by Konstantine Tsiolkovsky and the first technical publication on the subject was in 1924 by Fredrik Tsander. In his paper

Tsander identified several useful configurations and made calculations of interplanetary trajectories by a solar sailing spacecraft. It was Tsander who actually coined the term solar sailing. The concept of solar sailing lay dormant for approximately thirty years and it was not until 1951 when an American aeronautical engineer Carl Wiley revived the idea. Fearing for his professional credibility Wiley published an article in "Astounding Science Fiction" under the pseudonym of Russel Sanders [63]. He discussed the design of a feasible Solar Sail and strategies for orbit raising. After this revival of Solar Sail many conceptual missions have been proposed but it was not until 2010 when the Japan Aerospace Exploration Agency (JAXA)[22] successfully launched the first solar sail. A time-line of the history of sailcraft is shown in Fig. 1.1.

1.2 Past researches

The Solar Sail artificial equilibrium points have interesting application in space mission but they are not intrinsically stable. Therefore, many authors have already developed systems and models to obtain controlled trajectories, contributing to consolidate the viability of this technology.
In past studies, it is possible to find station-keeping strategies for classical libration point involving discrete, impulsive velocity corrections to be applied with thrusters. Starting from Howell in Ref. [31], where a method is presented that uses manoeuvres executed (impulsively) at discrete time intervals to keep the spacecraft on the nominal path. Again Howell in further studies [30] develops a stationkeeping strategy for Libration point L1 orbit, but this time including the possible estimation error of the spacecraft trajectory.
However, the usage of the Solar Sail technology introduces the possibility of using changes in the sail orientation (and potentially the sail area) to generate various "thrust" magnitudes and directions, and, thus, to provide stationkeeping capabilities. Therefore, in Ref. [44] by McInnes, an adaptation of the station-keeping method originally introduced by Howell in [31] is developed, modified such that the manoeuvres are computed in terms of sail orientation angles rather than velocity changes, since the sail thrust magnitude is a function of the attitude of the sail normal to the spacecraft-Sun line. A similar study has been carried out by Lawrence [36], in which a 10000 m^2 sail is considered and showed that it is controllable on the station-keeping manifold in the case of a circular Earth orbit about the Sun, and further, indicated whether orbit injection errors are correctable for a given mission profile and quantified tracking error correctability, by using a controllability Gramian approach. Another work by Bookless & McInnes [12] treated the three-body problem as a perturbed two-body and presented a design of an optimal controller aimed to select control gains that minimize the sail area or pitch-angle variation required to control displaced non-Keplerian orbits. A more recent study by Bombardelli [11] involved a stability analysis on minimum-control artificial equilibrium points properties in the planar

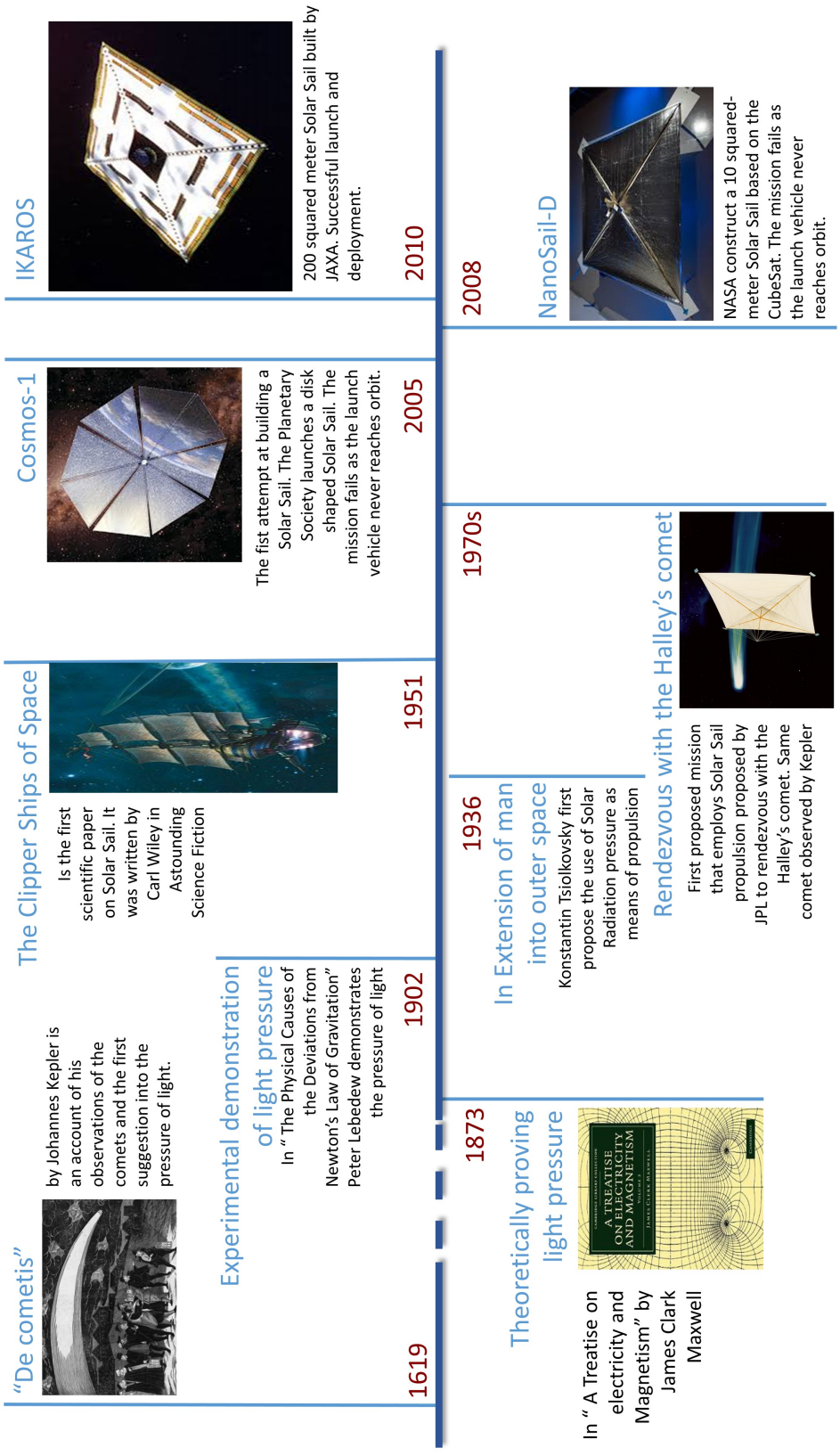

Figure 1.1: Solar sail historical time line

CRTBP, demonstrating that minimum-control equilibrium is obtained when the space-craft is almost co-orbiting with the second primary and in addition, a stability condition

related to mass ratio of the two primaries and their separation. Rios-Reyes in Ref. [53] develops a new control law for maintaining a flat, ideal solar sail orbiting an equilibrium point of the CRTBP and tracking neighbouring halo orbits. In his work, he designed a sail with an excess of thrust, allowing it to follow a nominal mission as long as it had this property in excess. It is worth to mention, another research line carried by Soldini and Colombo [56, 55], in which is investigated a Hamiltonian structure-preserving (HSP) control involving the acceleration of solar radiation pressure for the stabilization of unstable periodic orbits in the circular restricted three-body problem. In note [56] these control types are used to stabilise, in the sense of Lyapunov, an unstable distant prograde orbit in the CRTBP, exploiting the SRP as controller action and tuning its magnitude with a sailcraft "morphing" deployable structure. In addition, it is shown that the proposed control admits different sets of gains to guarantee stability and it is possible to analytically find the minimum set of gains to have Lyapunov stability. Furthermore, in [55] the Hamiltonian structure-preserving control is then extended to a general case in which complex and conjugate eigenvalues occur at high-amplitude orbits, which are currently of interest to the European Space Agency because they require a lower insertion Δv.

Finally, a novel actuation method for solar sail control is introduced, which involves the so-called RCD (Reflectivity Control Devices), i.e. the mechanisms devolved to alteration of the reflectivity across the sail film, which can be achieved using electro-chromic coatings. In 2010, IKAROS verified the techniques of using RCD for the attitude control [58]. The RCD was used to generate torque by changing the induced force on each small element's surface by switching between power on and off states [47]. The idea of adjusting the reflectivity states of the RCD for orbit control and attitude-orbit control has been discussed in the GeoSail Mission [50, 49], and Artificial Lagrange Point Mission [1, 25]. Furthermore, Gong and Li in [24] proposed a new elliptic displaced orbit using a Solar Sail with RCD. In another recent study instead, Borggräffe and Heiligers [13] exploit this property with two approaches: first a continuous reflectivity distribution to control the sail attitude under the influence of external disturbances, and second approach assuming discrete on/off reflectivity regions across the surface. In a more recent note by Biggs and Negri [8] the RCD technology is applied to control of unique Solar Sail orbits, known as highly non-Keplerian orbits. A practical case is designed in which the sail surface consists of a finite number of RCDs each having the capability to switch between reflection and absorption for attitude control. In other work, Biggs [6] intends to develop an active disturbance model estimator for the robust, in-situ, tracking of the sail characteristic acceleration based on an extended state observer and an adaptive stochastic gradient descent method. The estimator is coupled with an active disturbance rejection control in simulation to show improved performance of the tracking in the presence of uncertainties in gravitational fields and characteristic acceleration.

Due to the simplicity of the linear time-invariant (LTI) models of Solar Sail in the CRTBP,

several Linear Quadratic Regulator (LQR) controllers for stationkeeping have been presented. Gong and Baoyin in Ref. [23] outline the characteristics of the relative motion around a displaced solar orbit and propose some possible control strategies. They include in first control formation, the two attitude angle and the lightness number and derive control gain with LQR theory. Biggs and McInnes in Ref. [7] consider using a continuous linear quadratic regulator controller in the solar sail ERTBP to track a periodic reference orbit using variations in the sail's orientation, showing also that a reference orbit from the solar sail CRTBP is not adequate for tracking in the elliptical case. Meanwhile, Gong and Li employ the typical LQR method to stabilize the relative motion of a Solar Sail on an inclined periodic orbit to the ecliptic, with its orbital plane in synchronous rotation with the Sun. A more recent study by Mu and Gong [49], discusses a coupled attitude control and orbit dynamics of the sail in a GeoSail orbit, where the relative attitude and orbit equations of motion are incorporated and linearised into the coupled equations, and a control law based on the LQR is designed to this linearised system. A similar coupled attitude-orbit control exploiting the LQR method is treated in Ref.[32] where the model is augmented with flexible properties of the Solar Sail. Another recent study about the flexible solar sail is carried out by Liu and Rong in Ref. [38], where a dynamic model is implemented for attitude/vibration controller design which in the study is an LQR based and optimal proportional-integral (PI) based controller.

1.3 Novel contributions of the thesis to Solar Sail control

This thesis aims to expand knowledge on the Solar Sail control strategies for the stabilization of artificial stationary points. Firstly, consolidated control actuation mechanisms, such as the thrust vectoring through attitude control [31, 44], and the application of a reflective control device on the solar sail film to produce torque [58, 47, 8] have been analysed. Subsequently, different combinations of actuation mechanisms, based on LQR theory [23, 7], have been implemented with the objective to develop new successful control schemes. In particular, a new concept that fuses two different technologies (RCD and heliogyro) has been proposed. Furthermore, algorithms involving all the designed mechanisms were developed and applying each of them to the Solar Sail dynamics, it was possible to compare their control capabilities. A comparison aimed to determine which would be the most suitable, in terms of Solar Sail parking in the CRTBP.
In addition, the research presents a new control design, exploiting thrust vectoring through attitude control. It differs from the previous linear control because it is implemented without the linearisation with respect to the control, but only the state. For this purpose, an algorithm aimed at *mapping* an ideal feed-back acceleration within a loop has been designed. This algorithm exploits the Newton method in such a way that the peculiar Solar Sail acceleration reproduces exactly the ideal control, whose station keeping capabilities

have been demonstrated. The process is achieved by tuning attitude angles, which are variables of the acceleration function.

Chapter 2

Solar Sail background

This second chapter presents a general outlook on Solar Sails' existing configurations, and the theory behinds the characteristic force thanks to which these are propelled. In addition, there is an overview of the Solar Sail acceleration parameters which will be employed as control variables in the future control designs.

2.1 Fundamentals of Solar Sailing

2.1.1 Solar Sail structural configurations

There exist three different configurations that meet these requirements, each of them should provide a force that maintains the sail film flat. The first concept is the square solar sail, which consists of four deployable spars cantilevered from a central load-bearing hub. The payload and spar deployment mechanism, are contained in the hub (see Fig. 2.1). The second configuration is the so-called "heliogyro", which differentiates form the previous by presence of spin-induce tension. This design involves a number of long slander blades which are again attached to a central load-bearing hub. The heliogyro slowly spins to maintain a flat, uniform surface Fig. 2.2.
Both configurations have pros and cons. While the square Solar Sail is a good concept, the cantilevered spars are subject to bending loads and so must be sized consequently, representing a massive mass fraction of the sail. On the other hand, the heliogyro blades may require edge stiffeners to transmit radial loads and to provide torsional stiffness to allow cyclic blade rotations.
The final concept is the disc Solar Sail in which a continuous film, or elements of film, are held flat, again using spin-induced tension, as shown in Fig. 2.3. The disc Solar Sail offers the same potential advantages as the heliogyro in reducing structural mass, but avoids extremely long slender blades.

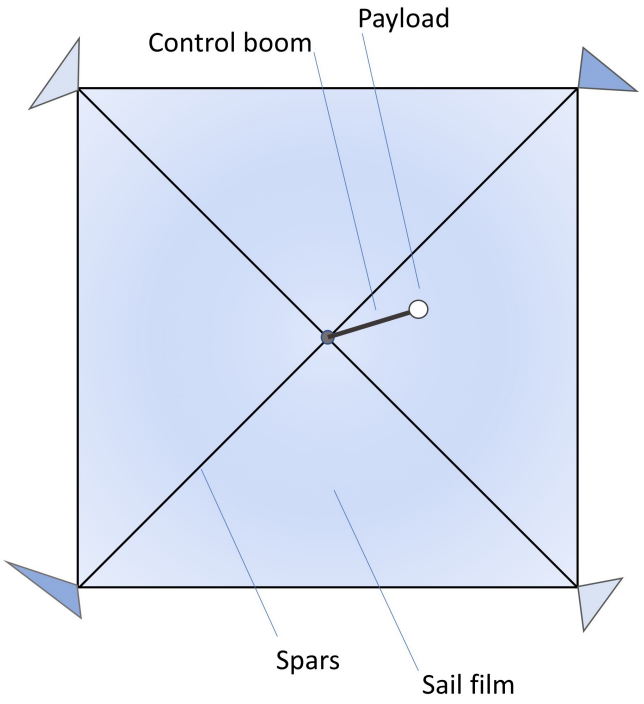

Figure 2.1: Classical solar sail configuration

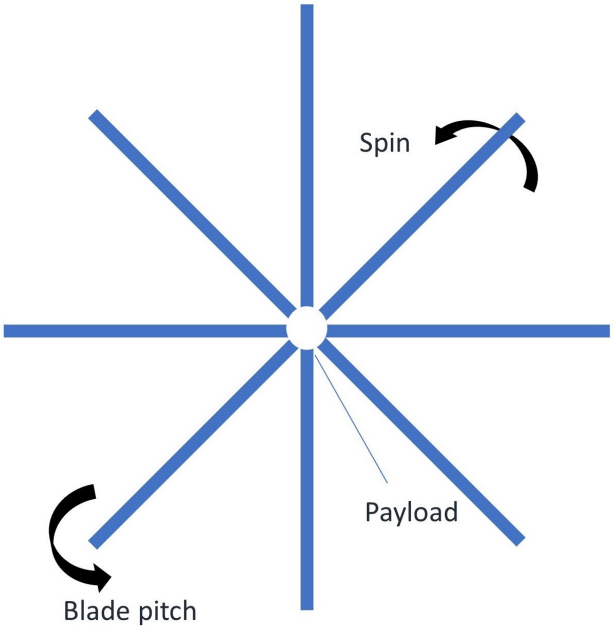

Figure 2.2: Heliogyro configuration

2.1.2 Performance parameters

In order to compare Solar Sail designs, a standard performance metric is required. The peculiar parameter used is the Solar Sail characteristic acceleration, i.e. the Solar Radiation Pressure acceleration experienced by a Solar Sail facing the Sun at a distance of one

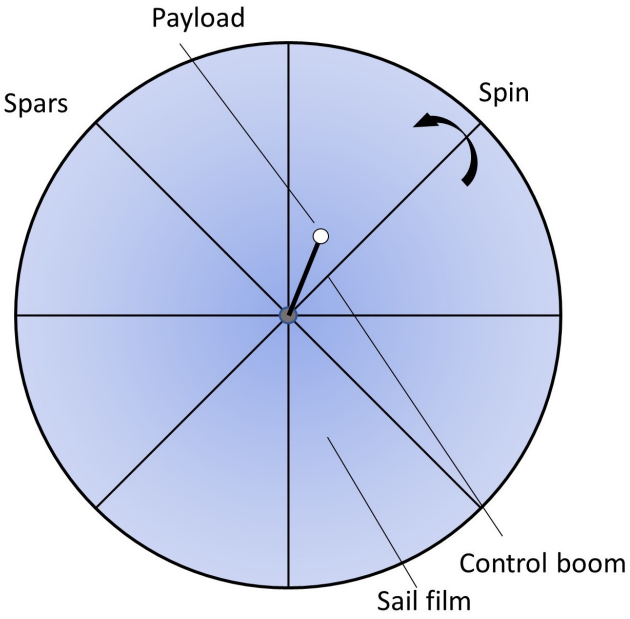

Figure 2.3: Disk shaped configuration

astronomical unit (AU), the mean distance of the Earth from the Sun. At this distance from the Sun, the magnitude of solar radiation pressure P is $4.56 \times 10^6\ Nm^{-2}$.
Hence, multiplying this pressure by the sail area$A$ yields the solar radiation pressure **force** exerted on the solar sail. Dividing by the sail mass m yields the solar sail acceleration. A factor of 2 must also be added to account for the sail reflectivity since reflected photons impart a reaction of equal magnitude to incident photons. From this calculation in possible to define the solar sail characteristic acceleration a_0, then defined as:

$$a_0 = \frac{2P}{\sigma},\ \sigma = \frac{m}{A} \tag{2.1}$$

where σ is the Solar Sail mass per unit area, termed the *sail loading*. The characteristic Solar Sail Acceleration allows a comparison of sailcraft design concepts.

2.1.3 Solar Sail orbits

As mentioned before, the solar radiation action on the sail can be visualised considering the transfer of momentum to the Solar Sail by photons, the quantum packets of the energy of which light is composed. When photons arrive at sail surface, they impart momentum to it, this phenomena leads to an impulse generator for the entire sail. A second impulse is generated when the photons are reflected again. The union of these two impulses is responsible for a force-directed normal to the solar sail surface, as shown in Fig. 2.4. An important parameter is the so-called clock angle α which describes the orientation of sail to the Sun, therefore the force vector. It can vary in a range between $-\pi/2$ and $\pi/2$,

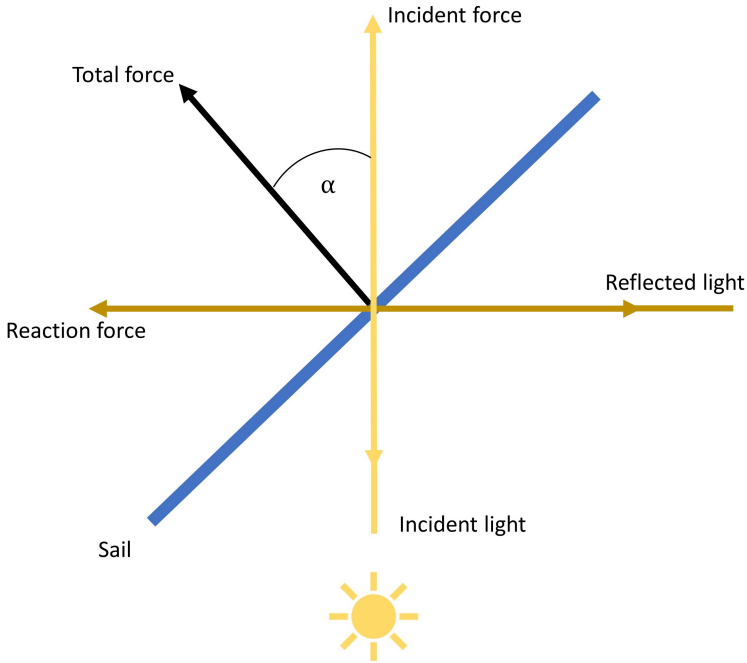

Figure 2.4: Force vector components

to have the sail reflecting surface always directed toward the sun. It follows that as the clock angle increases, the magnitude of solar radiation pressure force decreases due to the reduction in the projected sail area and the reduction in the component of solar radiation pressure force directed normal to the sail surface.
Solar sails are continuously accelerated so that their orbits are quite different from the usual ballistic arcs followed by conventional spacecraft. By choosing either a negative or positive sail pitch angle the Solar Sail will either spiral inwards towards the Sun or outwards away from the Sun. In this thesis, however, focus will be placed on control strategies used for Solar Sail parking, i.e. forcing the spacecraft to be steady into one of its equilibrium points of CRTPB (see Chapter 2). The resulting orbit, in this case, will be circular around the CRTBP centre of mass. It is worth to be said that by an appropriate sequence of sail orientations, any point in the solar system can be reached. Optimization methods can be used in such instances to determine the best sail orientation time history to minimize the transfer time to the target body.

2.2 Solar Radiation Pressure

Solar Sail acceleration is induced by the pressure exerted on the surface due to photons' momentum. The physics of SRP could be analysed by considering the two physical descriptions of the momentum transfer process. Here the first method will be exploited, which includes the quantum description of radiation and packets of energy, in which the photons can be visualised while travelling radially outward from the Sun and scattering

off the sail thus imparting momentum. Following this model, the pressure exerted on the solar sail is computed by considering the momentum transported by a flux of photons, which is related to the energy flux of them hitting the surface W. The term W designates the energy flux (energy crossing unit area in unit time) at a distance r from the Sun. This quantity can be written in terms of solar luminosity L_S and scaled by the Earth-Sun distance R_E as:

$$W = W_E \left(\frac{R_E}{r} \right)^2 \tag{2.2}$$

$$W_E = \frac{L_s}{4\pi R_E^2} \tag{2.3}$$

Where W_E is the energy flux at the Earth distance, so it is a well known quantity. From the flux term it is possible to derive the energy ΔE across a surface of area A normal to the incident radiation at time Δt, it is given by the formula:

$$\Delta E = WA\Delta t \tag{2.4}$$

This energy transports a momentum Δp given by:

$$\Delta p = \frac{\Delta E}{c} \tag{2.5}$$

The pressure P that acts on the surface can be finally computed as:

$$P = \frac{1}{A} \left(\frac{\Delta p}{\delta t} \right) \tag{2.6}$$

Therefore using the definition of W and Eq. 1.4 it is possible to define the solar radiation pressure as:

$$P = \frac{W}{c} \tag{2.7}$$

2.3 Solar Sail ideal force

The force exerted on an ideal, perfectly reflecting Solar Sail and the consequent acceleration is described below. The Solar Sail is an oriented surface, therefore to compute the acceleration the sail attitude must be considered. Naming $\mathbf{n}$ the unit vector normal to sail surface, $\mathbf{u_i}$ the direction of incident photons and A the area of the sail, the force exerted on the latter due to the energy flux coming from the Sun is:

$$f_i = PA(\mathbf{u_i} \cdot \mathbf{n})\mathbf{u_i} \tag{2.8}$$

Taking into account that the reflected photons will exert a pressure equal in magnitude with respect ot the incident ones, the total force expression will be:

$$f_i = 2PA(\mathbf{u_i} \cdot \mathbf{n})\mathbf{u_i} \tag{2.9}$$

Then, using Eqs. 2.3, 2.4 and 2.7 this total force may be written as:

$$f_i = \frac{2AW_e}{c}\left(\frac{R_e}{r}^2\right)\cos^2\alpha\mathbf{n} \tag{2.10}$$

where $\cos\alpha$ is the result of dot product between the direction vector of incident photons and Solar Sail normal. From now on, the vector $\mathbf{u}_i$ will be renamed $\mathbf{r}_1$ which corresponds to the unit vector from the Sun to the sail.
Therefore, dividing the force by solar sail mass it is possible to derive the expression of the *solar sail acceleration*:

$$a = \frac{2W_E}{c}\frac{1}{\sigma}\left(\frac{R_E}{r}\right)^2\cos\alpha^2\mathbf{n} \tag{2.11}$$

Where σ defines the ratio A/m and α is the clock angle, defined before. For a solar sail in heliocentric orbit, as the case of this thesis, the radiation direction $\mathbf{u_i}$ can be substituted with the unit radial vector $\mathbf{r}_1$ from the Sun to the sail. Furthermore, it is useful to express $\mathbf{a}$ in terms of solar gravitational acceleration as [42]

$$\mathbf{a} = \beta\frac{GM_S}{r^2}(\mathbf{r}_1 \cdot \mathbf{n})^2\mathbf{n} \tag{2.12}$$

where M_s is the solar mass and G is the universal gravitational constant. The dimensionless sail loading parameter β corresponds to the ratio of solar radiation pressure acceleration to the solar gravitational one. This parameter is also referred as the *lightness number* of the sail, which results independent of the Sun-sail distance.
By exploiting the Eqs. 2.3 and 2.12 it is possible to write the Solar Sail lightness number as

$$\beta = \frac{\sigma^*}{\sigma} \tag{2.13}$$

And the critical sail loading parameter:

$$\sigma^* = \frac{L_S}{2\pi GM_s c} \tag{2.14}$$

It is found to be $1.53gm^{-2}$. This is a unique constant which is function of the solar mass and the solar luminosity.
The parameter β will be of great relevance in following analysis, constituting an important

control parameter, especially for heliogyro.

Another formulation of the Solar Sail ideal acceleration, which will be useful in this study, is the dimensionless form of SSCRTBP (Solar Sail Circular Restricted Three-Body Problem) with Sun and Earth as primaries.

$$\mathbf{a} = \beta \frac{1-\mu}{|\mathbf{r}|^2} cos\alpha^2 \mathbf{n}. \tag{2.15}$$

Where μ is the mass ratio of the system and r_1 the distance from the Sun to the sail.

2.4 Solar sail non-ideal force

The acceleration computed in the previous section was obtained by considering a perfect reflective Solar Sail, but such an idealised model is not sufficient for our study. Therefore, it is necessary to include a non-perfect force model, called *optical model*, considering reflection, absorption, and re-radiation by the sail. The total force exerted on the solar sail due to solar radiation pressure may be rigorously written as

$$f = f_r + f_a + f_e \tag{2.16}$$

where f_r is the force due to reflection, f_a is the force due to absorption and f_e is the force due to emission by re-radiation. The main optical properties of the sail film can now be defined by the reflection coefficient $\tilde{r}$, absorption coefficient a and transmission coefficient τ, with the constraint:

$$\tilde{r} + a + \tau = 1. \tag{2.17}$$

Since $\tau = 0$ on the reflecting side of the sail, the relation becomes:

$$a = 1 - \tilde{r} \tag{2.18}$$

The solar sail orientation is again defined by a vector $\mathbf{n}$ normal to sail surface, and a tangent unit vector $\mathbf{t}$ normal to $\mathbf{n}$. In addition, a unit vector of incident photons $\mathbf{u}$ and a unit vector of specular reflected photons $\mathbf{s}$ will be defined. Between these two vectors exist two relations:

$$\mathbf{u} = \cos\alpha \mathbf{n} + \sin\alpha \mathbf{t} \tag{2.19}$$

$$\mathbf{s} = -\cos\alpha \mathbf{n} \tag{2.20}$$

By manipulating the definition of $\mathbf{s}$, it is possible to write it in a useful form, in relation to $\mathbf{u}$:

$$\mathbf{s} = \mathbf{u} - 2cos\alpha \mathbf{n} \tag{2.21}$$

Once the component vectors are defined, it is possible to introduce the force components exerted by photons on a non perfectly reflecting Solar Sail surface.
For the sake of completeness, it will be explained, firstly, the most rigorous way to express that force [43], but in further computation, the employed model would be a simplified one [62].

2.4.1 Force optical model

In the complete non-ideal solar sail model [43] the force is composed of three contributions: one due to absorption photons, and the others related to re-emission and re-radiation. The first contribution is given by $PA\cos\alpha\mathbf{u}$, where $A\cos\alpha$ is the projected sail area in direction $\mathbf{u}$. Resolving this force into normal and transverse components, using Eq. 2.21, it is found that

$$f_a = PA(\cos^2\alpha\mathbf{n} + \cos\alpha\sin\alpha\mathbf{t}) \tag{2.22}$$

Hereafter, are instead explained the contributions due to the photons which are specular reflected and photons which are uniformly scattered:

$$f_{rs} = -(\tilde{r}s)PA\cos\alpha\mathbf{s} \tag{2.23a}$$

$$f_{ru} = B_f\tilde{r}(1-s)PAcos\alpha\mathbf{n} \tag{2.23b}$$

The coefficient s indicates the fraction of photons specular reflected, while the coefficient B_f indicates that the front surface of the sail is non-Lambertian. A Lambertian surface is one which appears equally bright when viewed from any aspect angle. The non-Lambertian coefficient then describes the deviation from this condition. The total force due to reflected photons is now given by $f_{rs}+f_{ru}$ Therefore, the force due to reflection can be written in terms of normal and transverse directions:

$$f_r = PA[(\tilde{r}s\cos^2\alpha + B_f(1-s)\tilde{r}\cos\alpha)\mathbf{n} - \tilde{r}s\cos\alpha\sin\alpha\mathbf{t}] \tag{2.24}$$

The final component of force, that should be analysed, is the force due to the re-emission of light from the Solar Sail. The power emitted from a unit area of the sail at temperature T is $\varepsilon\tilde{\sigma}T^4$, where $\tilde{\sigma}$ is the Stefan-Boltzmann constant and ε is the surface emissivity. Therefore, allowing for the non-Lambertian nature of the front and back sail surfaces, and assuming the sail has uniform temperature, the force due to emission by re-radiation is given by:

$$f_e = \frac{\tilde{\sigma}T^4}{c}(\varepsilon_f B_f - \varepsilon_b B_b)\mathbf{n} \tag{2.25}$$

where ε_f and ε_b are the front and back emissivities, and as previously mentioned B_f and B_b are front and back Lambertian coefficients [46].
Therefore, substituting for the sail equilibrium temperature, the force exerted on the solar sail due to emission by re-radiation is given by

$$f_e = PA(1-\tilde{r})\frac{(\varepsilon_f B_f - \varepsilon_b B_b)}{\varepsilon_f + \varepsilon_b}\cos\alpha\mathbf{n} \tag{2.26}$$

Adding all of the derived force contributions, and subdividing it in normal(**n**) and tangential (**t**) components, we are able to obtain a complete expression for the total force on a Solar Sail system.

$$f_n = PA\left((1-\tilde{r}s)\cos\alpha^2 + Br(1-s)\tilde{r}\cos\alpha + (1-\tilde{r})\frac{\varepsilon_f B_f - \varepsilon_b B_b}{\varepsilon_f + \varepsilon_b}\cos\alpha\right)\mathbf{n} \tag{2.27}$$

$$f_t = PA(1-\tilde{r}s)\cos\alpha\sin\alpha\mathbf{t} \tag{2.28}$$

From the force, it is easy to obtain the acceleration. It is computed dividing the force by Solar Sail mass, and pointing out the Solar Sail lightness number β, it results:

$$\begin{aligned}\mathbf{a} = \frac{1}{2}\beta\frac{GM_s}{|\mathbf{r}|^2}\Bigg(&((1-\tilde{r}s)\cos\alpha^2 + Br(1-s)\tilde{r}\cos\alpha + (1-\tilde{r})\frac{\varepsilon_f B_f - \varepsilon_b B_b}{\varepsilon_f + \varepsilon_b}\cos\alpha)\mathbf{n} \\ &+ ((1-\tilde{r}s)\cos\alpha\sin\alpha)\mathbf{t}\Bigg)\end{aligned} \tag{2.29}$$

2.4.2 Simplified force optical model

After the explanation of the most rigorous model of the Solar Sail specific force, a simplified model from [62] will be discussed.
In that model the contribution of re-emitted photons is neglected and therefore only the force parts due to absorption, specular and diffuse reflection are included. These three are related by the formula:

$$\rho_a + \rho_s + \rho_d = 1 \tag{2.30}$$

The SRP force acting on such a flat, Lambertian surface is modelled as

$$\begin{aligned} f &= PA\left[\rho_a\cos\alpha\hat{r}_1 + 2\rho_s\cos\alpha^2\mathbf{n} + \rho_d\cos\alpha\left(\hat{r}_1 + \frac{2}{3}\mathbf{n}\right)\right] \\ &= PA\cos\alpha\left[(\rho_a+\rho_d)\mathbf{r}_1 + \left[2\rho_d\cos\alpha + \frac{2}{3}\rho_d\right]\mathbf{n}\right] \\ &= PA\cos\alpha\left[(1-\rho_d)\mathbf{r}_1 + \left[2\rho_s\cos\alpha + \frac{2}{3}\rho_d\right]\mathbf{n}\right] \end{aligned} \tag{2.31}$$

where P s the nominal solar-radiation-pressure, A is the surface area, $\hat{n}$ is a unit vector normal to the surface, and $\mathbf{r}_1$is a unit vector pointing from the Sun to the surface.
For case with $\rho_d \approx 0$, the SRP force can be expressed as

$$f = PA\cos\alpha[(1-\rho_s)\mathbf{r}_1 + 2\rho_s\cos\alpha\mathbf{n}] \tag{2.32}$$

It worth to express Eq. 2.32 even in terms of tangential and normal components, as follows:

$$\begin{aligned} f_n &= PA\cos\alpha^2(1+\rho_s) \\ f_t &= PA\cos\alpha\sin\alpha(1-\rho_s) \end{aligned} \tag{2.33}$$

Finally, it is possible to derive the simplified non-ideal Solar Sail acceleration as:

$$\mathbf{a_{sail}} = \frac{1}{2}\beta\frac{(1-\mu)}{|\mathbf{r}^2|}[(1-\rho_s)\mathbf{r}_1 + 2\rho_s\cos\alpha\mathbf{n}] \tag{2.34}$$

To complete the formulation of the non-ideal SRP force exerted on a solar sail, in addition to $\mathbf{n}$, there is the thrust unit vector $\mathbf{m}$, which points along the direction of the SRP force. While for ideal reflective model the SRP force is always along the direction of the sail normal vector, i.e. $\mathbf{m} = \mathbf{n}$, in non perfectly reflective model an angle exists between $\mathbf{n}$ and $\mathbf{m}$ called centreline angle ϕ (see Fig. 2.5), which is strictly related to reflection coefficient ρ.

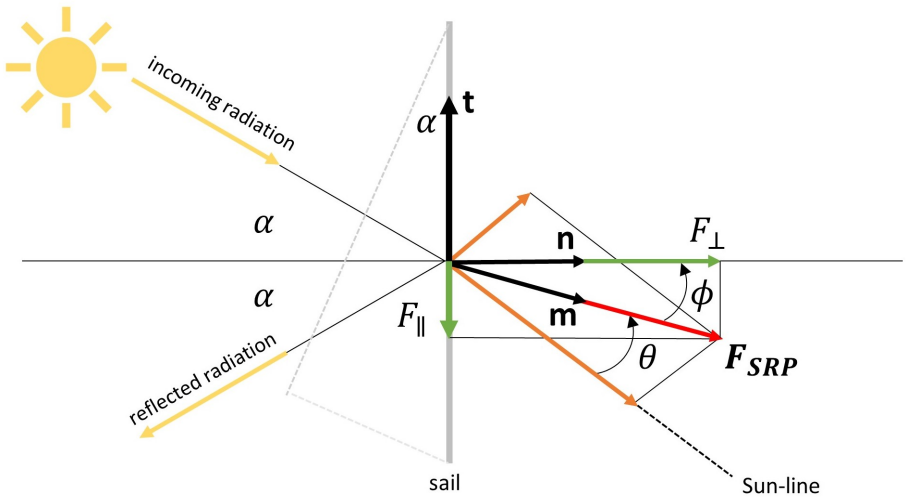

Figure 2.5: SRP force on a non-perfectly reflecting sail

2.4.3 Control variables

Once the solar sail force formulations have been explained, it is possible to list all the parameters related to that function, which are used as input variables in designed linear control systems.

Attitude angles

One of the most exploited parameters in Solar Sails attitude control is certainly its orientation vector **n** because the magnitude and direction of the induced thrust force strictly depend on the sail's attitude to the Sun. In this study *attitude angles* γ and δ have been employed, which represent the orientation of the sail with respect to the reference system taken into account (i.e. the rotating frame xyz presented in Chapter 3). The components of **n** in the rotating frame are

$$n = [\cos\gamma\cos\delta \;\; \cos\gamma\sin\delta \;\; \sin\gamma] \tag{2.35}$$

It worth to mention that for states with γ and δ equal to zero, the control developed with angles attitudes has resulted not adequate.
Constraints:
It is important to bear in mind that to represent a real situation of Solar Sail, driven by solar radiation, constraints on attitude angles should be imposed. The solar radiation pressure force vector can never be directed sun-ward ($\mathbf{r}_1 \cdot \mathbf{n} \geq 0$). In terms of attitude angles, this translates into the constraints $-\frac{\pi}{2} < \gamma < \frac{\pi}{2}$, while $0 < \delta < \pi$.

Lightness number β - Heliogyro

As said in the introduction, different sail configurations exist, including a traditional flat sail (either square or disc-shaped) and a heliogyro, which divides the sail membrane into several long, slender blades (see Fig. 2.6), analogous to a helicopter rotor. The potentiality of this configuration were stated by MacNeal [39] in 1967. He developed heliogyro design concept, proving that this was superior to other systems employing chemical or electrical propulsion for many missions requiring a large total impulse. Later, Blomquist in Ref. [9] studied the effects of blades configuration on acceleration, and examined two methods for deploying the blades from their rolled up configuration. The heliogyro Solar Sail is being re-examined by NASA, as a potential game-changing architecture for future solar sailing missions in [64], with a technology demonstration concept of small-scale heliogyro. Again Blomquist in Ref. [10] verified control models and appropriate operation strategies which allow heliogyro design.
Recalling that the magnitude and direction of the induced thrust force depends on the sail's attitude to the Sun, at each *cone* angle, a flat sail can only generate a force of par-

ticular magnitude and direction, while has been demonstrated by Heiligers in [27] that a heliogyro can arbitrarily reduce the magnitude of the thrust vector through the additional control of pitching the blades.
For the heliogyro, the scalable lightness number is an additional control, to account both for the attitude of the heliogyro and the effect of pitching the blades. Therefore, this configuration can be regarded as enabling a highly-variable lightness number, allowing it to scale the solar radiation pressure force between zero and that of an equivalent-area flat solar sail.

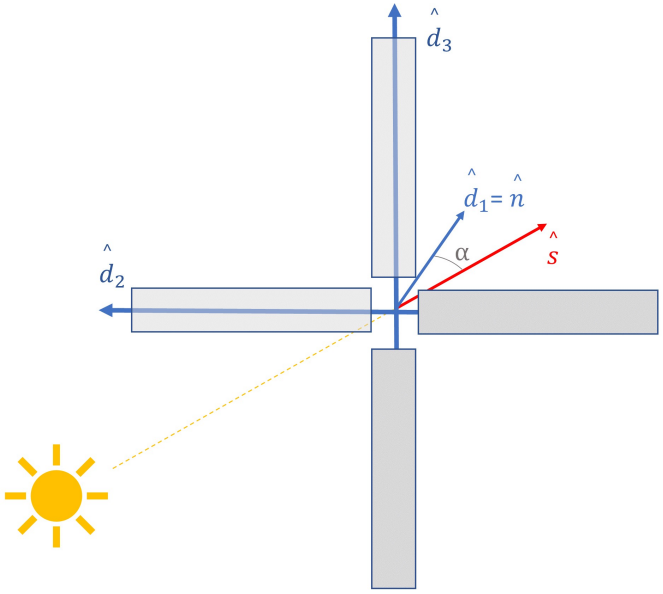

Figure 2.6: Heliogyro blades configuration

Specular reflectivity ρ - RCD

Previously, the two classic methods used to control the attitude of the sails has been introduced: such as varying the attitude angles or changing its surface exposed to the Sun. However, there is another method. It is the use of devices capable of changing the reflectivity properties of the sail. A reflectivity control device (RCD) is a thin film device capable of controlling the reflectivity characteristic of the Solar Sail [17].
In the majority of past studies, RCDs have been used as elements for the control of solar sail attitude in discrete way (on/off behaviour). In this thesis, instead, Solar Sail reflectivity parameter is a continuous control variable, assuming that it can vary continuously to satisfy the required control action. Therefore, the sail will be considered as a system capable of adapting the reflectivity of its surface to the required values. Focus will not be placed on how this happens, but following similar conducted researches [28]. It is necessary to impose constraints on this value, which cannot be too different from the nominal range, to have a feasible application.

Chapter 3

Solar Sail dynamics and Equilibrium points

To provide the basis for control analysis, it is necessary to build the equations that characterize the Solar Sail dynamics and analyse its characteristic equilibrium points.
In this research, the Solar Sail has been considered as the third body of a Circular Restricted Three-Body Problem (SSCRTBP), with the Earth and Sun as the two primaries, and the equations of motion are developed in a rotating frame of reference, convenient for the numerical continuation strategy and control development. Subsequently, the stationary points of the Solar Sail dynamics have been computed, involving both ideal and non-ideal Solar Sail dynamics.
It is necessary to state that this procedure has been carried out in several works. Concerning the case of the ideal dynamics, the first has been McInnes, in Ref. [43], which identified regions of existence of artificial Lagrange points, with the required sail orientation and the required sail loading in the Sun-Earth restricted three-body system determined. Much later, the concept of Solar Sail equilibrium points has been investigated by Verrier [59] who presented a detailed investigation of the dramatic changes that occur in the L1 halo family when radiation pressure is introduced into the Sun-Earth circular restricted three-body problem, demonstrating that even at small values of β there is significant difference to the classical CRTBP. A further study has been done again by McInnes in Ref. [4] which investigates the existence of equilibrium points in the elliptical restricted three-body problem.
The study of Solar Sail equilibration points is of great interest especially for their possible application in the development of halo orbits. This analysis has the foundation in libration point halo orbits for the classical restricted three-body problem, see the works of Farquhar [19], Farquhar et al. [20], Howell [29], Breakwell and Brown [14] and many others. A specific application for Solar Sail has been done by Baoyin in Ref. [3], where it is shown that periodic orbits can be developed that are displaced above or below the plane of the restricted three-body system. Again Baoyin in Ref. [4] investigates halo

orbits for solar sails, this time specifically at Sun-Earth L1 points, deriving a third-order approximate solution. In particular, two families of halo orbits are explored as defined by the sail attitude. Successively, Li Xuqiang in Ref. [65] analyses the variation of the position of the artificial L1 point with the lightness number of the Solar Sail, the effect of the difference of the lightness number and the out-of-plane amplitude on the orbit, and the variation of the orbit period with the lightness number.
There exist also studies on Solar Sail orbits involving the Earth-Moon system, as in Ref. [28] which research is aimed to find Solar Sail periodic orbits in the Earth-Moon three-body problem, in particular, Lagrange-point orbits. Differently, from Sun-Earth, this system is not autonomous and constraints on the orbital period need to be imposed. In that paper, the problem is solved as a two-point boundary value problem together with a continuation approach.
As for the determination of equilibrium points for the non-ideal dynamic model, even this approach has already been dealt with and solved in previous works. Starting from Ref. [41] by McInnes, where the problem of artificial Lagrange points generated by using Solar Sail spacecraft, are re-examined with a partially reflecting solar sail. In this study is demonstrated that, apart from reducing the magnitude of the radiation pressure force exerted on the sail, the absorption of the latter means that the radiation pressure force vector is no longer directed normal to the sail surface. Later, in Ref. [16] Dachwald proved that involving the non-perfect reflecting Solar Sail acceleration, in artificial Lagrangian points, leads to a reduction in the volume of space available for equilibrium solutions about L2. As the sail degrades, the coefficient of reflection decreases and therefore the points of equilibrium decrease, changing the behaviour of the Solar Sail in CRTBP.
The whole of these works has been taken into account to develop these two sets of artificial equilibrium points, which exact values are essential to future analyses of this research.

3.1 Circular Restricted Three-Body Problem

The CRTPB is a particular version of the classic restricted three-body problem which is concerned with the motion of an infinitesimal body in the gravitational field of two massive primary bodies. In CRTBP the motion of two primary bodies is constrained to circular orbits about their barycentre [61].
The Circular Restricted Three-Body Problem was originally formulated by Euler in 1772 for the Sun–Earth-moon system to study the motion of the moon about the Earth but perturbed by the sun.
In this section, we consider the Sun-Earth–Solar Sail system, illustrated in Fig. 3.1. It is assumed that the spacecraft mass is insignificant compared to the masses of two primary bodies. Hence, the orbital motion of the two primary bodies is not affected by the spacecraft. Therefore, it is simply described by the two-body problem in which the two primary

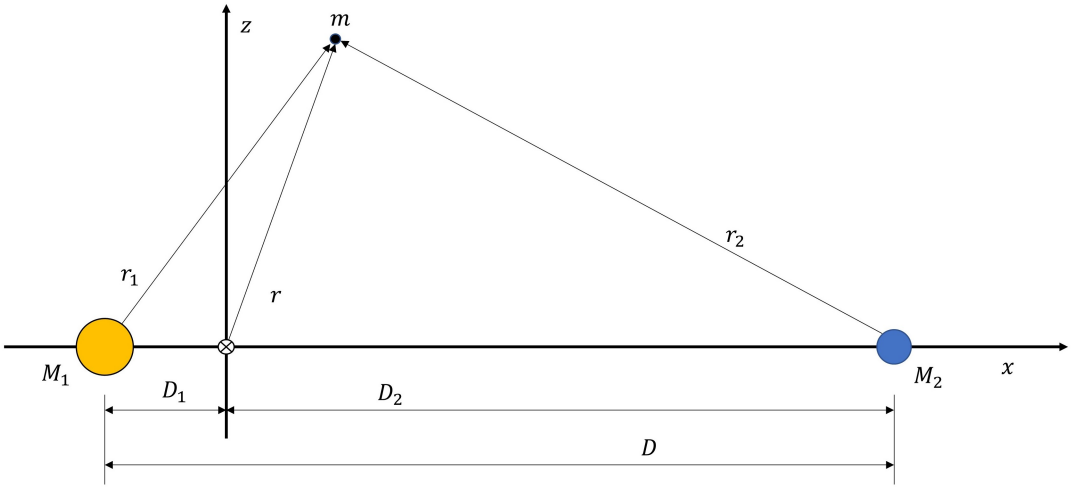

Figure 3.1: Circular restricted three-body problem

bodies rotate about their composite centre of mass (barycentre). It can be further assumed that the two primary bodies rotate about their barycentre in circular orbits. It derives that Sun-Earth system rotates with a constant angular velocity

$$\omega = \sqrt{G(M_1 + M_2)/D^3} \tag{3.1}$$

where M_1 and M_2 are the masses of the Sun and the Earth, respectively, and D is the constant distance between them. For the Sun-Earth system, the parameters are:

$$\begin{gathered} M_1 = 1.989\ 10^{30} kg \\ M_2 = 5.972\ 10^{24} kg \\ D = 1.5\ 10^{11} m \\ D_1 = 4.5\ 10^{5} m \\ D_2 = 1.49\,10^{11} m \\ \omega = 1.9881\,10^{-7} rad/s \\ \mu_1 = GM_1 \\ \mu_2 = GM_2 \end{gathered}$$

where D_1 is the distance between M_1 and the barycentre, D_2 is the distance between M_2 and the barycentre, and $D = D_1 + D_2$.

The position vector of the spacecraft relative to the barycentre is expressed in terms of basis vectors $(\mathbf{x}, \mathbf{y}, \mathbf{z})$ of a rotating reference frame with an angular velocity of $\omega\mathbf{z}$ and with its origin at the barycentre, as follows:

$$\mathbf{r} = X\mathbf{x} + Y\mathbf{y} + Z\mathbf{z} \tag{3.2}$$

Considering that $\dot{\mathbf{x}} = \omega\mathbf{y}$, $\dot{\mathbf{y}} = -\omega\mathbf{x}, and \dot{\mathbf{z}} = 0$, the inertial acceleration of the spacecraft can be found as

$$\ddot{\mathbf{r}} = (\ddot{X} - 2\omega\dot{Y} - n^2X)\mathbf{x} + (\ddot{Y} + 2n\dot{X} - n^2Y)\mathbf{y} + \ddot{Z} \tag{3.3}$$

The equation of motion of the spacecraft is then simply given by

$$m\ddot{\mathbf{r}} = -\frac{GM_1m}{r_1^3}\mathbf{r}_1 - \frac{GM_2m}{r_2^3}\mathbf{r}_2 \tag{3.4}$$

where m is the mass of the spacecraft (Solar Sail in our case), $r_1 = |\mathbf{r}_1|, r_2 = |\mathbf{r}_2|$ and

$$\mathbf{r}_1 = -D_1\mathbf{x} + \mathbf{r}$$
$$; \mathbf{r}_2 = D_2\mathbf{x} + \mathbf{r}\ .$$

Eq. 3.4 can be written as:

$$\ddot{\mathbf{r}} = -\left(\frac{\mu_1}{r_1^3}\right)\mathbf{r}_1 - \left(\frac{\mu_2}{r_2^3}\right)\mathbf{r}_2 \tag{3.5}$$

Equating the components of the inertial acceleration and the gravitational acceleration in Eq. 3.5, CRTBP equations of motion are obtained:

$$\ddot{X} - 2\omega\dot{Y} - \omega^2 = \frac{\mu_1(X - D_1)}{r_1^3} - \frac{\mu_2(X + D_2)}{r_2^3} \tag{3.6}$$

$$\ddot{Y} + 2\omega\dot{X} - n^2Y = -\frac{\mu_1Y}{r_1^3} - \frac{\mu_2Y}{r_2^3} \tag{3.7}$$

$$\ddot{Z} = -\frac{\mu_1Z}{r_1^3} - \frac{\mu_2Z}{r_2^3} \tag{3.8}$$

The terms $2\omega\dot{Y}$ and $2\omega\dot{X}$ are the Coriolis acceleration, and ωX and $\omega^2 Y$ are centrifugal acceleration terms.

The equations of motion, given by Eqs. 3.6, 3.7, and 3.8, for restricted three-body problem can also be expressed in terms of a pseudo-potential $U = U(X,Y,Z)$ as follows:

$$\ddot{X} - 2\omega\dot{Y} = \frac{\partial U}{\partial X} \tag{3.9}$$

$$\ddot{Y} + 2\omega\dot{X} = \frac{\partial U}{\partial Y} \tag{3.10}$$

$$\ddot{Z} = \frac{\partial U}{\partial Z} \tag{3.11}$$

where the pseudo-potential U, which is the centrifugal plus gravitational force potential, is defined as

$$U = \frac{1}{2}\omega^2(X^2 + Y^2) + \frac{\mu_1}{r_1} + \frac{\mu_2}{r_2} \tag{3.12}$$

where $\mu_1 = GM_1$, $\mu_2 = GM_2$, $r_1 = \sqrt{(X-D1)^2+Y^2+Z^2}$, and $r_2 = \sqrt{(X-D2)^2+Y^2+Z^2}$. In the next section, the dimensionless version of this set will be derived, useful to define the Solar Sail equations of motion.

3.2 Solar Sail equations of motion

The dimensionless equations of motion are derived using a rotating frame of reference $(\mathbf{x},\mathbf{y},\mathbf{z})$ in which the primary masses are fixed, the x-axis points between the primary masses, the z-axis is the axis of rotation, and the y-axis completes the triad. The angular velocity of the frame is therefore $\omega = \mathbf{z}$.
To derive these equations, we should start by introducing the mass ration *mu* of The Sun-Earth system as

$$M_2/(M_1+M_2) = \mu = 3e-6$$
$$M_1/(M_1+M_2) = 1-\mu$$

therefore, we rewrite the equations of motion in dimensionless form:

$$\ddot{X} - 2\dot{Y} - X = -\frac{(X+\mu)(1-\mu)}{r_1^3} - \frac{\mu(X-1+\mu)}{r_2^3} \tag{3.13}$$

$$\ddot{Y} + 2\dot{X} - Y = -\frac{(1-\mu)Y}{r_1^3} - \frac{\mu Y}{r_2^3} \tag{3.14}$$

$$\ddot{Z} = -\frac{(1-\mu)Z}{r_1^3} - \frac{\mu Z}{r_2^3} \tag{3.15}$$

where

$$r_1 = \sqrt{(X+\mu)^2+Y^2+Z^2}$$
$$r_2 = \sqrt{(X-1+\rho)^2+Y^2+Z^2}$$

Time is units of $\frac{1}{\omega}$ and X,Y,Z,r_1 and r_2 are units of D. A scheme of this reference system is represented in Fig. 3.2. As we said in Section 2.1, an alternative way to express this equations is involving the pseudo-potential U, this time expressed in dimensionless coordinates.

$$\ddot{\mathbf{r}} + 2\nabla \times \mathbf{r} = \nabla U \tag{3.16}$$

where dimensionless U is:

$$U = -\left(\frac{1-\mu}{r_1} + \frac{\mu}{r_2}\right) - \frac{1}{2}|\omega \times \mathbf{r}| \tag{3.17}$$

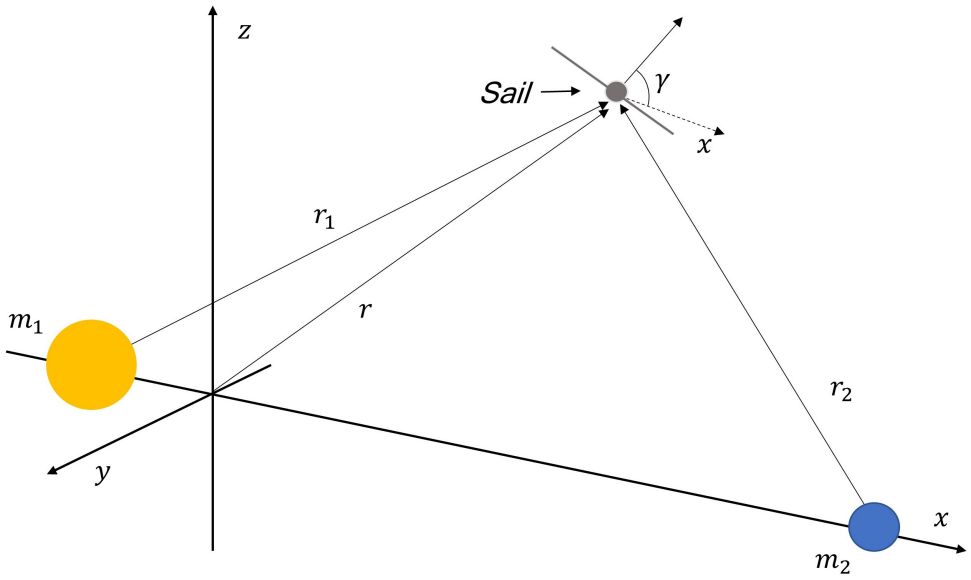

Figure 3.2: The rotating coordinate frame and the sail position therein

In order obtain the Solar Sail equations of motion in CRTBP, the sail acceleration vector (Eq. 2.15) is summed to Eq. 3.16.

$$\ddot{\mathbf{r}} + 2\nabla \times \mathbf{r} = \nabla U + a_{sail} \tag{3.18}$$

Expanding Eq. 3.18 the equations of the Solar Sail dynamics are obtained, and these will be useful in further analyses:

$$\ddot{X} - 2\omega\dot{Y} - X = \frac{(X+\mu)(1-\mu)}{r_1^3} - \frac{\mu(X-1+\mu)}{r_2^3} + a_x \tag{3.19}$$

$$\ddot{Y} + 2\omega\dot{X} - Y = -\frac{(1-\mu)Y}{r_1^3} - \frac{\mu Y}{r_2^3} + a_y \tag{3.20}$$

$$\ddot{Z} = -\frac{(1-\mu)Z}{r_1^3} - \frac{\mu Z}{r_2^3} + a_z \tag{3.21}$$

where a_x, a_y and a_z are Solar Sail radiation acceleration components in rotating frame.
In order to express the Solar Sail radiation acceleration in the rotating frame, two sail angles are used to describe the spacecraft orientation. There are two definitions of sail angles in the literature. The first definition uses the *cone* and *clock* angle, while the second definition the *pitch* and *azimuth* angle. The pitch angle γ and the azimuth angle δ have been used in this thesis. In Fig. 3.3, the layout of these two angles, where x, y, z are the axes of the rotating frame. The solar radiation acceleration is in the opposite direction of $\mathbf{n}$, i.e. $\mathbf{a} = -a\mathbf{n}$.

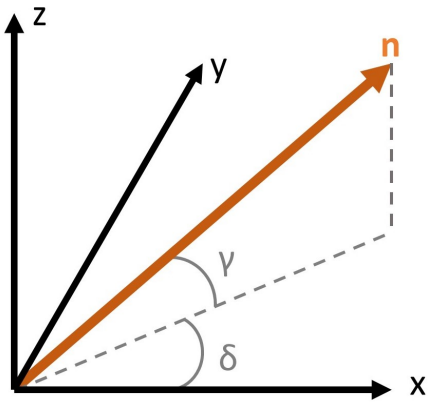

Figure 3.3: Attitude vector components

Thus, the acceleration scalar components in terms of the control angles are:

$$\begin{bmatrix} a_x \\ a_y \\ a_z \end{bmatrix} = \beta \frac{1-\mu}{|\mathbf{r}^2|} \begin{bmatrix} \cos\gamma\cos\delta \\ \cos\gamma\sin\delta \\ \sin\gamma \end{bmatrix} \tag{3.22}$$

As exposed before, the Solar sail acceleration is linked to the force formulation adopted, and it depends on the accuracy required by the problem. In next section, both *ideal solar sail acceleration* and simplified *non-ideal acceleration* formulas will be used.

3.3 Equilibrium points for ideal solar sail

Once the equations of motion are derived, it is straightforward to compute the set of artificial equilibrium points of the Solar Sail dynamics in CRTBP.

3.3.1 Computation

Here after the procedure adopted to derive equilibrium points is explained. These are computed by looking at the stationary solution of the Eq. 3.18, therefore to find them it is necessary to impose the conditions:

$$\begin{aligned} \ddot{\mathbf{x}} = \dot{\mathbf{x}} = 0 \\ \ddot{\mathbf{y}} = \dot{\mathbf{y}} = 0 \\ \ddot{\mathbf{z}} = \dot{\mathbf{z}} = 0 \end{aligned}$$

which lead to the identity

$$\mathbf{a} - \nabla U = 0 \tag{3.23}$$

The classical Circular Restricted Three-Body Problem has five equilibrium solutions Lj (j = 1-5) where an infinitesimal mass will remain at rest with respect to two primary masses in orbit about their common centre-of-mass, and these are the well known Lagrange points. The classical restricted problem has been extended to include radiation pressure exerted on the infinitesimal mass from either or both of the primary masses. This formulation generates four new additional equilibria with interesting stability characteristics. However, for a point mass the radiation pressure force vector is constrained to lie along the line connecting the source of radiation pressure and the mass. For the planet-Sun-sail three-body problem however, the sail attitude may be freely oriented so that the direction of the solar radiation pressure force vector is not constrained in this way. Furthermore, the magnitude of the solar radiation pressure force may be chosen through the solar sail lightness number β.
Since these parameters can be chosen at will, it is clear that this set of five stationary solutions will be replaced by an infinite set of artificially generated solutions. This infinite set of solutions is parametrised into level surfaces by the sail loading parameter β. A particular stationary solution on a level surface is then defined by two specific attitude angles. Attention is focused on equilibrium points in $x-z$ plane, and to simplify the computation the sailcraft will be considered normal to this plane, so that $\delta = 0$ and $y = 0$.
Firstly, the Solar Sail equilibrium points for the dynamics including the ideal acceleration formula of Eq. 2.15, will be computed.
The equilibrium points have been calculated by exploiting the Matlab® function *fsolve*, aimed at the resolution of non-linear equations system, of the form:

$$F(x) = 0 \tag{3.24}$$

Where $F(x)$ is a vector function, such as Eq. 3.23 representing Solar Sail dynamics.
Therefore, expanding Eq. 3.23 the equations system, to solve, will be obtained:

$$F(1) = X - \frac{(X+\mu)(1-\mu)}{r_1^3} - \frac{\mu(X-1+\mu)}{r_2^3} + a_x \tag{3.25a}$$

$$F(2) = Y - \frac{(1-\mu)Y}{r_1^3} - \frac{\mu Y}{r_2^3} + a_y \tag{3.25b}$$

$$F(3) = -\frac{(1-\mu)Z}{r_1^3} - \frac{\mu Z}{r_2^3} + a_z \tag{3.25c}$$

It is known that the acceleration of Eq. 3.15 depends on β and attitudes angles. Therefore, equilibrium points have been computed in $x-z$ plane, parametrizing the Eq. 3.25 in function of β and attitude angle γ (since δ has been imposed equal to 0).
The sections of level surfaces generated by Eq. 3.25 are shown in Figs. 3.4 and 3.5. The sections define families of one parameter level curves representing subsets of the

continuum of new artificial stationary solutions with equal sail loading β. These are generated connecting the stationary solutions of Eq. 3.25, for values of γ which range is from $-\pi/2$ to $\pi/2$, values that derive from the assumption that Solar Radiation Pressure force vector can never be directed Sun-ward.

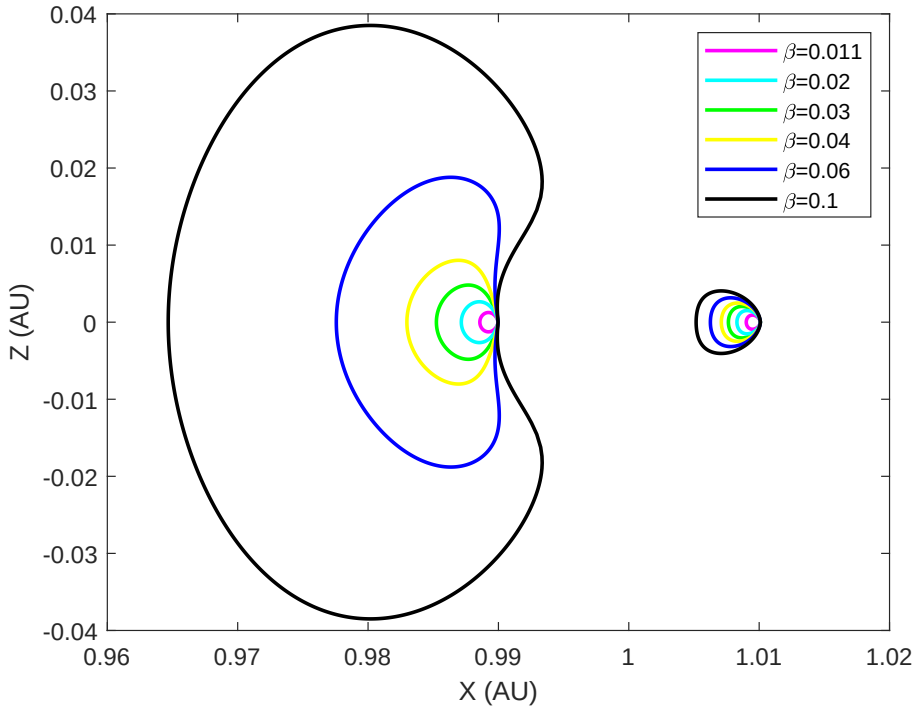

Figure 3.4: Section of the level surfaces in the near Earth region normal to the plane of the system, for $\beta = [0.011, 0.02, 0.03, 0.04, 0.06, 0.1]$. Ideal Solar Sail case

It is possible to appreciate in Fig. 3.4 that equilibrium points are divided in two groups, which are in correspondence of Lagrangian point L_1 and L_2. In fact, the computation of equilibrium points is strictly related to *initial conditions* of system integration, that were imposed equal to L_1 and L_2. Since the equilibrium points will be employed in further computations of control designs, these have been computed in a very accurate way, imposing a tolerance limit of 10^{-12} to the system solver.

3.4 Equilibrium points for non-ideal solar sail

Another set of artificial equilibrium points should be computed, including, this time, the Solar Sail dynamics with *non-ideal acceleration*, due to the requirement to have one of these equilibrium points for the implementation of linear control models.

3.4.1 Computation

Looking at Eqs. 2.34, it is clear that the difference with ideal acceleration is in the second part of the formula, in which appears the additional term: ρ. As mentioned in Chapter

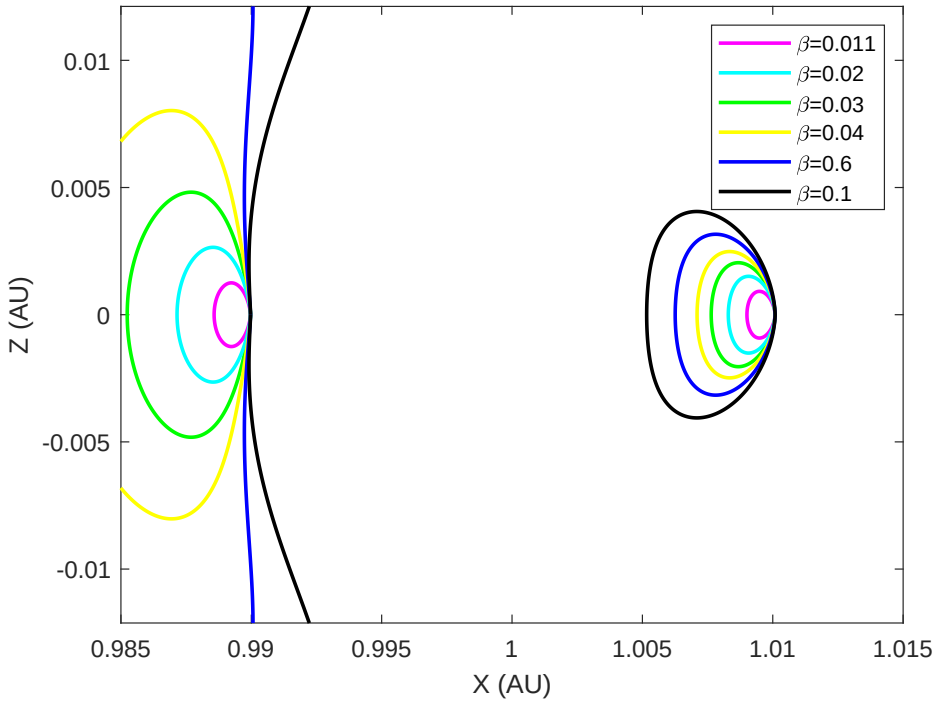

Figure 3.5: Particular of the section of the level surfaces in the near Earth region normal to the plane of the system, for $\beta = [0.011, 0.02, 0.03, 0.04, 0.06, 0.1]$. Ideal solar sail case

2, it represents the specular reflectivity of the solar sail and it is different from 1 because it is necessary to consider even a non-perfectly reflecting sail model. As has been done in mentioned researches, the simplified non-ideal acceleration formula, presented in Eq. 2.34 is exploited, and used in Eq. 3.25.

In this computation, the data will be taken from the Solar Sail of NEA Scout project [51], with a mass and sail area of $12kg$ and $86m^2$ respectively, that results in ideal lightness parameter β is 0.011 and $\rho = 0.91$.

Following the same procedure of Subsection 3.3.1, another set of equilibrium points is calculated (see Figs 3.6 and 3.7). Comparing equilibrium surfaces in Figs. 3.4 and 3.6, firstly it can be seen that for non-ideal Solar Sail case, the volume of space available for equilibrium solutions about L2 is significantly reduced, as it has been demonstrated in [18]. For solutions near L1 the main effect of the non-ideal sail is to displace the equilibrium solutions towards the Earth. This is due to the reduction in the SRP force magnitude rather than the centreline angle. In general, we can state that equilibrium solutions sun-ward of L1 are not greatly affected by non perfect reflecting properties while equilibrium solutions about L2 are severely restricted.

3.5 Equilibrium point stability

Now that the existence of artificial stationary solutions has been established, it is necessary to examine their stability. We will numerically demonstrate that the system does not

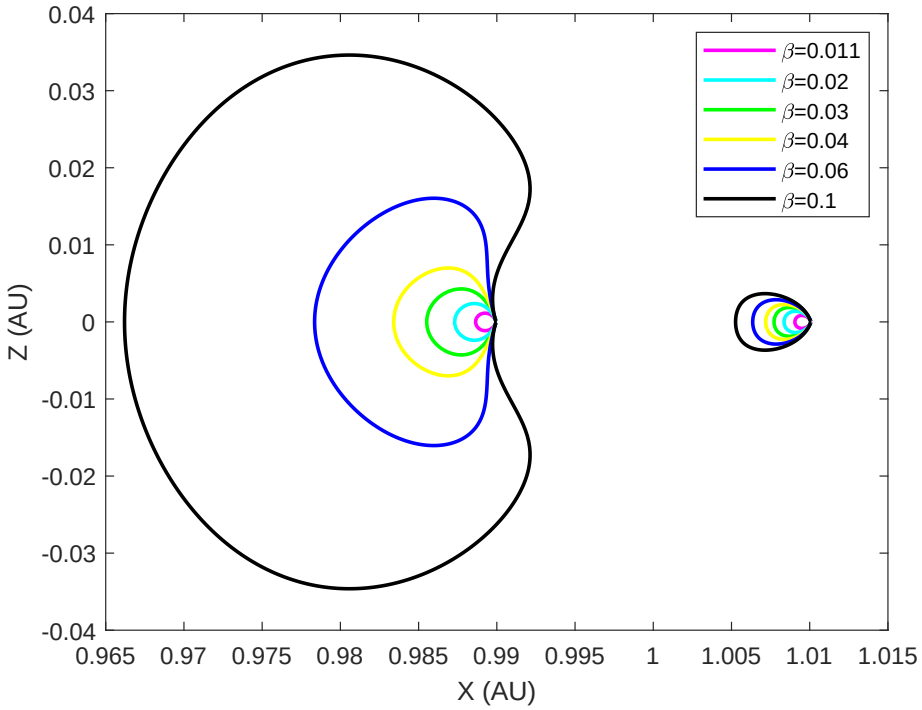

Figure 3.6: Section of the level surfaces in the near Earth region normal to the plane of the system, for $\beta = [0.011, 0.02, 0.03, 0.04, 0.06, 0.1]$. Non-ideal Solar Sail case

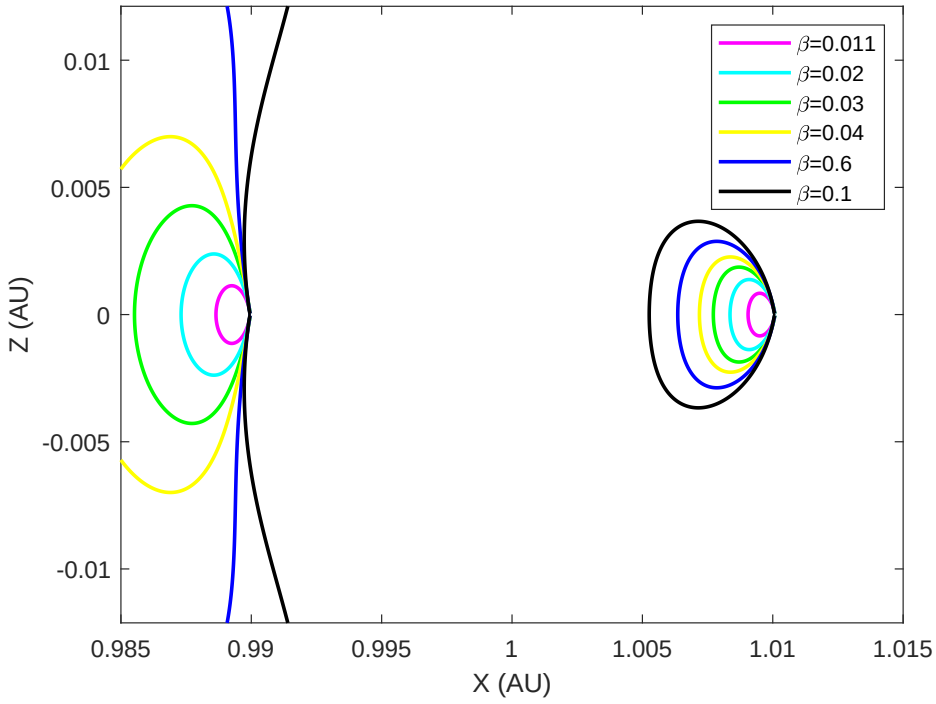

Figure 3.7: Particular of the section of the level surfaces in the near-Earth region normal to the plane of the system, for $\beta = [0.011, 0.02, 0.03, 0.04, 0.06, 0.1]$. Non-ideal Solar Sail case

naturally possess asymptotic stability, and so it is necessary to implement a control aimed to keep a Solar Sail in its equilibrium position of the pulsating rotating frame.

Here it will not be proved theoretically, but experimentally by some tests. That is, a ran-

dom point will be taken and the stability of the system will be analysed at that point. This empirical check is reinforced by reference [43].

The general vector dynamics equation to analyse is given by Eq. 3.18. It will be assumed that the sail is stationary on some level surface at a point $\mathbf{r_{eq}}$. Then the dynamics equation in a local neighbourhood of $\mathbf{r_{eq}}$ is obtained in the usual manner using an arbitrary perturbation δ, such that $\mathbf{r_{eq}} \rightarrow \mathbf{r_{eq}} + \delta$. Since $\mathbf{r_{eq}}$ is a stationary solution, a variational equation is obtained.

$$\frac{d^2\delta}{dt^2} + 2\Omega \times \frac{d^2\delta}{dt^2} + \nabla U(\mathbf{r_{eq}} + \delta) - \mathbf{a}(\mathbf{r_{eq}} + \delta) \tag{3.26}$$

The potential gradient and the solar radiation pressure acceleration may be expanded in trivariate Taylor series about the stationary solution to first order as

$$\nabla U(\mathbf{r_{eq}} + \delta) = \nabla U(\mathbf{r_{eq}}) + \frac{\partial}{\partial \mathbf{r}} \nabla U(\mathbf{r}) \bigg|_{\mathbf{r}=\mathbf{r_{eq}}} \delta + o(|\delta|^2) \tag{3.27a}$$

$$\mathbf{a}(\mathbf{r_{eq}} + \delta) = \mathbf{a}(\mathbf{r_{eq}}) + \frac{\partial}{\partial \mathbf{r}} \mathbf{a}(\mathbf{r}) \bigg|_{\mathbf{r}=\mathbf{r_{eq}}} \delta + o(|\delta|^2) \tag{3.27b}$$

Then, since $\nabla U(\mathbf{r_{eq}}) = \mathbf{a}(\mathbf{r_{eq}})$ for a stationary solution, a linear variational equation is obtained [43]

$$\frac{d^2\delta}{dt^2} + \mathbf{S}\frac{d^2\delta}{dt^2} + (\mathbf{A_U} - \mathbf{A_a})\delta = 0 \tag{3.28}$$

where $\mathbf{A_U}$ and $\mathbf{A_a}$, the gravity and radiation gradient tensors and the skew symmetric gyroscopic matrix $\mathbf{S}$ are given by

$$\mathbf{S} = \begin{bmatrix} 0 & -2 & 0 \\ 2 & 0 & 0 \\ 0 & 0 & 0 \end{bmatrix}, \qquad \begin{aligned} \mathbf{A_U} = \{U_{ij}\},\ \mathbf{A_a} = \{a_{ij}\} \\ (i,j) \in (x,y,z) \end{aligned} \tag{3.29}$$

where U_{ij} is the (i,j) partial derivative of the potential with respect to the Cartesian axes and a_{ij} is the jth derivative of the jth component of the solar radiation pressure acceleration.

In order to investigate easily the stability of linearised system, a state space representation of the dynamics has been implemented.

Starting from the linearised dynamics equation (Eq. 3.27), and substituting δ with $\delta\mathbf{x}$, the system in *state space* form can be expressed as

$$\delta\dot{\mathbf{x}} = \mathbf{A}\delta\mathbf{x} \tag{3.30}$$

where $\mathbf{A}$ is the 6×6 Jacobian matrix composed by

$$\mathbf{A} = \begin{bmatrix} 0 & \mathbf{I} \\ \mathbf{A_u} + \mathbf{A_a} & -\mathbf{S} \end{bmatrix} \tag{3.31}$$

The second step of the analysis, has been to choose one equilibrium point, both for ideal and non-ideal case. They have not been selected in a completely random way, because we would avoid states which could generate singularities problems, such as point with γ and δ equal to 0. Therefore, the designed points were chosen far from x axis and they are characterized by following parameters: Once the state space representation has been set

Parameter	Value
γ	0.51730
δ	0
β	0.02
Position r_{eq}	[0.988503049085796; 0; 0.00264908459384856] AU

Table 3.1: Equilibrium point chosen for stability analysis at ideal case

Parameter	Value
γ	0.51730
δ	0
β	0.011
ρ	0.91
Positionr_{eq}	[[0.989173986828632; 0; 0.00112441672663063] AU

Table 3.2: Equilibrium point chosen for stability analysis at non-ideal case

and the points evaluated, the equilibrium stability could be analysed. Matlab® function *eig*, which returns a vector containing the eigenvalues, was applied to the matrix $\mathbf{A}$ of Eq. 3.31. The components of matrices $\mathbf{A_U}$ and $\mathbf{A_a}$ have been computed two times, considering both acceleration formulas presented in Chapter 2. Therefore the stability check has been done for both the dynamics.

Stability analysis for the ideal Solar Sail

Firstly, the Jacobian of pseudo-potential function U has been computed, in order to obtain matrix $\mathbf{A_U}$:

$$\mathbf{A_U} = \begin{bmatrix} U_{xx} & 0 & U_{xz} \\ 0 & U_{yy} & 0 \\ U_{zx} & 0 & U_{zz} \end{bmatrix} \tag{3.32}$$

where u_{ij} are the second partial derivatives of U evaluated at the equilibrium point (x_0, y_0, z_0). The complete set is in Appendix A. Here after the components of matrix in Eq. 3.32,

which are different from zero.

$$U_{xx} = 1 + \frac{3\mu(x-1+mu)^2}{r_2^5} - \frac{\mu}{r_2^3} + \frac{3(1-mu)(\mu+x)^2}{r_1^5} - \frac{1-\mu}{r_1^3} \tag{3.33a}$$

$$U_{xz} = \frac{3\mu(x-1+\mu)z}{r_2^5} + \frac{3(1-\mu)(\mu+x)z}{r_1^5} \tag{3.33b}$$

$$U_{yy} = 1 + \frac{3\mu y^2}{r_2^5} - \frac{\mu}{r_2^3} + \frac{3(1-\mu)y^2}{r_1^5} - \frac{1-\mu}{r_1^3} \tag{3.33c}$$

$$U_{zz} = \tag{3.33d}$$

recalling $r_1 = \sqrt{(X+\mu)^2+Y^2+Z^2}$ and $r_2 = \sqrt{(X-1+\rho)^2+Y^2+Z^2}$.
Substituting the value of Tab. 2.1 it results that:

$$\mathbf{A_U} = \begin{bmatrix} 6.51171 & 0 & -1.21323 \\ 0 & -1.89657 & 0 \\ -1.21323 & a_{zy} & -2.61514 \end{bmatrix} \tag{3.34}$$

Then, the matrix $\mathbf{A_a}$ is evaluated considering $\mathbf{a}$ from Eq. 2.15 and computing the Jacobian of acceleration function at equilibrium point (x_0, y_0, z_0)

$$\mathbf{A_a} = \begin{bmatrix} a_{xx} & a_{xy} & a_{xz} \\ a_{yx} & a_{yy} & a_{yz} \\ a_{zx} & a_{zy} & a_{zz} \end{bmatrix} \tag{3.35}$$

The computation of the partial derivatives for each component of the acceleration vector is shown in the Appendix B. Hereafter the results will be reported:

$$\mathbf{A_a} = \begin{bmatrix} -0.0273137 & 0 & 0.0153482 \\ 0 & 0 & 0 \\ -0.0155413 & 0 & 0.00873305 \end{bmatrix} \tag{3.36}$$

Finally matrix $\mathbf{A}$, has been calculated by summing Eqs. 2.34 and 3.36:

$$\mathbf{A} = \begin{bmatrix} -0.0273137 & 0 & 0.0153482 \\ 0 & 0 & 0 \\ -0.0155413 & 0 & 0.00873305 \end{bmatrix} \tag{3.37}$$

and substituting the obtained matrix in Eq. 3.31 it results that:

$$\mathbf{A_{ideal}} = \begin{bmatrix} 0 & 0 & 0 & 1 & 0 & 0 \\ 0 & 0 & 0 & 0 & 1 & 0 \\ 0 & 0 & 0 & 0 & 0 & 1 \\ 6.4844 & 0.0080 & -1.1979 & 0 & 2 & 0 \\ 0 & -1.8966 & 0 & -2 & 0 & 0 \\ -1.2288 & 0 & -2.6064 & 0 & 0 & 0 \end{bmatrix} \tag{3.38}$$

Once all the "ingredients" to apply the *eig* function have been collected, it is possible to check the stability of that point. Then the resultant eigenvalues vector is evaluated in order to apply **LTI** system stability theory [5]. One of the eigenvalues summarized in Tab. 3.3 (λ_2) presents positive real part, which is symptom of system instability.

Eigenvalues	
λ_1	$-1.9988 + 0.0000i$
λ_2	$+1.9988 + 0.0000i$
λ_3	$+1.8898i$
λ_4	$-1.8898i$
λ_5	$+1.5628i$
λ_6	$-1.5628i$

Table 3.3: Eigenvalues of linearised ideal dynamic system

Stability analysis for non-ideal Solar Sail

For non-ideal case a parallel analysis was carried out. First of all, computing Jacobian of pseudo-potential function U, it results that:

$$\mathbf{A_U} = \begin{bmatrix} 7.73177 & 0 & -0.727469 \\ 0 & -2.40386 & 0 \\ -0.727469 & 0 & -3.32791 \end{bmatrix} \tag{3.39}$$

After that, Jacobian of $\mathbf{a_{sail}}$ is computed again, which this time is equivalent to Eq. 2.34. The components of acceleration Jacobian are the partial derivatives of $\mathbf{a_{sail}}$, as follows:

$$\mathbf{A_a} = \begin{bmatrix} -0.0144699 & 0.00798037 & -0.0000328964 \\ -0.00772743 & 0.00484138 & -0.0000175679 \\ 0 & 0 & 0.000444503 \end{bmatrix} \tag{3.40}$$

Even in this case, matrix $\mathbf{A}$, is computed by summing matrices of Eq. 3.39 and Eq. 3.40. Therefore by replacing these values in Eq. 3.31, it derives state matrix as follows:

$$\mathbf{A_{non\,ideal}} = \begin{bmatrix} 0 & 0 & 0 & 1 & 0 & 0 \\ 0 & 0 & 0 & 0 & 1 & 0 \\ 0 & 0 & 0 & 0 & 0 & 1 \\ 7.7173 & 0.0080 & -0.7275 & 0 & 2 & 0 \\ -0.0077 & -2.3990 & -0.0000 & -2 & 0 & 0 \\ -0.7275 & 0 & -3.3275 & 0 & 0 & 0 \end{bmatrix} \tag{3.41}$$

The stability analysis is done looking at eigenvalues:

Eigenvalues	
λ_1	-2.2525
λ_2	$+2.2490$
λ_3	$0.0015 + 1.9642i$
λ_4	$0.0015 - 1.9642i$
λ_5	$0.0003 + 1.7936i$
λ_6	$0.0003 - 1.7936i$

Table 3.4: Eigenvalues of linearised non-ideal dynamic system

Comparing Tab. 3.3 with Tab. 3.4, it is possible to appreciate the differences between ideal and non-ideal Solar Sail dynamics. Tab. 3.4 shows that all the eigenvalues except one, have positive real part. It means that the non-ideal solar sail model is intrinsically more unstable than the ideal one. And it requires a more robust control action.

Chapter 4

Linear Feedback controls

Once clarified that the Solar Sail artificial Libration points do not possess asymptotic stability, it is straightforward to think about implementing a control system related to them.

4.1 Control design principles

4.1.1 Feedback control

It worth to mention some theories on the feedback control system, in order to understand the operating principle of our control algorithm.
In the analysis and design of a feedback control system, the mathematical model of the latter (in this case, the system developed in Chapter 3) is dealt with, not with the actual physical system. Consequently, special care must be taken regarding uncertainties in the mathematical model because no mathematical model of a physical system is exact. A closed-loop feedback control system maintains a specified relationship between the actual output and the desired output or the reference input by using the difference of these outputs, called the error signal (see scheme in Fig. 4.1). In a feedback control system, a controller also called *compensator* or *control logic* is designed to manipulate or process the error signal so that certain specifications are satisfied in the presence of system disturbances. In the study of control systems, the dynamic behaviour or characteristics of the system under consideration is analysed. In the design or synthesis, it is important to devise a feedback control system that will achieve the desired system characteristics.

4.1.2 Lqr theory

In the design of linear controllers, a widely used technique, called optimal **linear quadratic regulator**, has been exploited. Thereafter, its theoretical principles [33] and how this method has been fitted to our problem will be explained.

A prerequisite to LQR is ***controllability***. Considering a mathematical model of the form

$$\dot{\mathbf{q}} = \mathbf{A}\mathbf{q} + \mathbf{B}\mathbf{u}$$

controllability describes the ability of the actuator $\mathbf{u}$ to influence the state $\mathbf{q}$.
The following discussion assumes we deal with a linear model. Such a system is said to be ***controllable*** on the time interval $[0,\ T]$ if given any initial state $\mathbf{q}_0$, and final state $\mathbf{q}_f$, there exists a control $\mathbf{u}$ that will steer from the initial state to the final state. Controllability is a property that is easy to test [48]: a necessary and sufficient condition is that the controllability matrix

$$\mathbf{C} = \begin{bmatrix} \mathbf{B} & \mathbf{AB} & \mathbf{A}^2\mathbf{B} & \ldots & \mathbf{A}^{\mathbf{n}-1}\mathbf{B} \end{bmatrix} \tag{4.1}$$

have full rank $(rank = n)$. Where, n is the dimension of the state space, so $\mathbf{q}$ is a vector of length n and $\mathbf{A}$ is a $n \times n$ matrix.
Returning to linear quadratic regulator (LQR) problem, it is stated as follows: find the control $u(t)$ to minimize the quadratic objective function

$$J(\mathbf{f}) = \int_0^\infty \mathbf{q}^\mathbf{T}\mathbf{Q}\mathbf{q} + \mathbf{u}^\mathbf{T}\mathbf{R}\mathbf{u}\,dt \tag{4.2}$$

subject to the state dynamics

$$\dot{\mathbf{q}}(t) = \mathbf{A}\mathbf{q}(t) + \mathbf{B}\mathbf{u}(t) \tag{4.3}$$

The matrices $\mathbf{Q}$ and $\mathbf{R}$ are *state* and *control weighting operators* and may be chosen to reach the desired properties of the closed-loop system.
It is necessary that $\mathbf{Q}$ is non-negative definite and $\mathbf{R}$ is positive definite, for the LQR problem to have a solution. Also, $(A,\ B)$ must be controllable. This problem is called linear because the dynamic constraints are linear, and quadratic since the objective function is quadratic. The controller is called a regulator because the optimal control will drive the state error to zero.
The solution to this problem can be obtained by applying the necessary conditions of the calculus of variations. One finds that under the above assumptions, the solution to this problem is given by the feedback control

$$\mathbf{u}(t) = -\mathbf{K}\mathbf{q}(t), \quad \mathbf{K} = \mathbf{R}^{-1}\mathbf{B}^T\mathbf{P}$$

where the matrix $\mathbf{K}$ is called the feedback gain matrix, and the symmetric matrix $\mathbf{P}$ is the solution of the **algebraic Riccati equation**

$$\mathbf{A}^T\mathbf{P} + \mathbf{P}\mathbf{A} - \mathbf{P}\mathbf{B}\mathbf{R}^{-1}\mathbf{B}^T\mathbf{P} + \mathbf{Q} = 0. \tag{4.4}$$

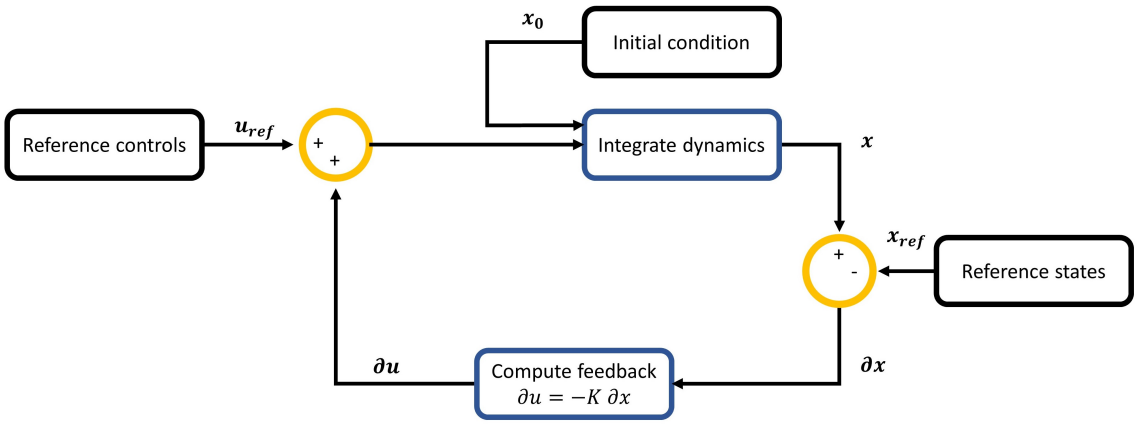

Figure 4.1: Scheme of feed-back linear control applied to Solar Sail dynamics

This is a quadratic matrix equation and has many solutions, but only one positive definite solution, which is the one desired. Equations of this type may be solved easily, for instance using the ®Matlab command *lqr*.
The LQR is designed for linear systems, therefore all the computation has been done starting from Solar Sail linearised dynamics Eq. 3.28, which provides the matrix **A** for Eq. 4.3. To add the control action to the system, the matrix **B**, denominated *input matrix* in the state-space formulation, has been calculated case-by-case. Similarly to the state matrix, **B** corresponds to the Jacobian of the system, derived for input variables, evaluated at the equilibrium point and it results different for each control algorithms because they differ by input variables.
All *LQR feedback control* developed and presented in this Chapter take the same scheme (see Fig 4.1). *Matrix* **K** will be different for each model, because it depends on *input matrix*. Also the *Reference controls* will be different in every case, it represents the value of the input variables at equilibrium. *Reference states* will be always the equilibrium point coordinates in CRTBP.

4.1.3 Introduction to actuation mechanisms

In this research, we take advantage of these mentioned analyses, to develop controls aimed to stabilize the equilibrium points. Four different linear controls are implemented exploiting LQR theory, starting from the linearised SSCRTBP (Solar Sail Circular Restricted Three-Body Problem) dynamic system, after ensuring that each of them was controllable. Designed control models are based on Solar Sail peculiar actuation mechanism, to exploit the sail-craft potentialities, without introducing external mechanisms. The first control model relies on sail orientation angles, even called *Attitude angles*, which represent the orientation of the solar sail normal vector. As affirmed in previous studies [31], changing the attitude means changing the thrust given by SRP. The second control scheme includes

orientation of attitude angles coupled with the tuning of lightness number β as in [23]. It means to have the Solar Sail with heliogyro configuration, which allows changing the area hit by SRP. The third involves a non-ideal Solar Sail concept and relies on attitude angles orientation but this time coupled with a variable surface reflectivity distribution of the sail, which allows the SRP force modulation. The last model is a novelty presented in this research. The station-keeping control has been realized excluding the attitude angles, and combining the potentiality of heliogyro configuration, to change the area surface subject to SRP, with a continuous RCD as in Ref. [13]. In the following sections, the feed-back theory will be presented with a special focus on LQR, which is at the basis of all designed algorithms. After that, the Solar Sail variables employed in the actuation mechanism will be summarised. Finally, the implemented algorithms and their respective results will be shown, comparing them by following some specific parameters.

4.2 Control performance metrics

The results of the four control methods will be examined and compared, taking into account specific parameters, which are:

Attraction radius

This parameter refers to the maximum distance from the equilibrium point in which the Solar Sail can be injected such that it returns to the equilibrium position, thanks to controlling action. This maximum distance is just a radius from the point of equilibrium. Therefore, the solar sail can be injected at this distance into all three spatial coordinates. From this it derives that attraction area will be a sphere around a steady solution.
The attraction area radius has been established empirically, conducting several simulations in which the injection error was increased time by time.

Steady state error

SSE (Steady state error) is a property of the input/output response of a linear system. If the desired value of the output for a system is r and the actual output is $y(t)$, the steady-state error is defined as:

$$e_{ss} = \lim_{t \to \infty} r - y(t)$$

In this case, the desired state r is the equilibrium point. As $\lim_{t \to \infty}$ to infinity is considered the instant when the system dynamics reaches a steady state (stops oscillating). In that instant $y(t)$ is recorder and the error is calculated. A powerful control model is characterized by a small SSE.

Variables rate of change

In order to obtain feasible controllers which respect the limit of actuation mechanism, it is necessary to impose a rate limiter on input variables. This requirement involves the attitude angles, which physical constraint is imposed with a rate of deflection of maximum $1deg/h$. The attitude angles rate of change constitutes a performance parameter because the smaller is this value, the higher is the feasibility of the actuation mechanism.

Convergence rate

Finally, the convergence rate represents the measure of how quickly control algorithm can bring the system to the desired state.
In further computations, the convergence rate evaluated with the ratio between is the time spent to reach the steady-state and the path necessary to reach it. A system is in a steady state if the variables (called state variables) which define the behaviour of the system are unchanging in time. It has been assumed that the state exactly converge when it results

$$\frac{d\mathbf{x}}{dt} = 0, \qquad \text{for all } t.$$

being $\mathbf{x}$ the state vector.

4.3 Control algorithms implementation

In this section, the whole procedure for the implementation of linear control algorithms will be reported. It will be explained how the state-space model for each of the four control typologies has been developed, linearising the dynamics of the system about equilibrium points values.
The state matrix $\mathbf{A}$ computation follows the same procedure of Section 3.5, and it is needed to complete the model by deriving the *input matrix* $\mathbf{B}$. Similarly to the state matrix, it corresponds to Jacobian of dynamic equations, but this time, about input variables and so it will be different for each control algorithm. $\mathbf{B}$ matrix is composed as follow

$$\mathbf{B} = \begin{bmatrix} \mathbf{B}_0 \\ \mathbf{B_J} \end{bmatrix} \tag{4.5}$$

where $\mathbf{B}_0$ is a $3 \times n$ matrix of zeros, and B_j a $3 \times n$ matrix of dynamics partial derivative with respect to actuation variables:

$$\mathbf{B_j} = \frac{\partial f(\mathbf{q}, \mathbf{u})}{\partial \mathbf{u}} \tag{4.6}$$

with f equivalent to Solar Sail dynamics equation vector:

$$f = a_{sail} - \nabla U \tag{4.7}$$

and $\mathbf{u}$ the $n \times 1$ linearised control vector.
As the second step, it will be explained how the LQR theory was applied for the calculation of gain matrix $\mathbf{K}$. It has been necessary to set up the state and control weighting operators $\mathbf{Q}$ and $\mathbf{R}$, thus several values were tested, proceeding with the tuning process and finally, those that corresponded to the best control performances were chosen. Once the state space and weighted matrices are computed, $\mathbf{K}$ is derived by using the ®Matlab function *lqr* as $K = lqr(A,B,Q,R)$. Therefore the dynamic system state space model is updated, recalling from Section 4.2 that $\mathbf{u} = -\mathbf{Kq}$, obtaining the same general form for all the control algorithm:

$$\dot{\mathbf{q}} = (\mathbf{A} - \mathbf{BK})\mathbf{q} \tag{4.8}$$

The last step is then a new check on the stability of the linearised system, considering this time the controlled version highlighted in Eq. 4.8.

4.3.1 Attitude angles

First designed control has been called *Attitude angles* because its actuation mechanism is based only on the attitude angles (γ and δ) orientation. The control will be tested on the same unstable equilibrium point used in Chapter 3, the point of Tab. 3.1. This point, characteristic of the ideal solar sail model, has been chosen for the sake of simplicity.

State space

Concerning state space realization, state matrix $\mathbf{A}$ is equivalent to Eq. 3.38. The control vector is $\mathbf{u} = [\gamma\ \delta]$ and therefore *input matrix* $\mathbf{B}$, has composed by $\mathbf{B}_0$ equivalent to a zeros matrix of 3×2 dimensions, and $\mathbf{B_j}$ as follows

$$\mathbf{B_j} = \begin{bmatrix} \frac{\partial f_x}{\partial \gamma} & \frac{\partial f_x}{\partial \delta} \\ \frac{\partial f_y}{\partial \gamma} & \frac{\partial f_y}{\partial \delta} \\ \frac{\partial f_z}{\partial \gamma} & \frac{\partial f_z}{\partial \delta} \end{bmatrix} \tag{4.9}$$

where f is equivalent to Eq. 4.7 with a_{sail} ideal Solar Sail acceleration, i.e. Eq. 2.15. By replacing derivatives results in the state matrices, it follows:

$$\mathbf{A} = \begin{bmatrix} 0 & 0 & 0 & 1 & 0 & 0 \\ 0 & 0 & 0 & 0 & 1 & 0 \\ 0 & 0 & 0 & 0 & 0 & 1 \\ 6.4844 & 0 & -1.1979 & 0 & 2 & 0 \\ 0 & -1.8966 & 0 & -2.0000 & 0 & 0 \\ -1.2288 & 0 & -2.6064 & 0 & 0 & 0 \end{bmatrix}. \tag{4.10}$$

$$\mathbf{B} = \begin{bmatrix} 0 & 0 \\ 0 & 0 \\ 0 & 0 \\ -0.0229 & 0 \\ 0 & 0.0135 \\ 0.0048 & 0 \end{bmatrix} \tag{4.11}$$

LQR and Stability check

Once the state space has been built, it is necessary to establish that the system in question is controllable. This check was done with the help of *ctrb* ®Matlab function, which returns the controllability matrix ($\mathbf{C}$) of the system described by matrices $\mathbf{A}, \mathbf{B}$. Once computed $\mathbf{C}$, its rank is evaluated easily, by using *rank* ®Matlab function. It results equal to 6 which is the maximum value, therefore this system is controllable.
Now it is possible to apply LQR to the model. The designed $\mathbf{Q}$ and $\mathbf{R}$ are:

$$\mathbf{Q} = \mathbf{I}_{6\times 6}, \qquad \mathbf{R} = \begin{bmatrix} 10 & 0 \\ 0 & 100 \end{bmatrix} \tag{4.12}$$

where $\mathbf{I}$ identify $n-by-n$ identity matrix with 1 on the main diagonal and 0 elsewhere. These weights where chosen to minimize steady state error and reduce oscillations. At last, we could compute the LQR control gain matrix $\mathbf{K}$, which results as

$$\mathbf{K}_1 \begin{bmatrix} -494.0767 & 93.1442 & 57.4872 & -155.4398 & -88.3218 & 30.0988 \\ 186.3153 & -34.7723 & -19.8945 & 50.6739 & 46.6616 & -6.1169 \end{bmatrix} \tag{4.13}$$

Adding this feed back control to the Solar Sail dynamic systems, we get the state space of the controlled system. Therefore, it is possible to check the power of control in stabilize equilibrium point, recomputing eigenvalues vector of the new system, which has as state matrix $\mathbf{A}_{con} = (\mathbf{A} - \mathbf{BK})$. Again, is applied the *eig* function to $\mathbf{A}_{con}$ and we can appreciate that all the eigenvalues have a negative real part, so the system is stabilized.

Eigenvalues	
λ_1	$-2.0578+0.0000i$
λ_2	$-1.9428+0.0000i$
λ_3	$-0.1024+1.8839i$
λ_4	$-0.1024-1.8839i$
λ_5	$-0.0650+1.5659i$

Table 4.1: Eigenvalues of dynamic system controlled by Attitude angles linear control

4.3.2 Attitude angles and Heliogyro Configuration

The second control model, relies on two actuation mechanism: attitude angles orientation coupled with heliogyro configuration. As previously explained, this particular configuration allows to change the parameter β as needed. In the design this is evaluated as a continuous variable, which is a feasible assumption because the β variation derives from the possibility of pitching the heliogyro blades, an operation that can been done in a continuous mode [27].

State space

The state space formulation must be updated with respect to the previous case, because this time a linearised control with respect to the angles of attitude and lightness number β is analysed. Since the control variables do not include the reflection coefficient, the Solar Sail dynamics represented by the equations of motion with the ideal acceleration will be considered.
To simplify the computation, the equilibrium point of Tab. 3.1, as a reference point to which linearise the system will be employed again. Therefore, the matrix $\mathbf{A}$ (i.e. state matrix) is equivalent to that previously compute in Eq 3.38. This time the control vector is
$\mathbf{u} = [\gamma\ \delta\ \beta]$, which leads to an input matrix $\mathbf{B}$ of the form $\mathbf{B} = [\mathbf{B_0}; \mathbf{B_j}]$ where:

$$\mathbf{B_0} = \begin{bmatrix} 0 & 0 \\ 0 & 0 \\ 0 & 0 \end{bmatrix} \tag{4.14}$$

and

$$\mathbf{B_j} = \begin{bmatrix} \frac{\partial \mathbf{f_x}}{\partial \gamma} & \frac{\partial \mathbf{f_x}}{\partial \delta} & \frac{\partial \mathbf{f_x}}{\partial \beta} \\ \frac{\partial \mathbf{f_y}}{\partial \gamma} & \frac{\partial \mathbf{f_y}}{\partial \delta} & \frac{\partial \mathbf{f_x}}{\partial \beta} \\ \frac{\partial \mathbf{f_z}}{\partial \gamma} & \frac{\partial \mathbf{f_z}}{\partial \delta} & \frac{\partial \mathbf{f_x}}{\partial \beta} \end{bmatrix} \tag{4.15}$$

where f is equivalent to Eq. 4.7, with Solar Sail ideal acceleration. Substituting the derivatives values, the matrices results as follows:

$$\mathbf{B} = \begin{bmatrix} 0 & 0 & 0 \\ 0 & 0 & 0 \\ 0 & 0 & 0 \\ -0.0229 & 0 & 0.6740 \\ 0 & 0.0135 & 0 \\ 0.0048 & 0 & 0.3835 \end{bmatrix} \tag{4.16}$$

LQR and stability check

Controllability test gives as result that the $\mathbf{C}$ matrix has a maximum rank ($rank = 6$). Therefore it is possible to develop a new LQR controller, with attitude angle orientations and heliogyro configuration as actuation mechanisms. The weighting matrices are subjected to tuning process, and the following have been selected, in order to increase convergence rate:

$$\mathbf{Q} = \mathbf{I}_{6\times 6}, \qquad \mathbf{R} = \begin{bmatrix} 1000 & 0 & 0 \\ 0 & 10 & 0 \\ 0 & 0 & 0.00001 \end{bmatrix} \tag{4.17}$$

Finally, the LQR control gain matrix $\mathbf{K}$ can be computed, which results as

$$\mathbf{K} = \begin{bmatrix} -8.109\times 10^{-5} & -4.626\times 10^{-5} & -6.814\times 10^{-6} & 2.646\times 10^{-5} & 3.178\times 10^{-5} & 4.621\times 10^{-5} \\ 0.023 & -0.0024 & 0.0067 & 0.0014 & 0.0122 & -0.0024 \\ 2.138\times 10^{3} & -882.61 & 491.54 & 461.34 & 384.54 & -159.66 \end{bmatrix} \tag{4.18}$$

With new matrix $\mathbf{K}$, a new state space model of the Solar Sail controlled dynamics is obtained, which this time is augmented by attitude and β control All that must be done is check for stability, computing the eigenvalues of new controlled state matrix:
$\mathbf{A}_{con} = (\mathbf{A} - \mathbf{BK})$.

4.3.3 Attitude angles and Reflectivity Control Device

The third implemented model, on the other hand, is addressed to non ideal solar sail. It includes as control variable the coefficient of specular reflectivity ρ_s (from now on renamed *rho*) together with attitude angles γ and δ. Therefore, it is based on two actuation mechanisms: attitude angles orientation and a continuous RCD. Differently from the previous models, this one has been developed starting from solar sail dynamics that includes non-ideal acceleration, and from now on, the simplified acceleration formula of Eq. 2.34 will be considered.

Eigenvalues	
λ_1	$-245.21+0.00i$
λ_2	$-0.14+1.61i$
λ_3	$-0.14-1.61i$
λ_4	$-1.61-0.86i$
λ_5	$-1.61+0.86i$
λ_6	$-1.00+0.00i$

Table 4.2: Eigenvalues of dynamic system controlled by Attitude angles and β linear control

This control aimed to solar sail parking, will be tested on a *non-ideal* unstable equilibrium point, and to simplify the calculation the point of Table 3.2 will be used again, which, in Chapter 3 has been used to check the instability of equilibrium points for non-ideal solar sail model.

State Space

State space model for this scheme, is implemented starting from last results of Section 3.4 where the linearisation matrix from non-ideal Solar Sail dynamics has been derived. Therefore, state matrix $\mathbf{A}$ is equivalent to Eq. 3.41. At this stage, it is clear that each control algorithm differs from the other thanks to the input matrix, which in turn depends on control vector. This time the input vector is $\mathbf{u} = [\gamma\ \delta\ \rho]$ which leads to a matrix $\mathbf{B}$ of the form $\mathbf{B} = [\mathbf{B}_0; \mathbf{B_j}]$ where:

$$\mathbf{B}_0 = \begin{bmatrix} 0 & 0 \\ 0 & 0 \\ 0 & 0 \end{bmatrix} \tag{4.19}$$

and

$$\mathbf{B_j} = \begin{bmatrix} \frac{\partial f_x}{\partial \gamma} & \frac{\partial f_x}{\partial \delta} & \frac{\partial f_x}{\partial \rho} \\ \frac{\partial f_y}{\partial \gamma} & \frac{\partial f_y}{\partial \delta} & \frac{\partial f_x}{\partial \rho} \\ \frac{\partial f_z}{\partial \gamma} & \frac{\partial f_z}{\partial \delta} & \frac{\partial f_x}{\partial \rho} \end{bmatrix} \tag{4.20}$$

Where f is dynamics function of Eq. 4.7, with non-ideal Solar Sail acceleration fro Eq. 2.34. Including numerical values the matrix becomes:

$$\mathbf{B} = \begin{bmatrix} 0 & 0 & 0 \\ 0 & 0 & 0 \\ 0 & 0 & 0 \\ -0.0117 & 1.815\,10^{-5} & 0.0025 \\ 0.0024 & 9.997\,10^{-6} & 0.0042 \\ -2.844\,10^{-7} & 0.0077 & -5.553\,10^{-6} \end{bmatrix} \tag{4.21}$$

LQR and stability check

The system's controllability was also checked for the third control scheme, and even here the test is passed, being the matrix of maximum rank ($rank = 6$). Successively weighting matrices **Q** and **R** have been obtained by trial and error, looking for the values giving maximum convergence rate and minimum rate limit of attitude angles.

$$\mathbf{Q} = \mathbf{I}_{6\times 6}, \qquad \mathbf{R} = \begin{bmatrix} 10 & 0 & 0 \\ 0 & 10 & 0 \\ 0 & 0 & 10 \end{bmatrix} \tag{4.22}$$

The third control matrix **K** is then computed

$$\mathbf{K} = \begin{bmatrix} -1215.798\,10^3 & 225.654 & 68.250 & -351.941 & -211.861 & 30.494 \\ -76.861 & 14.569 & 4.323 & -22.100 & -13.416 & 2.554 \\ 595.491 & -110.536 & -33.724 & 172.025 & 104.364 & -14.968 \end{bmatrix} \tag{4.23}$$

The last step is to check control model power, by checking controlled system stability. So linear system eigenvalues are computed and its real part must be observed (see Tab. 4.3). All eigenvalues real parts are negative, so the control is effective.

Eigenvalues	
λ_1	$-2.2528 + 0.0000i$
λ_2	$-2.2486 + 0.0000i$
λ_3	$-0.0021 + 1.9642i$
λ_4	$-0.0021 - 1.9642i$
λ_5	$-0.0014 + 1.7936i$
λ_6	$-0.0014 - 1.7936i$

Table 4.3: Eigenvalues of dynamic system controlled by Attitude angles and ρ linear control

4.3.4 Heliogyro configuration and Reflectivity Control Device

The latest designed control is a new model, which does not appear among the control methods for Solar Sail. Here are involved, as input variables, the lightness number β and the reflectivity coefficient ρ, excluding the attitude angles. This control has been designed with the objective to avoid attitude angles orientation as a control mechanism. All the systems saw so far required the ability to orient the attitude angles and so displacing the sailcraft, but it should be said that attitude control of a large flexible structure, as Solar Sail, is complex. This new model, instead, involves as actuation mechanism a continuous reflectivity distribution applied on a Solar Sail with heliogyro configuration (see Fig 4.2).

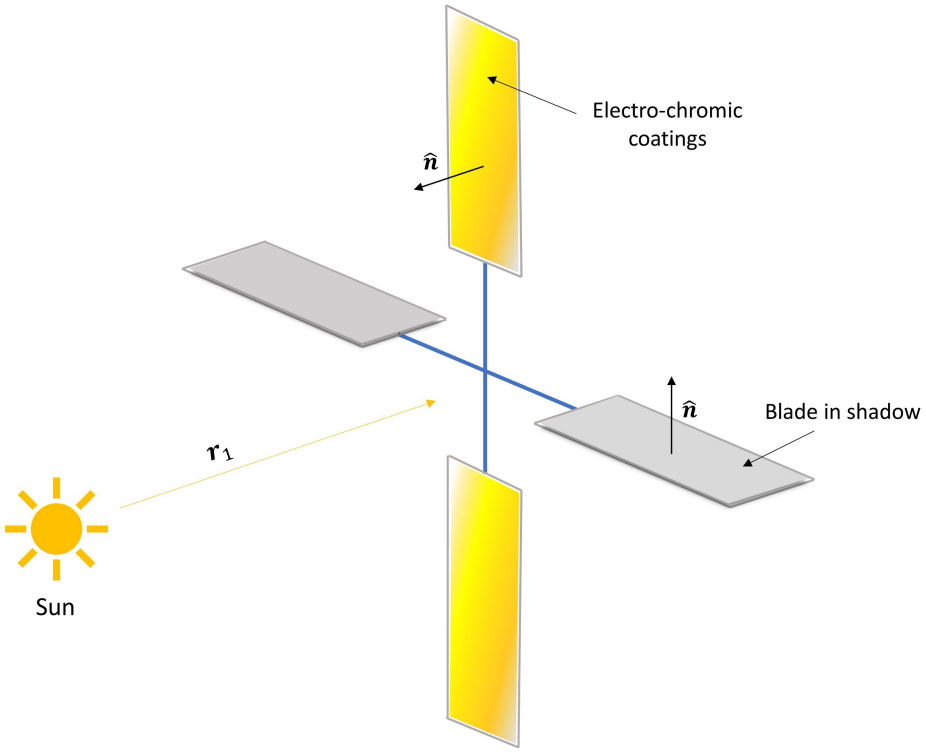

Figure 4.2: Heliogyro and RCD configuration

To approximate a continuous reflectivity distribution, it is ideally assumed that the entire sail area A is covered with electro-chromic coating elements that are able to change their reflectivity in the interval $\rho \in [0,1]$ [13]. Changing the reflectivity of the surface leads to difference SRP magnitude, which is then exploited as a control force. As known, the heliogyro configuration is a particular sail divided into some blades, which are independent in their behaviour. Depending on their orientation, each of them will or will not contribute to the total acceleration of the Solar Sail, which is expressed by the summation:

$$\mathbf{a_{tot}} = \sum_{i=1}^{N} \mathbf{a_i} \tag{4.24}$$

where N is the total number of blades and $\mathbf{a_i}$ is the acceleration produced on each of them:

$$\mathbf{a_i} = \frac{1}{2}\beta_i \frac{(1-\mu)}{|\mathbf{r_i}^2|}[(1-\rho_s)\mathbf{r}_1 + 2\rho_s \cos\alpha_i \mathbf{n_i}] \tag{4.25}$$

If a blade that composes the heliogyro is placed in the direction of the SRP, i.e. with the normal vector $\mathbf{n_i}$ parallel to it, its action is added to the total acceleration. If instead, it is disposed transversely, with the normal vector perpendicular to the SRP, it will not be hit and therefore will not be subjected to the action of the SRP. There can also be an intermediate configuration, in which the SRP vector and the normal to the blade form an angle. The ability to change the are is contained in β parameter.

State space

Since we are dealing with non ideal solar sail model, the control algorithm has been developed starting from an equilibrium point derived with *non-ideal* Solar Sail model, which is the same point employed by third control model (Table 3.2). A particular attention will be directed to controllability analysis of this new system, because it is not intuitive that this is controllable in all three axes. The state matrix **A** is obtained by linearising the Solar Sail dynamics equations around the non-ideal equilibrium point of Tab. 3.2, as follows:

$$\mathbf{A} = \begin{bmatrix} 0 & 0 & 0 & 1 & 0 & 0 \\ 0 & 0 & 0 & 0 & 1 & 0 \\ 0 & 0 & 0 & 0 & 0 & 1 \\ 7.7173 & 0.0080 & -0.7275 & 0 & 2 & 0 \\ -0.0077 & -2.3990 & -0.0000 & -2 & 0 & 0 \\ -0.7275 & 0 & -3.3275 & 0 & 0 & 0 \end{bmatrix} \tag{4.26}$$

Input matrix **B** instead is computed by deriving the Solar Sail dynamics equation with respect to the input vector $\mathbf{u} = [\beta \;\; \rho]$:

$$\mathbf{B_j} = \begin{bmatrix} 0 & 0 \\ 0 & 0 \\ 0 & 0 \\ \frac{\partial f_x}{\partial \beta} & \frac{\partial f_x}{\partial \rho} \\ \frac{\partial f_y}{\partial \beta} & \frac{\partial f_y}{\partial \rho} \\ \frac{\partial f_z}{\partial \beta} & \frac{\partial f_z}{\partial \rho} \end{bmatrix} \tag{4.27}$$

where f is dynamics function of Eq. 4.7, with non-ideal Solar Sail acceleration fro Eq. 2.34. Substituting numerical values in each derivatives, input matrix results:

$$\mathbf{B} = \begin{bmatrix} 0 & 0 \\ 0 & 0 \\ 0 & 0 \\ 0.6506 & 0.0025 \\ 0.3474 & 0.0042 \\ 4.54372\,10^{-5} & -5.5534\,10^{-6} \end{bmatrix} \tag{4.28}$$

LQR and stability check

Controllability matrix **C** even for this new system has maximum rank ($rank = 6$). It is possible to implement last control model with LQR. The weight matrices have been tuned to find the minimum steady state error and the maximum convergence rate, and the

Eigenvalues	
λ_1	$-73.742+0.0000i$
λ_2	$-0.0592+1.8312i$
λ_3	$-0.0592-1.8312i$
λ_4	$-1.0022+0.0000i$
λ_5	$-1.7504+1.0964i$
λ_6	$-1.7504-1.0964i$

Table 4.4: Eigenvalues of the dynamic system controlled by β and ρ linear control

best achievements were found for:

$$\mathbf{Q} = 100\,\mathbf{I}_{6\times 6}, \qquad \mathbf{R} = \begin{bmatrix} 0.0001 & 0 \\ 0 & 1 \end{bmatrix} \tag{4.29}$$

Then, the control gain matrix $\mathbf{K}$ is computed

$$\mathbf{K} = \begin{bmatrix} 249.345 & 7.483 & 94.847 & 152.988 & -60.919 & -112.307 \\ -0.0486 & 0.06002 & 0.2957 & -0.0689 & 0.1328 & -0.1277 \end{bmatrix} \tag{4.30}$$

Finally, analysing the eigenvalues of the linearised controlled system including the last $\mathbf{u}$ and $\mathbf{K}$, it appears that even this new model is effective in Lagrangian point station keeping.

4.4 Simulations

After designing models, simulations were carried out with Simulink®, to test the response of solar sail dynamics (described in Eqs. 3.19, 3.20, 3.21) to these linear control algorithms.
Although several tests have been carried out, controlled dynamics in two cases will be reported. The first one, in which the simulation starts exactly from the equilibrium point and the second one in which the initial condition, will be displaced from equilibrium point of a distance denominated, in this work, as *maximum attraction radius*. This term, refers to the maximum radial distance from the equilibrium point such that control inputs still have authority over the Solar Sail and bring it back to the equilibrium point.
The parameters to be set in the simulations, which are essentially the integration of controlled dynamics for a determined amount of time will briefly be explained.
First of all, the initial condition, which will be equivalent to equilibrium point in simulations without injection error and in the other case, it will be displaced from the equilibrium of a distance equal to the maximum injection error. This parameter is expressed in *Astronomic Unit* (AU) because the equations of dynamics for the solar sails, that will be integrated, are dimensionalised compared to the distance Earth-Sun, which corresponds to the unit of measurement *AU*.
The second parameter to be set is the integration time, which has been changed for each simulation, according to the time taken by the system to converge. Finally, it has not imposed specific indications to the solver, except to the *relative tolerance* which is the largest acceptable solver error, relative to the size of each state during each time step, and the *absolute tolerance* that specify the largest acceptable solver error, as the value of the measured state approaches zero. These parameters have been decreased with respect to the default value, especially for simulations that include the maximum rate change of the angles. The simulations of controlled state dynamics starting from equilibrium points will present an unexpected analysis in terms of convergence rate and steady-state error. This is because, even if the computation of equilibrium points has been done very precisely, the model is subjected to little numerical errors. Therefore, linearising the dynamics around an equilibrium point which is slightly different from the real one, leads the control to bring the state not exactly at is equilibrium in the simulations.

4.4.1 Attitude angles

The first model simulation includes, as input variables, angles γ and δ. It is tested on an ideal solar sail of *lightness number* $\beta = 0.02$, which should be kept at the equilibrium point, equivalent to the point in Tab 3.1.

No injection error

The purpose of this simulation is to analyse the first control model's ability, to stabilize solar sail equilibrium points. The dynamics integration has been set according to the following parameters (see Tab. 4.5). We can then observe the solar sail dynamics in the

Parameter	Values
Initial condition (position)	$[0.988503049085796; 0; 0.00264788459384856;]\ AU$
Initial condition (velocity)	$[0;0;0]\ AU/s$
Integration time	$6\ 10^4\ s$
Tolerance (relative and absolute)	10^{-12}

Table 4.5: Integration parameters of Solar Sail dynamics simulation controlled by Attitude angles, starting from equilibrium point.

following plots, where Fig. 4.3 represents a zoomed view on the controlled behaviour of state coordinates x and y, while Fig. 4.4 includes zoomed view on the third coordinate of the state, z, and the velocities trend in three directions.

In term of deg$/h$ the angles rate of change correspond to $1.45 deg/h$, which is slightly

Parameter	Results
Steady state error	$28\,m$
Convergence rate	$0.628\,m/s$
Angles rate of change	$7\,10^{-6}\,rad/s$

Table 4.6: Results of Solar Sail dynamics simulation controlled by Attitude angles, starting from equilibrium point

higher than the stated rate limit [7].

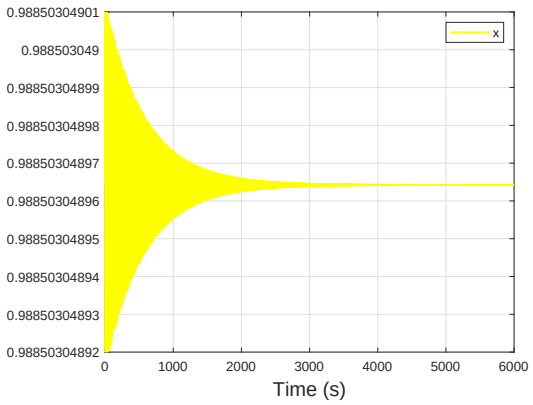

(a) X state coordinate

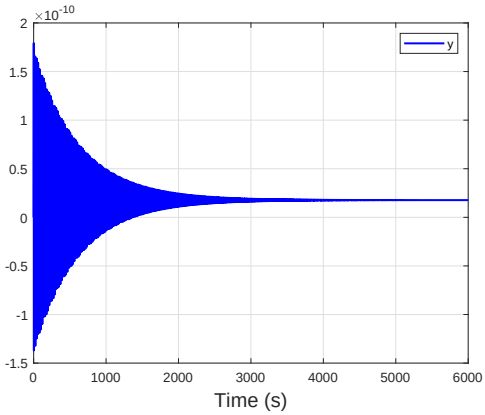

(b) Y state coordinate

Figure 4.3: X and Y state coordinates controlled by attitude angles linear control starting from equilibrium point.

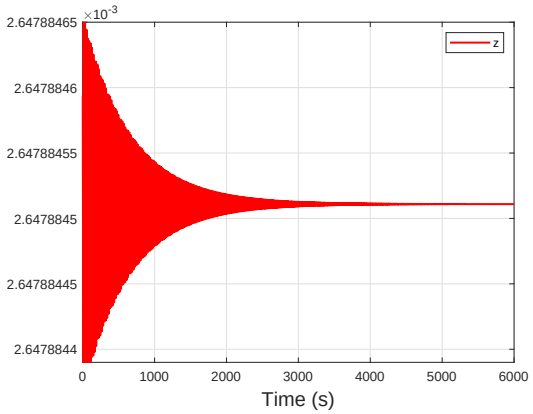

(a) Z state coordinate

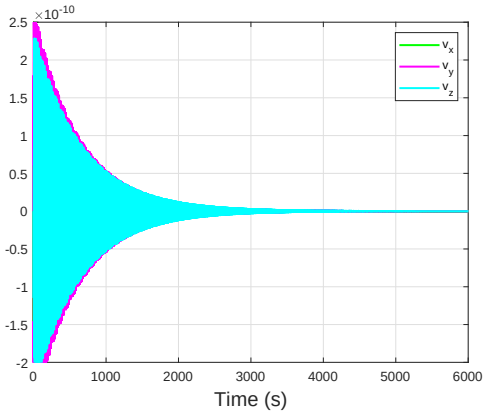

(b) V_x, V_y, V_z state velocities

Figure 4.4: Z state coordinate and velocities in three directions controlled by attitude angles linear control starting from equilibrium point

Maximum injection error

The objective of this second simulation has been to investigate the system dynamics, in case the sail is not exactly at the predetermined equilibrium point. Several tests have been carried out, gradually displacing the sail from the equilibrium point, until the last point where the control still manages to work, bringing the state back to equilibrium, is found. The distance of this last point, is exactly what has been defined as the *Attraction radius* or *maximum injection error*, which here results as $2.5\,km$ equivalent to $1.677\,10^{-8} AU$.
Together with position displacement, we have tested also the maximum velocity at which the sail can be injected into the site. Because, it is more reasonable to think that Solar Sail, once released into space, has an inherited speed.
Therefore, 2^{nd} dynamics integration has been set according to the parameters (see Tab 4.7). where,initial condition is *equilibrium point + maximum injection error* considering

Parameter	Values
Initial condition (position)	$[0.9885030490658; 1.67\,10^{-8}; 2.6479\ \ 10^{-3};]\ AU$
Initial condition (velocity)	$[0.08\,10^{-8}; 0.08\,10^{-8}; 0.08\ \ 10^{-8}]\ AU/s$
Integration time	$1.2\ 10^{4}\,s$
Tolerance (Absolute and Relative)	10^{-12}

Table 4.7: Integration parameters of Solar Sail dynamics simulation controlled by Attitude angles, starting from maximum injection error.

position and velocity.
Reported below the dynamic state plots of solar sail starting from displaced point. In Fig. 4.5 a zoomed view on the controlled behaviour of state coordinates x and y, and in Fig. 4.6 the third coordinate of the state, z, and the velocities trend in all the directions. Therefore, it is possible to derive the results for this second simulation (Tab. 4.8). Another interesting plot, is the one representing Solar Sail dynamics, injected at maximum error and under the control action (Fig. 4.7). We can appreciate the control power,because the solar sail is moved to the desired point.

Parameter	Results
Steady state error	$28\,m$
Convergence rate	$0.0222\,km/s$
Angles rate of change	$7\,10^{-6}\,rad/s$

Table 4.8: Results of Solar Sail dynamics simulation controlled by Attitude angles, starting from maximum injection error.

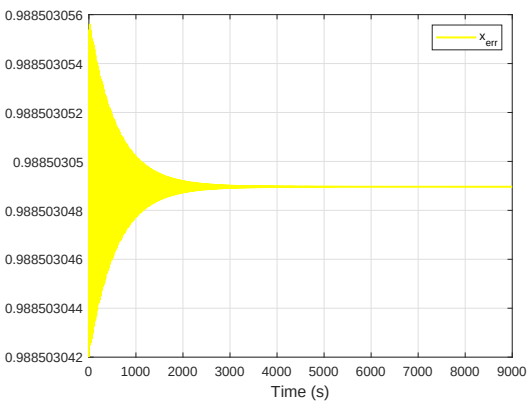

(a) X state coordinate

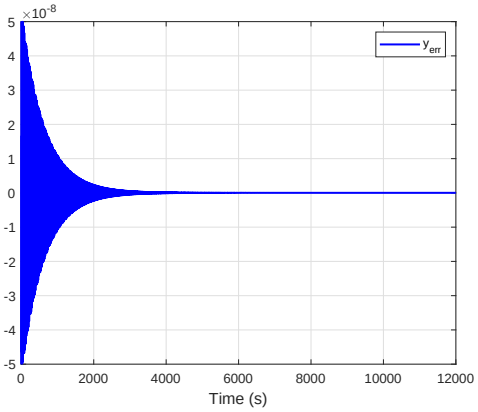

(b) Y state coordinate

Figure 4.5: X and Y coordinates controlled by attitude angles linear control starting from maximum injection error

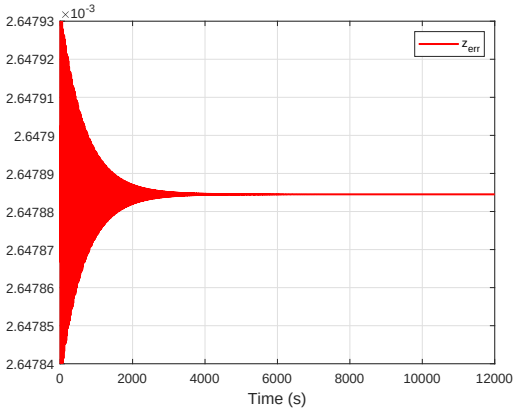

(a) Z state coordinate

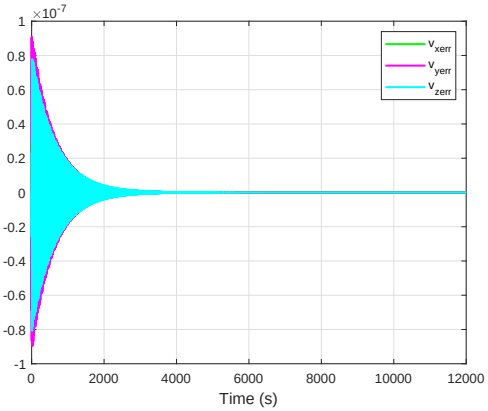

(b) V_x, V_y, V_z state velocities

Figure 4.6: Z state coordinate and velocities in three directions controlled by attitude angles linear control starting from maximum injection error.

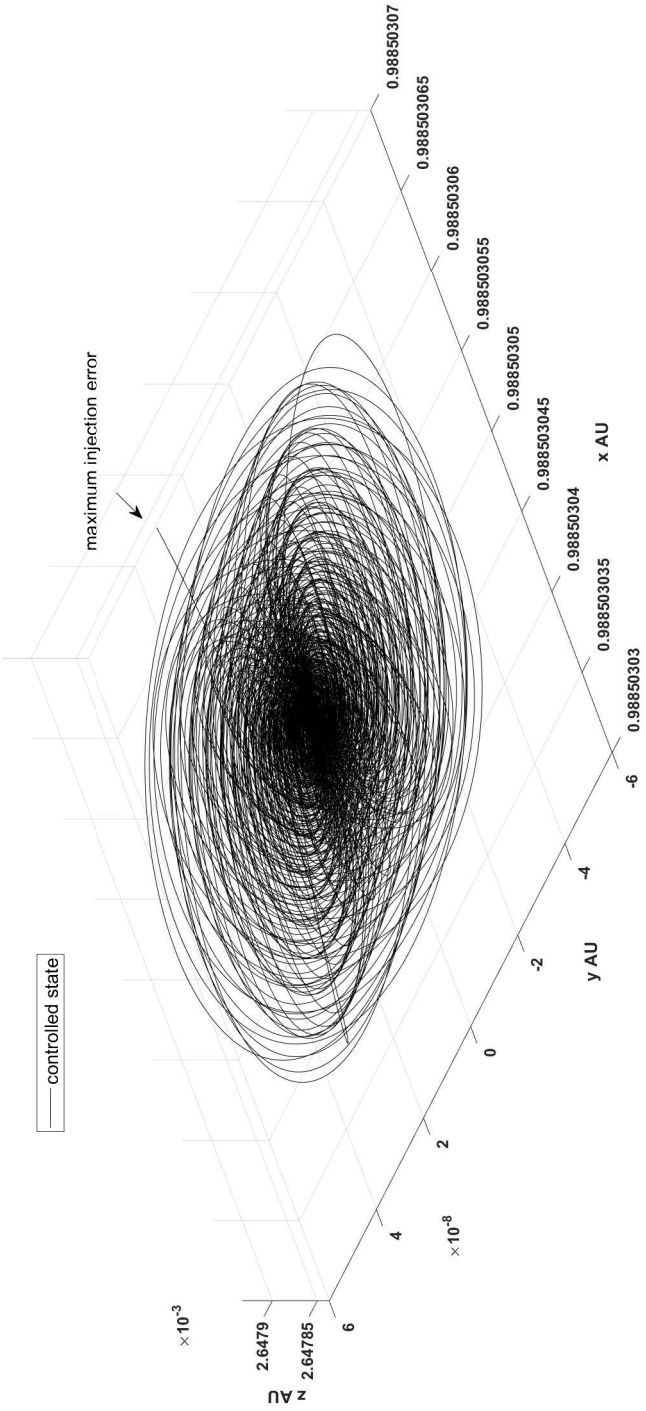

Figure 4.7: State trend subjected to attitude angles linear control starting from maximum injection error

At this point, it is possible to compare the two simulations and it can be noticed that in the absence of injection error the system converges faster. In addition, the dynamics in case of Solar Sail fixed at the point of equilibrium, oscillates with a significantly smaller amplitude about the steady-state, than in the second case. Looking at Fig. 4.5b and Fig. 4.7b, the difference in maximum oscillation amplitude, i.e. from $|2\,10^{-10}|$ to $|5\,10^{-8}|$ can be appreciated.

Attraction area

Finally, it has been elaborated a plot representing the *Attraction area* of linear control based on attitude angles orientation. It has been implemented considering the physical distance from the point of equilibrium, and the corresponding maximum speed at which the sail can be injected so that the control is still effective. In order to obtain these values, were carried 40 *simulations*. Starting from zero injection error, and zero injection velocity, these have been increased little by little to verify the system behaviour. The results have been recorded and used to build the following graph.

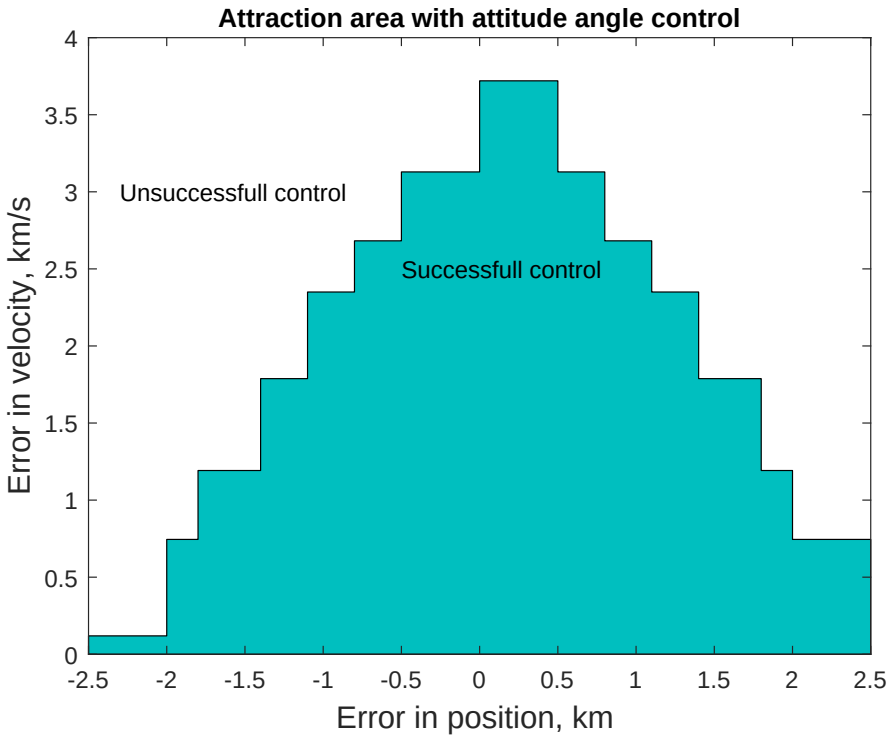

Figure 4.8: Attraction area for attitude angles controlled system

4.4.2 Attitude angles and Heliogyro Configuration

Second simulation realised, has been done using the same solar sail model of before. But this time β is a control variable together with γ and δ.

No injection error

First of all, solar sail dynamics, starting exactly from established equilibrium point will be simulated. The dynamic integration has been set according to the following parameters (see Tab. 4.9).

Parameter	Values
Initial condition (position)	$[0.988503049085796; 0; 0.00264788459384856]\ AU$
Initial condition (velocity)	$[0;0;0]\ AU/s$
Integration time	$10^3\ s$
Tolerance (Relative and Absolute)	10^{-12}

Table 4.9: Integration parameters of Solar Sail dynamics simulation controlled by Attitude angles and Heliogyro configuration, starting from equilibrium.

Simulated state dynamics is visible in Figs. 4.9 and 4.10, where the followed can be observed in order: zoomed view on the controlled behaviour of state coordinates x, y, z, and view of velocities in three directions.
With respect to the first model, the state converges more quickly but is characterized by a lot of noise. The results of this second controlled simulation are summarised in Tab. 4.10.

Parameter	Results
Steady state error	$17.4\,m$
Convergence rate	$0.165\,km/s$
Angles rate of change	$5\,10^{-6}\,rad/s$

Table 4.10: Results of Solar Sail dynamics simulation controlled by Attitude angles and Heliogyro configuration, starting from equilibrium.

Embedding β as input variable allows to lower the variables rate limit, for attitude angles, and that could mean a better applicability of the control.

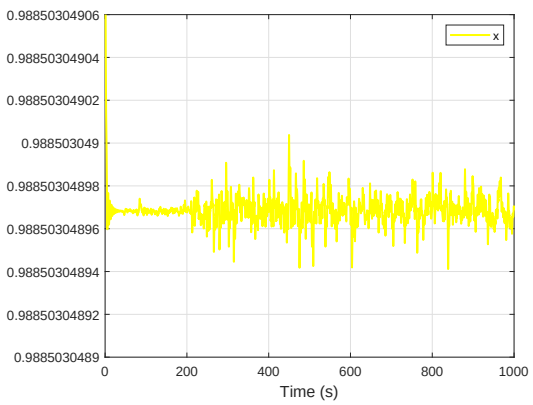

(a) X state coordinate

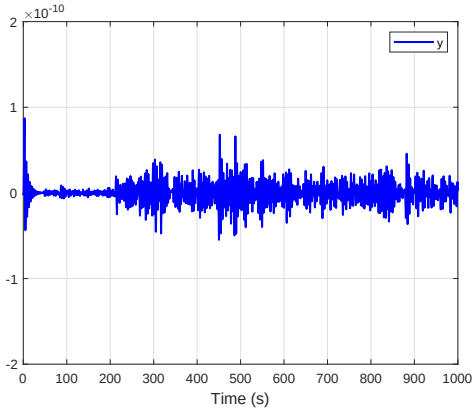

(b) Y state coordinate

Figure 4.9: X and Y state coordinates controlled by attitude angles/heliogyro linear control starting from equilibrium point

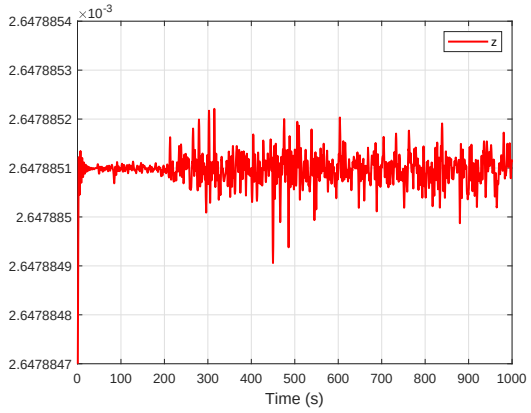

(a) Z state coordinate

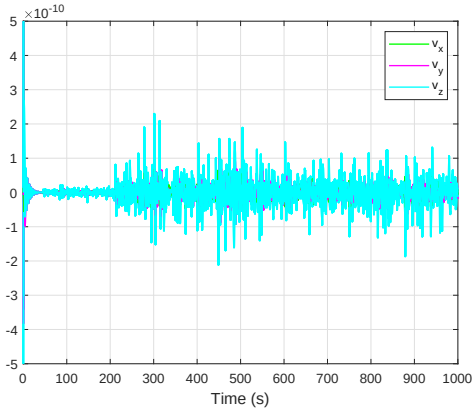

(b) V_x, V_y, V_z state velocities

Figure 4.10: Z anstatd Y state coordinates controlled by attitude angles/heliogyro linear control starting from equilibrium point

Maximum injection error

The second simulation purpose is to understand how far the Solar Sail injection point could be, but still, be driven by the Attitude angles/β model. Therefore, the attraction radius of the system is measured and it results to be very large, i.e. of the order of $10^{-5}AU$. More precisely, integration parameters are in Tab. 4.11.

Parameter	Values
Initial condition (position)	$[0.9875030491; 10^{-5}; 1.648\,10^{-5}]\,AU$
Initial condition (velocity)	$[10^{-5}; 10^{-5}; 10^{-5}]\,AU/s$
Integration time	$10^3\,s$
Tolerance (Relative and Absolute)	10^{-12}

Table 4.11: Integration parameters of Solar Sail dynamics simulation controlled by Attitude angles and Heliogyro configuration, starting from maximum injection error.

We have shown in Figs. 4.11 and 4.12 the states trends, starting from this far injection point. We should have expected, high oscillation amplitudes of the state before reaching the steady point. The results are summarized in Tab (3.12).

Parameter	Results
Steady state error	$17.4\,m$
Convergence rate	$1.6523\,km/s$
Angles rate of change	$5\,10^{-6}\,rad/s$

Table 4.12: Results of Solar Sail dynamics simulation controlled by Attitude angles and Heliogyro configuration, starting from maximum injection error.

It is possible to observe that the convergence rate, in case of error, has increased.
The system dynamics behaviour will be shown in 3-D space, under the control effect (Fig. 4.13). This model is theoretically very valid because it can attract the solar sail to the equilibrium from a position very far from the latter. The maximum injection error is much higher than the first control model. Besides, the maximum injection speed is also of the order 10^{-5}, which is unlikely but gives a lot of margin to the injection speed.
The *Attraction area* plot will be not shown because in this model there is no connection between the injection speed and the maximum injection error, but for each distance from the steady point, the maximum speed to have the system controlled is always $10^{-5}AU/s$.

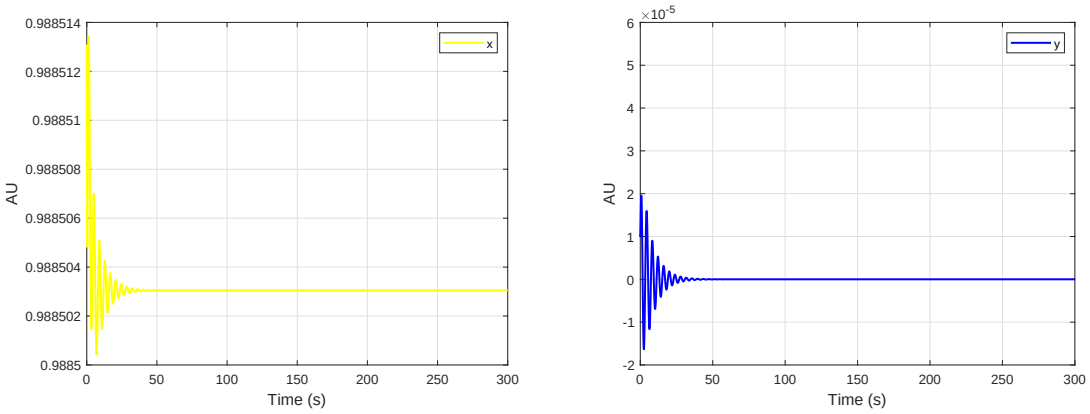

(a) X coordinate

(b) Y coordinate

Figure 4.11: X and Y state coordinates controlled by attitude angles/heliogyro linear control starting from maximum injection error

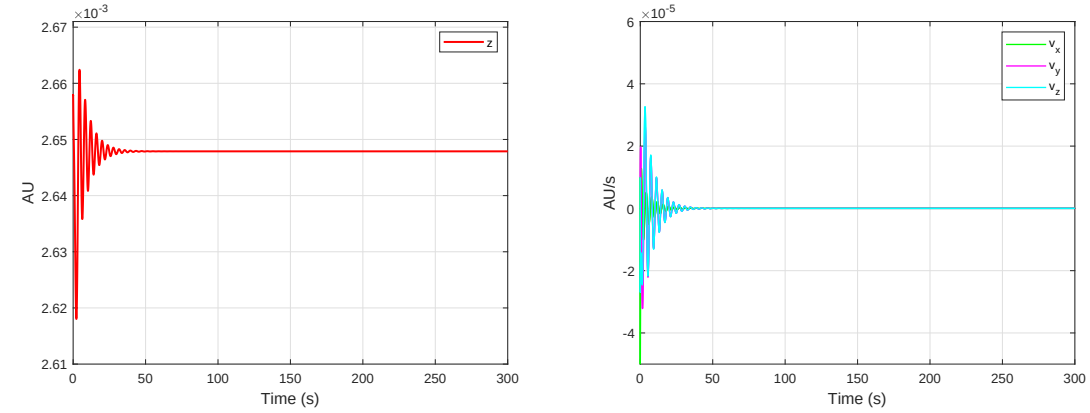

(a) Z coordinate

(b) V_x, V_y, V_z state velocities

Figure 4.12: Z state and velocities controlled by attitude angles/heliogyro linear control starting from maximum injection error

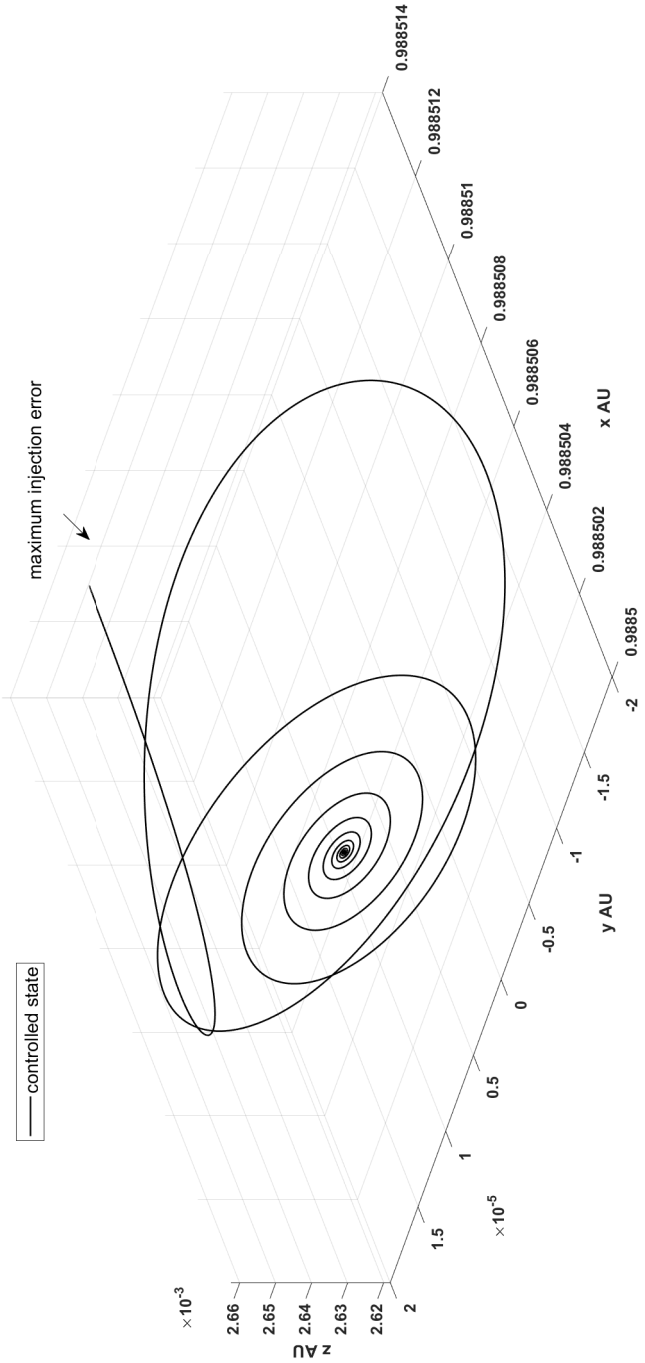

Figure 4.13: State trend subjected to attitude angles/heliogyro linear control starting from maximum injection error

4.4.3 Attitude angles and Reflectivity Control Device

The third simulated model includes as control variables the attitude of Solar Sail and an RCD device. It means that input variables will be angles γ, δ and the specular reflectivity coefficient ρ. Inevitably a non-ideal solar sail model must be used, to include in the acceleration formula, the coefficient ρ. Therefore, the model will be tested on the solar sail studied in Chapter 3, in the section focused on non-ideal model equilibrium computation (see Tab. 3.2).

No injection error

Concerning the first simulation in absence of position error, optimum integration parameters were set after some trial simulations (see Tab. 4.13)

Parameter	Values
Initial condition (position)	[0.989173986828632; 0; 0.00112441672663063] AU/s
Initial condition (velocity)	[0; 0; 0] AU/s
Integration time	$2\ 10^3\ s$
Tolerance (Relative and Absolute)	*Auto*

Table 4.13: Integration parameters of Solar Sail dynamics simulation controlled by Attitude angles and RCD, starting from equilibrium.

Here after, the most significant plots of the controlled states: in Fig. 4.14 and 4.15 respectively X, Z, Y and velocities. We have summarized simulations results of the system augmented with attitude and ρ control, in Tab. 4.14.

Parameter	Results
Steady state error	$0.03\,m$
Convergence rate	$1.245\,10^{-5} km/s$
Angles rate of change	$4.84\,10^{-8}\,rad/s$

Table 4.14: Results of Solar Sail dynamics simulation controlled by Attitude angles and RCD, starting from equilibrium.

It is observable that the rate limit is significantly lower than in previous cases and this characteristic certainly lead this control to be one of the best. On the contrary, the convergence rate is very low.

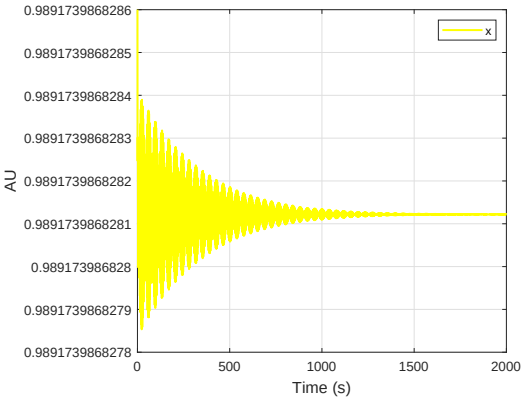

(a) X state coordinate

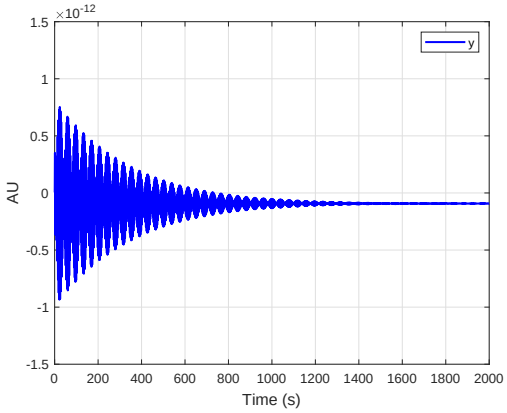

(b) Y state coordinate

Figure 4.14: X and Y state coordinates controlled by attitude angles/RCD linear control starting from equilibrium point

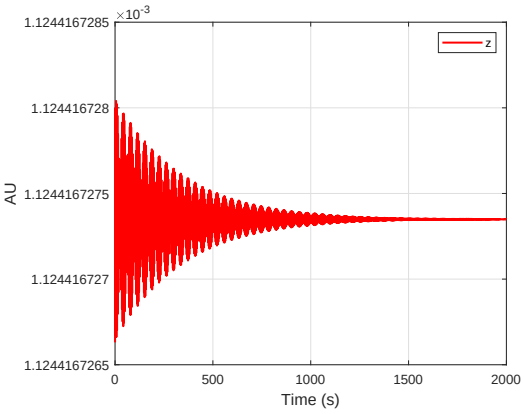

(a) Z state coordinate

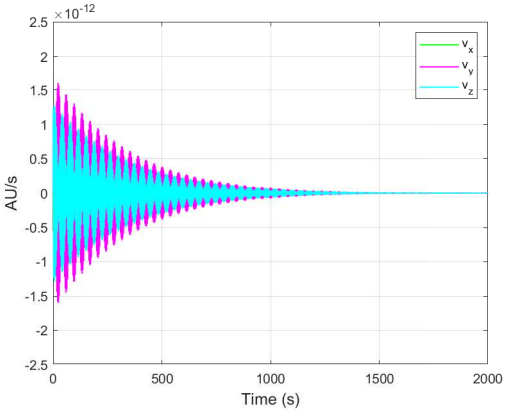

(b) V_x, V_y, V_z state velocities

Figure 4.15: Z state and velocities controlled by attitude angles/RCD linear control starting from equilibrium point

Maximum injection error

In this second simulation, it will be taken into account that this model can control even injection velocity different from zero. Therefore, after trying to find better performances, the integration parameters were set as values in Tab. 4.15. Special attention for integration time, which has increased, because the control demands more time to bring the sail to steady state, compared to the case where it is already in that point.

Parameter	Values
Initial condition (position	$[0.9891742888; 3\,10^{-7}; 1.12476\,10^{-3}]\,AU$
Initial condition (velocity)	$[9.4\,10^{-8}; 9.4\,10^{-8}; 9.4\ 10^{-8}]\,AU/s$
Integration time	$1\ 10^{4}\,s$
Tolerance (Relative and Absolute)	*Auto*

Table 4.15: Integration parameters of Solar Sail dynamics simulation controlled by Attitude angles and RCD, starting from maximum injection error.

Once again the results of simulated dynamics, in Figs. 4.16 and 4.17 are shown.
Most important results of controlled dynamics, starting from maximum injection error, are summarized in Tab. 4.15.

Parameter	Results
Steady state error	$0.073\,m$
Convergence rate	$0.5572 km/s$
Angles rate of change	$4.84\,10^{-3}\,rad/s$

Table 4.16: Results of Solar Sail dynamics simulation controlled by Attitude angles and RCD, starting from maximum injection error.

Compared to the case without injection error, an expectable slight increase in the steady state error and a decrease in convergence rate, due to the hight injection error are found. In addition, it is appreciable a sharp decrease in the minimum feasible value of attitude angles rate of change. It means that this of control, theoretically allows very high injection speed but it is at the disadvantage of control system effective implementation.
Again the behaviour of controlled Solar Sail, in a 3-D plot of the space near equilibrium point in *AU* (see Fig. 4.18) is shown.

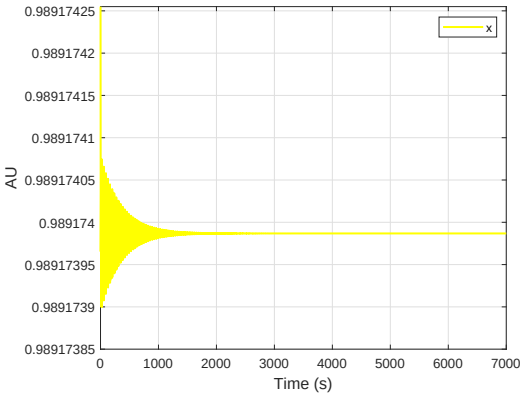

(a) X state coordinate

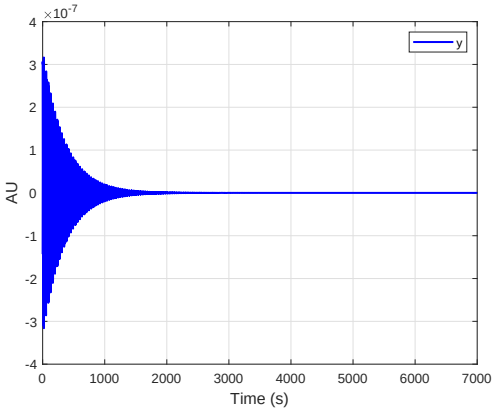

(b) Y state coordinate

Figure 4.16: X and Y state coordinates controlled by attitude angles/RCD linear control starting from maximum injection error

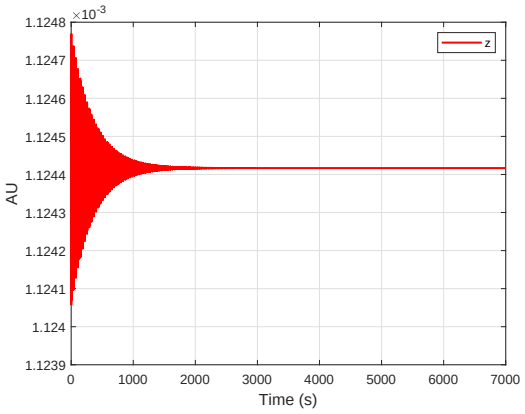

(a) Z state coordinate

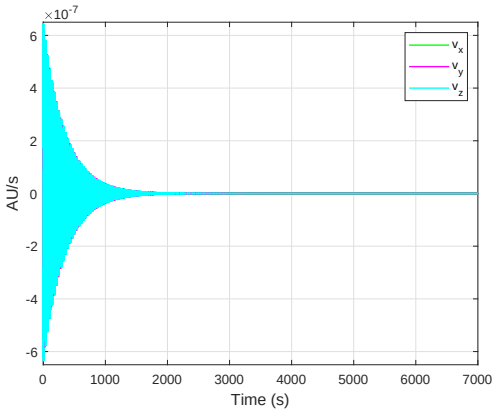

(b) V_x, V_y, V_z state velocities

Figure 4.17: Z state and velocities controlled by attitude angles/RCD linear control starting from maximum injection error

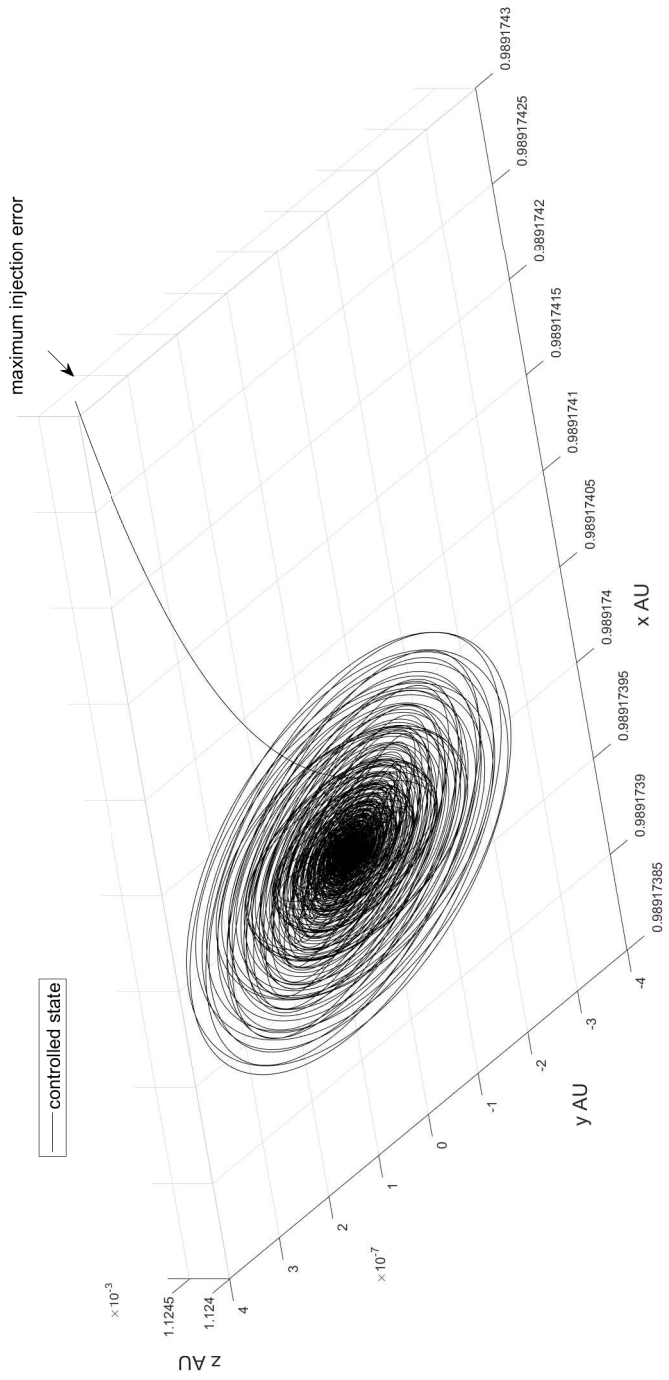

Figure 4.18: State trend subjected to attitude angles/RCD linear control starting from maximum injection error

Attraction Area

For this third type of control, it was possible to carry out the *Attraction area* analysis, as was done for the first model (see Fig. 4.19). This plot includes all the couples of maximum injection distance from equilibrium and corresponding injection velocity, which are acceptable by the control algorithm. In order to obtain these couples of values, 60 *simulations* were carried out. Starting from zero injection error, and zero injection velocity, these have been increased little by little to verify the system behaviour. The results have been recorded and used to build the following graph (see Fig. 4.19).
Comparing with the plot in Fig. 4.8, the x- and y-axis contain values of one order of magnitude more than the first model analysed. Thus, it can be said that this third model (which uses the RCD device) has a greater power of attraction than the previous one, both in terms of physical distance from the point of equilibrium and Solar Sail injection speed.

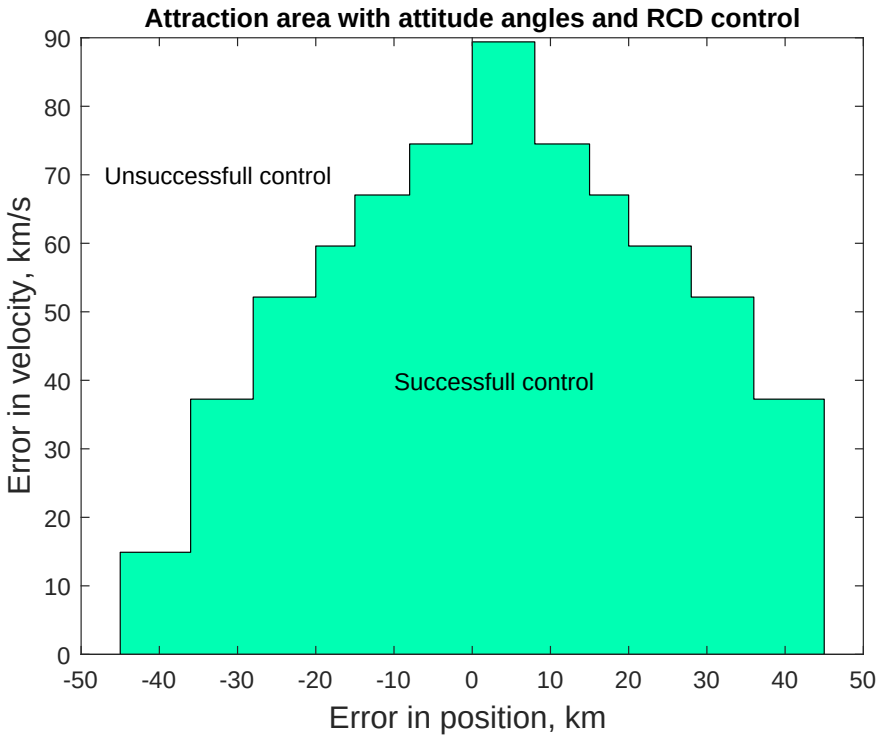

Figure 4.19: Attraction area for the system controlled by attitude and RCD

4.4.4 Heliogyro configuration and Reflectivity Control Device

The last control algorithm simulated is a new and unusual model, in which was avoided applying the most frequent control scheme, that embraces attitudes angles. This model is based only on β and ρ possible variations.
Again the algorithm on the non-ideal solar sail model should be tested and for the sake of simplicity, the same point of the previous model (point in Tab. 3.2) has been chosen.

No Injection Error

The first simulation has been set up as usual, with the solar sail already at the equilibrium point. The parameters of first integrations are in Tab. 4.16.

Parameter	Values
Initial condition (position)	[0.988503049085796; 0; 0.00264788459384856] AU
Initial condition (velocity)	[0; 0; 0] AU/s
Integration time	$1\ 10^3\,s$
Tolerance(Relative and Absolute)	10^{-3}

Table 4.17: Integration parameters of Solar Sail dynamics simulation controlled by Heliogyro configuration and RCD, starting from equilibrium.

A short integration time is characteristic of control which include beta, because they are fast in converging. The *integration tolerance* was fixed at 10^{-3}, because it has been proven that a more restrictive value had no beneficial effect on the simulation. It follows, the classical plot of coordinates and velocities of the state under control action (see respectively Fig. 4.20 and Fig. 4.21).
From these plots the results shown in Tab. 4.18 are derived.

Parameter	Results
Steady state error	$0.00953\,m$
Convergence rate	$2.754\,km/s$
Angles rate of change	not required

Table 4.18: Results of Solar Sail dynamics simulation controlled by Heliogyro configuration and RCD, starting from equilibrium.

Steady state error is the lower obtained until now, while convergence rate is quite hight.

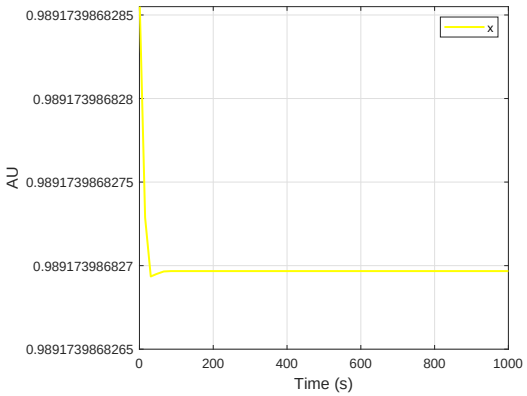

(a) X state coordinate

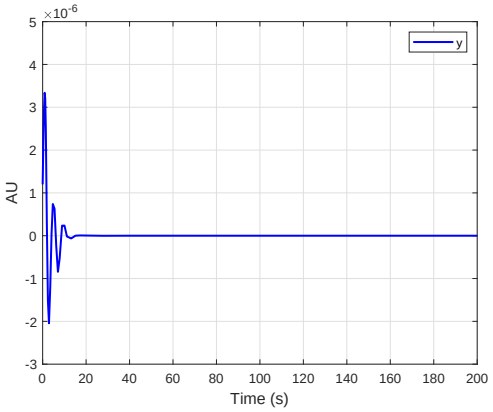

(b) Y state coordinate

Figure 4.20: X and Y state coordinates controlled by heliogyro/RCD linear control starting from equilibrium point

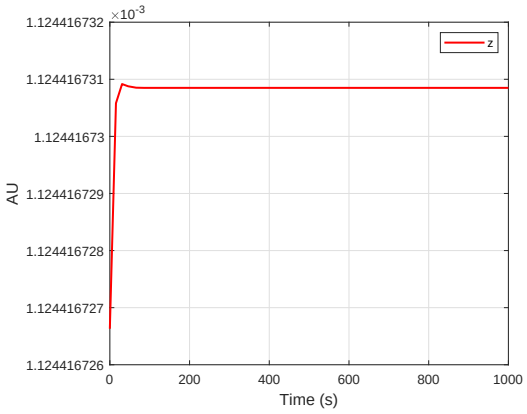

(a) Z state coordinate

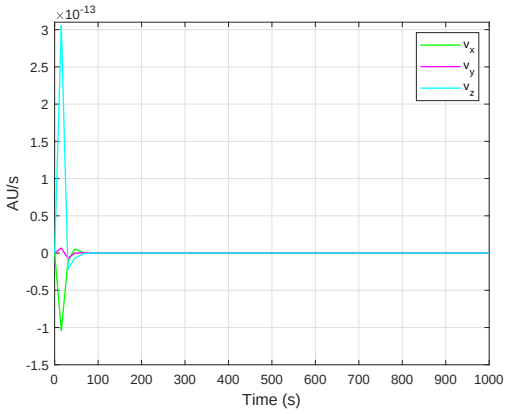

(b) V_x, V_y, V_z state velocities

Figure 4.21: Z state and velocities controlled by heliogyro/RCD linear control starting from equilibrium point

Maximum injection error

The last simulation was carried out by positioning the solar sail at the maximum distance point of the *Attraction Area*. However, this area is not well defined, since, in this model, there is not an inversely proportional correlation between maximum distance and controllable injection speed. Instead, a maximum acceptable value of the speed, which remains fixed even changing the injection error exists.
Dynamics integration follows the parameter of Tab. 4.19.

Parameter	Values
Initial condition (position)	$[0.988504249085796; 1.2\,10^{-6}; 0.00264908459384856]$ AU
Initial condition (velocity)	$[3\,10^{-6}; 3\,10^{-6}; 3\,10^{-6}]\ AU/s$
Integration time	$1\ 10^{3}\,s$
Tolerance(Relative and Absolute)	10^{-3}

Table 4.19: Integration parameters of Solar Sail dynamics simulation controlled by Heliogyro configuration and RCD, starting from maximum injection error.

A view of the solar sail state under the effect of this last control is in Fig. 4.22 and Fig. 4.23.
In Tab. 4.20 last simulations results.

Parameter	Results
Steady state error	$0.00953\,m$
Convergence rate	$2.31\,km/s$
Angles rate of change	not contemplated

Table 4.20: Results of Solar Sail dynamics simulation controlled by Heliogyro configuration and RCD, starting from maximum injection error.

Steady state error remains very small (of order of centimetres), while convergence rate decreases a bit but is still an high value, in fact β/ρ control is one of the fastest in leading the system to the steady state.
Finally, in the 3-D plot representing integrated dynamics, it is shown how solar sail reaches the desired state quickly, after a short oscillating trajectory (see Fig 4.24).

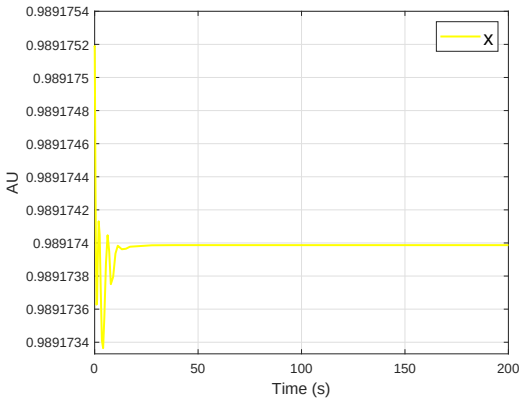

(a) X state coordinate

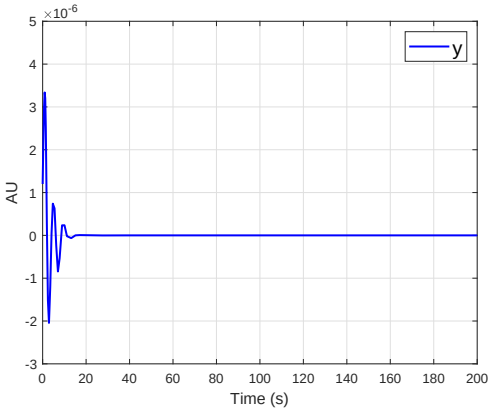

(b) Y state coordinate

Figure 4.22: X and Y state coordinates controlled by heliogyro/RCD linear control starting from maximum injection error

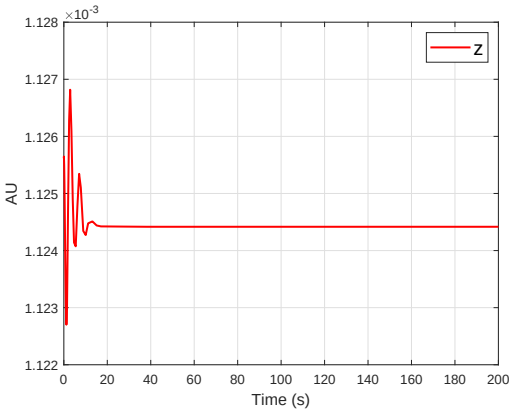

(a) Z state coordinate

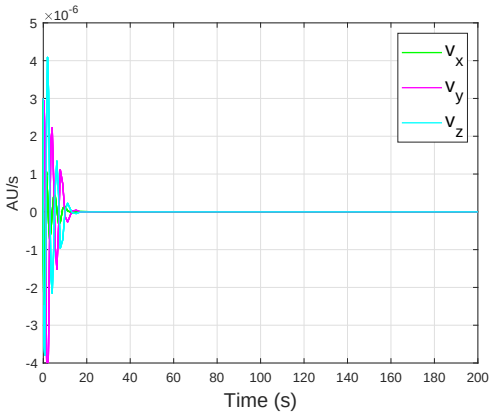

(b) V_x, V_y, V_z state velocities

Figure 4.23: Z state and velocities controlled by heliogyro/RCD linear control starting from maximum injection error

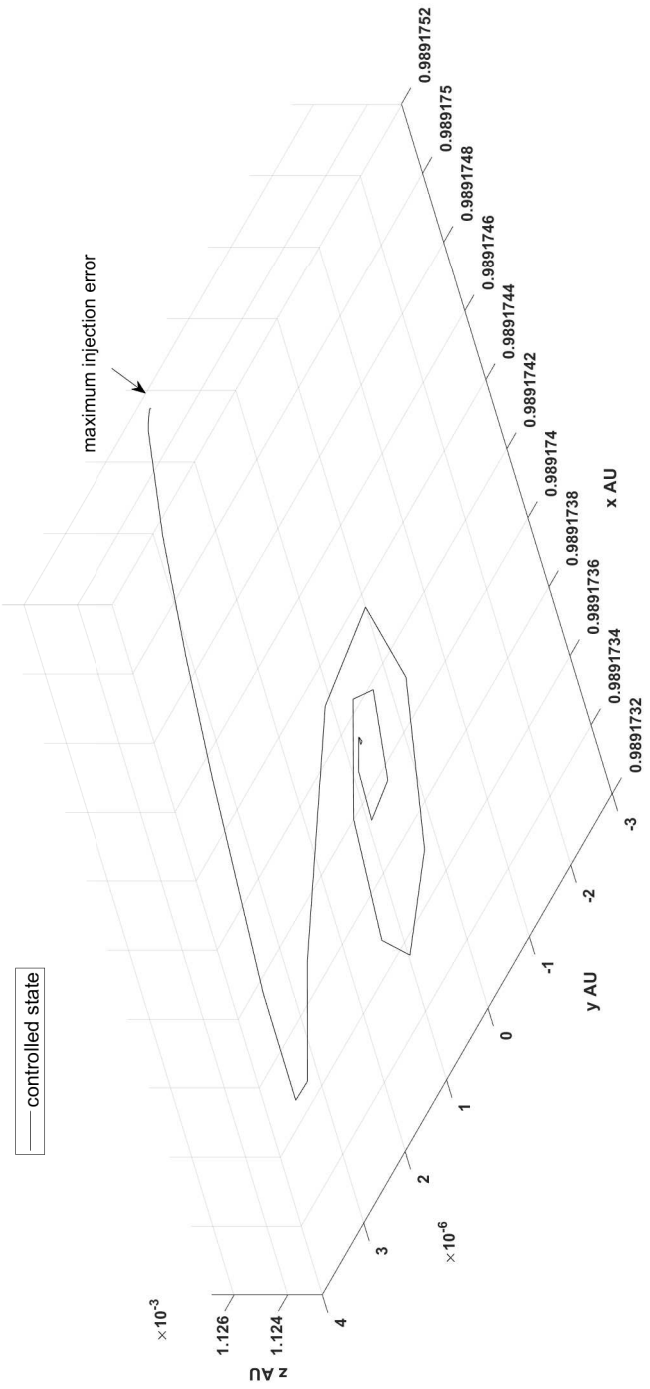

Figure 4.24: State trend subjected to heliogyro/RCD linear control starting from maximum injection error

4.5 Controls comparison

Finally, the results obtained by controlling the Solar Sail dynamics, with the four designed control models, are summarized with the aim to get an overview of the carried out analysis. All the parameters derived time by time are collected in the table below:

	Attitude	Beta+ Attitude	RCD+ Attitude	Beta+ RCD
Attraction area radius	2.5 km	1490 km	45 km	178.8 km
Steady state error (equilibrium)	28 m	17.4 m	0.03 m	0.00935 m
Steady state error (injection error)	28 m	17.4 m	0.03 m	0.00935 m
Attitude angles rate of change limit (equilibrium)	$7\,10^{-6}$ rad/s	$5\,10^{-6}$ rad/s	$5\,10^{-8}$ rad/s	—
Attitude angles rate of change limit (injection error)	$7\,10^{-6}$ rad/s	$5\,10^{-6}$ rad/s	$5\,10^{-3}$ rad/s	—
Convergence rate (equilibrium)	0.628 m/s	0.165 km/s	0.0125 m/s	2.754 km/s
Convergence rate (injection error)	22.2 m/s	1.6523 km/s	0.05572 m/s	3.31 km/s

Table 4.21: Comparison and summary of linear control systems

The first two models have been implemented on the *ideal Solar Sail dynamics* model, while the last two which involve the RCD, required to be implemented following the *non-ideal Solar Sail dynamics* model. Starting from analysing *Attraction area radius*, there is an appreciable difference between control that contains lightness number *beta* as input variable and the others. In that case, the radius is very large and it means that solar sail can be subject to very high injection error and still be brought back to the desired position. Going on with the analysis, *Steady state error* results very small for dynamics controlled by RCD, coupled with another actuation mechanism.
Another parameter investigated is the *Attitude angles rate of change* which is related only to models including angles as input variables. For the firsts two model, it is approximately 1 deg/h, while for *RCD+ Beta* model, the attitude angles minimum feasible rate

of change is $0,02\ deg/h$. So if the solar sail has a strong limitation in attitude changing, this control may be the right one. However, this same control is very disadvantaged in the case of injection error, because the value of the minimum feasible attitude rate of change increases to $206\ deg/h$.

The last variable analysed is the *Convergence rate* of the state toward the desired point. This parameter is mentioned even in the case of simulation starting at the equilibrium point already, because as it has been explained, the artificial Solar Sail Lagrangian points, do not possess intrinsically the stability. Therefore, it is necessary to employ control even in this case. The control action, on the other hand, is an external force applied to the state, which involves an acceleration. That is why the state follows a trajectory before reaching equilibrium.

The models that imply attitude angles show higher values of the convergence rate with the injection error. While models including β lead to a higher convergence rate than the others. Therefore it is convenient to choose one of them if it is required to reach the desired point as fast as possible.

Chapter 5

Mapping control

In the previous chapter, a comparative analysis of four control models, aimed at Solar Sails parking has been developed. In all cases, they were *linear controls* adapted to the non-linear solar sail dynamics.
However, it has to be said that linear control has some operating limits. Indeed, linear control methods rely on the key assumption of small range operations for the linear model to be valid. When the required operating range is large, a linear controller is likely to perform very poorly or to be unstable, because the non-linearities in the system cannot be properly compensated for. To achieve a more accurate control system, a *LQR mapping control* has been developed, a model which requires the linearisation of the state, in order to realize the ideal external LQR control, but not the linearisation the applied control. Indeed, the chosen actuation mechanism is forced to emulate the ideal control acceleration, by tuning its variables, without being subjected to the linearisation process. LQR mapping has already been investigated by Krishen in [35], where a control model is designed for a rotary inverted pendulum, based on a LQR stabilizing control emulated by a Mandani FIS.
In this last part of the research, in particular it has been attempted to implement a control model that could substitute the previous designed linear control including attitude angles (Section 4.4.1), in order to guarantee better performances and results. The mapping control was developed to emulate an ideal feed-back acceleration, which has been previously experimented on solar sail dynamics and its control power tested. Step by step, it will be explained how the algorithm has been achieved.
First of all, the ideal control, in the form of external acceleration, has been designed according to the LQR theory. Once tested, the effectiveness of this ideal control, aimed to steady one of the equilibrium points, a control model fitted to map the acceleration induced by the ideal control has been designed, using the attitude angles as variables. In order to obtain the required input values, a numerical optimization procedure, that seeks to find a_{sail} that minimises the following function, was employed

$$f = u_{ideal} + a_{sail}$$

where u_{ideal} is the LQR external function an a_sail the characteristic Solar Sail acceleration.

5.1 Ideal feed-back control

Let's start with the implementation of ideal acceleration finalized to state control. As mentioned, the ideal model has been realized following the LQR theory. Therefore, starting from solar sails dynamic equations (Eq. 3.18), is considered the ideal formulation of acceleration vector (a_{ideal} from Eq. 2.15), because there is no requirement to include non-ideal reflectivity coefficient in the equations.

Computation

Defining u_x, u_y and u_z as control acceleration components along X, Y, and Z axes, respectively, the non-dimensional equations of motion of the sailcraft in SSCRTBP Sun-Earth result as

$$\ddot{X} - 2\dot{Y} - X = -\frac{(X+\mu)(1-\mu)}{r_1^3} - \frac{\mu(X-1+\mu)}{r_2^3} + a_{ideal\,x} + u_x \tag{5.1}$$

$$\ddot{Y} + 2\dot{X} - Y = -\frac{(1-\mu)Y}{r_1^3} - \frac{\mu Y}{r_2^3} + a_{ideal\,y} + u_y \tag{5.2}$$

$$\ddot{Z} = -\frac{(1-\mu)Z}{r_1^3} - \frac{\mu Z}{r_2^3} + + a_{ideal\,z} + u_z \tag{5.3}$$

where

$$r_1 = \sqrt{(X+\mu)^2 + Y^2 + Z^2}$$
$$r_2 = \sqrt{(X-1+\rho)^2 + Y^2 + Z^2}$$

The non-dimensional linearised equations of motion in terms of x, y, and z can be derived in state space form as

$$\dot{\mathbf{x}} = \mathbf{A}\mathbf{x} + \mathbf{B}\mathbf{u} \tag{5.4}$$

where $x = (x, y, z, \dot{x}, \dot{y}, \dot{z})$, and $\mathbf{u} = (u_x, u_y, u_z)$ and

$$\mathbf{A} = \begin{bmatrix} 0 & 0 & 0 & 1 & 0 & 0 \\ 0 & 0 & 0 & 0 & 1 & 0 \\ 0 & 0 & 0 & 0 & 0 & 1 \\ U_{xx} & 0 & U_{xz} & 0 & 2 & 0 \\ 0 & U_{yy} & 0 & -2 & 0 & 0 \\ U_{zx} & 0 & U_{zz} & 0 & 0 & 0 \end{bmatrix}, \qquad \mathbf{B} \begin{bmatrix} 0 & 0 & 0 \\ 0 & 0 & 0 \\ 0 & 0 & 0 \\ 1 & 0 & 0 \\ 0 & 1 & 0 \\ 0 & 0 & 1 \end{bmatrix} \tag{5.5}$$

For point of Tab. 3.1 in Sun-Earth system, matrix components result:

$$U_{xx} = 6.1171, U_{xz} = -1.21323, U_{yy} = -1.89657, U_{zz} = -2.61514,$$

Starting from the linear system described by Eq. 5.4, it is possible to include a linear state-feedback controller of the form

$$\mathbf{u} = -\mathbf{K}(\mathbf{x} - \mathbf{x_r}) \tag{5.6}$$

where $\mathbf{K}$ is the gain matrix to be properly determined using LQR method, described in Chapter 4. Therefore, after having tuned weighting matrices $\mathbf{Q}$ and $\mathbf{R}$, the values that gave the better performance in term of oscillation amplitudes and convergence are:

$$\mathbf{Q} = 10000\,\mathbf{I}_{6\times 6}, \qquad \mathbf{R} = \begin{bmatrix} 0.001 & 0 & 0 \\ 0 & 0.001 & 0 \\ 0 & 0 & 0.01 \end{bmatrix} \tag{5.7}$$

which lead to the following gain matrix:

$$\mathbf{K} = \begin{bmatrix} 3168.77 & -2.00082 & -1.19515 & 3163.28 & 8.39259 & -0.00324 \\ 2.00082 & 3160.38 & -0.00037 & 18.39259 & 3163.27 & -1.35652\,10^{-6} \\ -1.22721 & 0.000119 & 997.397 & -0.00032 & -1.35652 & 1000.99 \end{bmatrix} \tag{5.8}$$

This control has been then tested with simulations. The same scheme of Fig. 4.1 have been implemented, where this time, $\mathbf{u}$ is added to equations system as an additional acceleration and will not substitute pre-existent equations components.

5.1.1 Results

The power of this control has been tested considering a big injection error with respect to equilibrium point. In Tab. 5.1 the integration parameter

Parameter	Values
Initial condition	$[0.98850315; 1\,10^{-7}; 0.0026486; 0; 0; 0]\ AU$
Integration time	$3\ 10^2\ s$
Tolerance (Relative and Absolute)	10^{-3}

Table 5.1: Integration parameter for ideal external control

The solar sail is rapidly brought back to its equilibrium point, as we can see in Figs. 5.1 and 5.2. The external control acceleration instead, goes to zero, once the solar sail has been brought to steady-state (see Fig. 4.3)

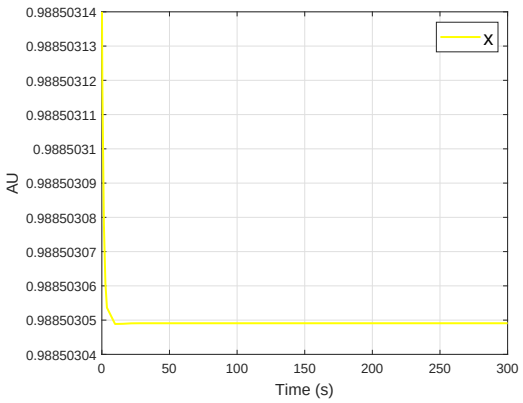

(a) X state coordinate

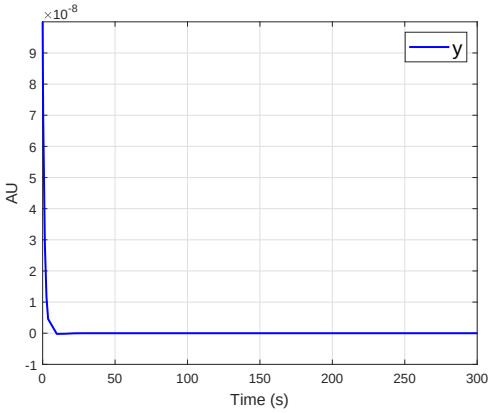

(b) Y state coordinate

Figure 5.1: X and Y state coordinates controlled by ideal external control

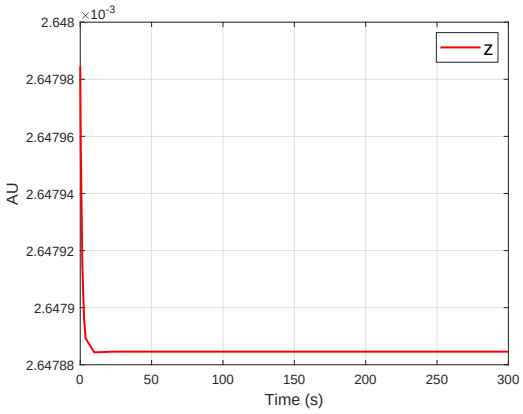

(a) Z state coordinate

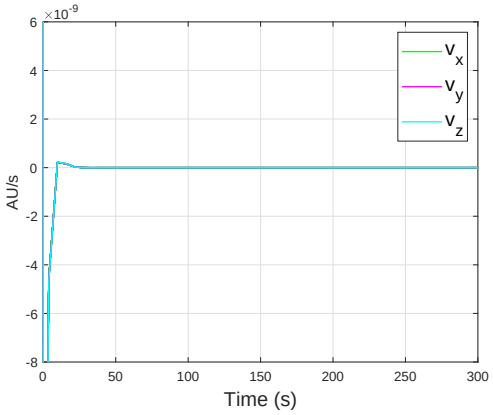

(b) V_x, V_y, V_z state velocities

Figure 5.2: Z state and velocities controlled by ideal external control

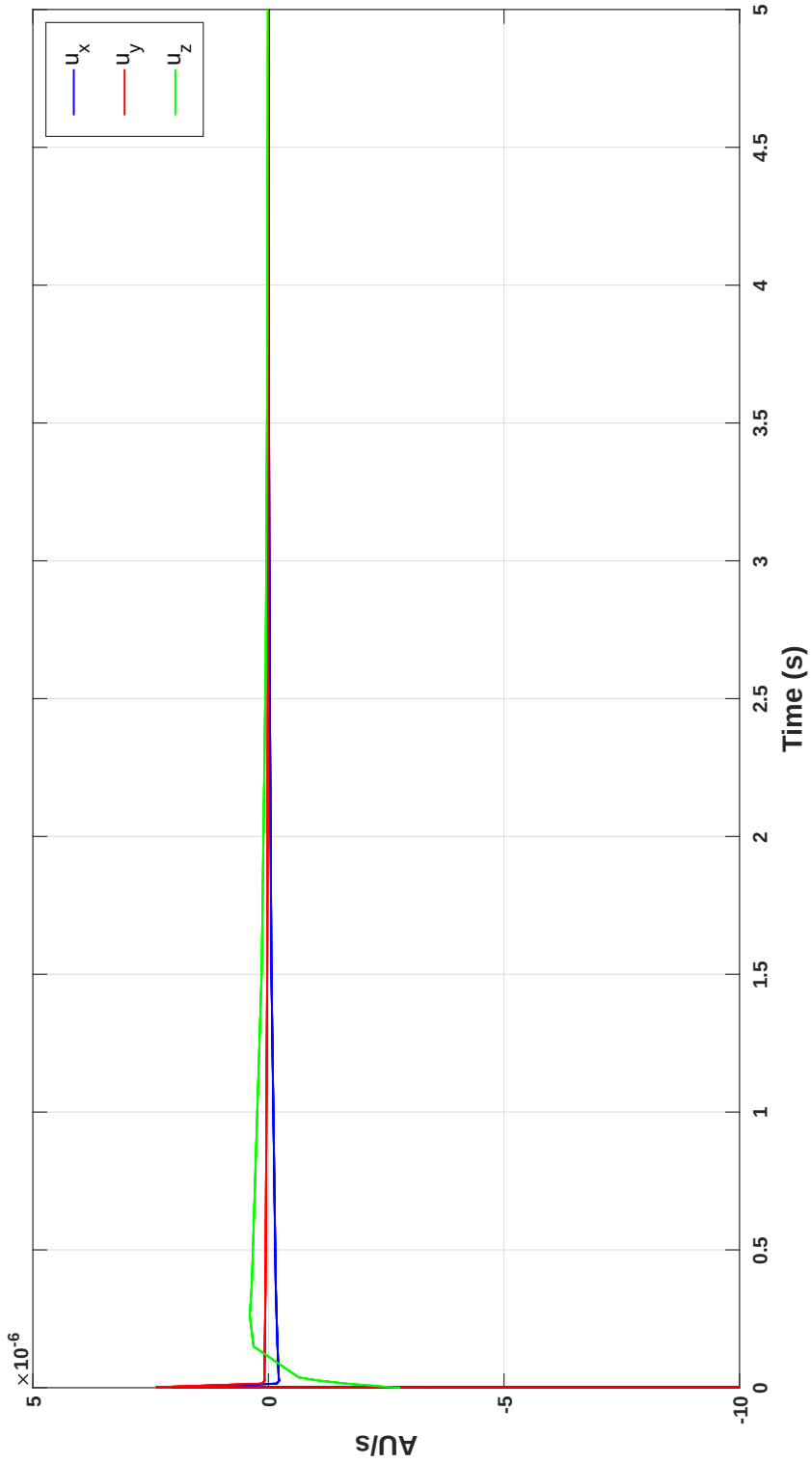

Figure 5.3: Ideal control variables

5.2 Mapping algorithm

In this section, it is explained how the ideal control has been mapped using attitude angles. An algorithm able to include the ideal acceleration in the solar sail acceleration has been built, by exploiting attitudes angles variation. To achieve this behaviour, the algorithm should satisfy the following statement:

$$\mathbf{f} = \left(\mathbf{u_{ideal}} - \mathbf{a_{sail}}\right) = 0 \tag{5.9}$$

Therefore, a *minimization problem* aimed to satisfy Eq. 5.9 has been designed, by including as variables the attitude angles γ and δ.
Since the system of equations that constitutes the objective function, is non-linear, to find its roots the computation has been set as a minimization process using Newton's method. In the next section, it follows an explanation of the method and how it has been applied to the problem.

5.2.1 Newton method

Newton's method [52] exploits information on the values of f function and its derivative (assuming this exists). For this purpose, it is reminded to the readers that the equation of the tangent to the curve $(x, f(x))$ in the point $x^{(k)}$ is

$$y(x) = f(x^{(k)}) + f'(x^{(k)})(x - x^{(k)}) \tag{5.10}$$

If we search for $x^{(k+1)}$ such that $y(x^{(k+1)}) = 0$, we found

$$x^{(k+1)} = x^{(k)} - \frac{f(x^{(k)})}{f'(x^{(k)})}, \;\; k \geq 0 \tag{5.11}$$

until $f'(x^k) \neq 0$. Eq. 5.11 allows to compute a sequence of values $x^{(k)}$ starting from an initial $x^{(0)}$. The method obtained in this way is known as *Newton's method* and it is equivalent to compute zeros of f substituting locally to f its tangent. Indeed, if it is developed f in Taylor series in a neighbourhood of a generic point x^k, it is found that

$$f(x^{(k+1)}) = f(x^{(k)}) + \delta^{(k)} f'(x^{(k)}) + \mathcal{O}((\delta^{(k)})^2) \tag{5.12}$$

where $\delta^{(k)} = x^{(k+1)} - x^{(k)}$. Imposing that $f(x^{(k+1)})$ is equal to zero and neglecting $\mathcal{O}((\delta^{(k)})^2)$,it can be derived $x^{(k+1)}$ function of $x^{(k)}$ as in Eq. 5.11. Therefore Eq. 5.12 can be seen as an approximation of Eq. 5.11. Newton method convergence is not guaranteed for every choice of $x^{(0)}$, but only for values of $x^{(0)}$ *sufficiently near* to α, i.e. belongings to a neighbourhood $I(\alpha)$ sufficiently small of α.

Newton method, once converging, gives back the exact value of α after an infinite number of iterations. Generally, it is enough to obtain the α within a fixed tolerance ε, therefore it is sufficient to stop at first iteration k_{min} such that it results:

$$\left|e^{(k_{min})}\right| = \left|\alpha - x^{(k_{min})}\right| < \varepsilon$$

It is a check on the error. Being this unknown, it is necessary to employ an *error estimation*, it means a quantity of easy calculation, thanks to which it is possible to increment the error itself. As error estimation for Newton method it has been employed the *differences between two consecutive iterations* and it is stopped in correspondence of the smaller integer k_{min} such that

$$\left|x^{(kmin)} - x^{(k_{min}-1)}\right| < \varepsilon \tag{5.13}$$

It is a check on the increment.

5.2.2 Application

Newton theory has been presented since it is the adopted method to obtain the solution of the objective function minimization (Eq. 5.9), in each step of the controlled dynamics integration. In its complete formulations, the objective function is

$$\mathbf{f} = \left((\mathbf{u_{ideal}} + \mathbf{a_{cost}}) - \mathbf{a_{sail}}\right) = 0 \tag{5.14}$$

where

- $\mathbf{u_{ideal}}$ is the ideal external acceleration, computed in Section 5.1.1,
- $\mathbf{a_{cost}}$ is the solar sail acceleration produced at those equilibrium point values and it is a constant vector,
- $\mathbf{a_{sail}}$ is the measure that solar sail should assume to embed the ideal control acceleration. The purpose of the algorithm is to ensure that the solar sail acceleration includes also the effect of ideal control.

Algorithm steps

Hereafter, it will be explained the structure of *Newton method solver*, implemented in ®Matlab, which is part of a ®Simulink model representing the dynamics controlled by the mapping control.
Firstly, the objective function has been defined (in Eq. 5.14) and called *target*, which is function of the unknowns δ and γ, of the state vector X and the ideal control vector u_c.
Then the proper Newton method solver has been exploited in an algorithm structured in this way:

- two required parameters have been fixed after some trial and error, i.e. the *tolerance* (5000) and *maximum iterations number* (1×10^{-8}),

- initial value $x^{(0)}$ has been imposed equal to equilibrium γ and δ, in order to have faster convergence,

- the *Jacobian* of *target* has been implemented, because it is an equations system and the derivative at denominator of Eq. 5.11 must be substituted by the function Jacobian,

- last step is to include Eq. 5.11 in a cycle that stops when the error is smaller that the tolerance. Therefore it is exploited ®Matlab *for* function, and in each k^{th} iteration the Eq. 5.15 is computed:

$$GD = GD - pinv(J) \cdot f \tag{5.15}$$

  where *GD* is the attitude angles vector, and $pinv(J)$ the pseudo-inverse matrix of Jacobian, which is a generalization of the inverse matrix. Then, the error between two successive iterations is computed. The algorithm found a solution and stops if, within several iterations equal to the *maximum iterations number*, an error less then the *tolerance* value is achieved.

Newton method solver is called by ®Simulink block described below.

5.2.3 Model

The controlled dynamics is then implemented in a model, which is outlined in Fig. 5.4. The dynamics block includes non-linear Solar Sail equations of motion, with the derivative of state vector $\mathbf{X_{state}} = [\mathbf{X}\ \dot{\mathbf{X}}]$ in evidence. Once the state is integrated, its values are used for the computation of state feedback control (see Eq. 5.6). Both state and ideal control vector constitute inputs for mapping control block, in which the Newton solver is called, and for each integration an *attitude angles control vector* is computed.

5.3 Simulations and results

To study and analyse the power of our new control model, a number of simulations (50) have been carried out, imposing each time different integration parameters, i.e. initial condition, the minimum rate of change, etc... Hereafter the results of two opposite situations will be shown, firstly without any injection error, and then with Solar Sail injected at maximum injection error, which has been found by trying to increase the injection error more and more and keeping track of the last value, for which the control still has the

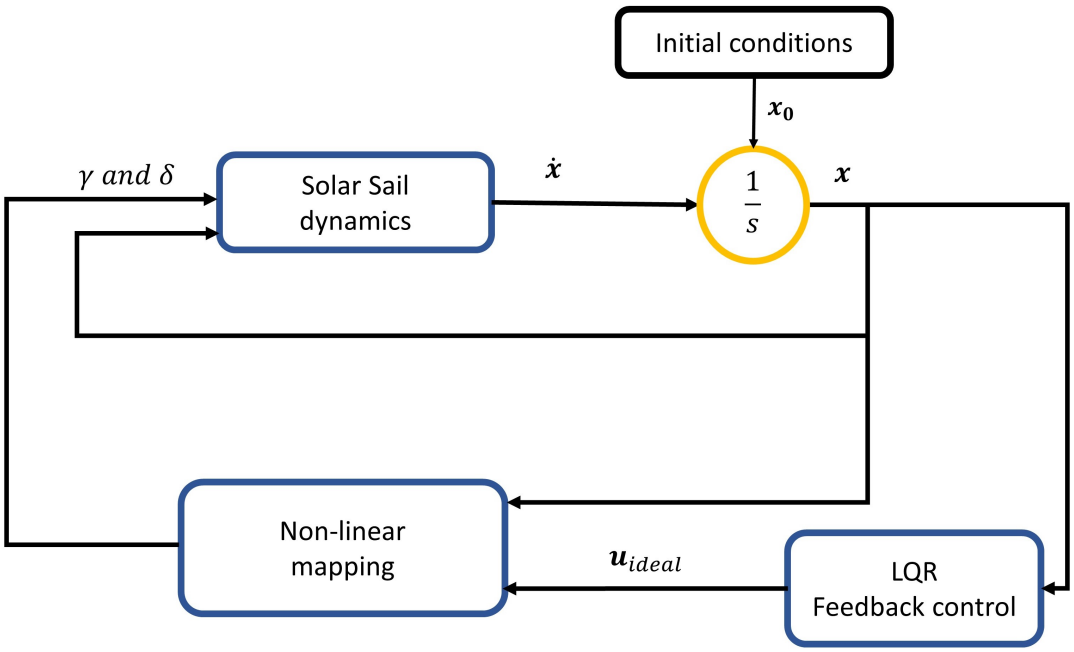

Figure 5.4: Mapping control system applied to Solar Sail dynamics

desired effect. Therefore, an *attraction area plot* will be introduced, which has been used in previous control analysis, to concretely see the differences between them.

5.3.1 Without injection error

The first simulation is characterized by the following parameters:

Parameter	Values
Initial condition	$[0.988503049085796; 0;$ $0.00264788459384856; 0; 0; 0]\ AU$
Integration time	$1\ 10^3\ s$
Tolerance (Relative and Absolute)	10^{-12}

Table 5.2: Integration parameters of Solar Sail dynamics simulation controlled by mapping model, starting from equilibrium point.

The controlled state is shown in Figs. 5.5 and 5.6, with the classical zoomed plot of all the state variables (coordinates and velocities). In Tab. 5.3, the obtained simulation results have been summarized, using the same parameters employed for linear control analysis, in the previous chapter.
By comparing the results of this simulation including the mapping control model, to the

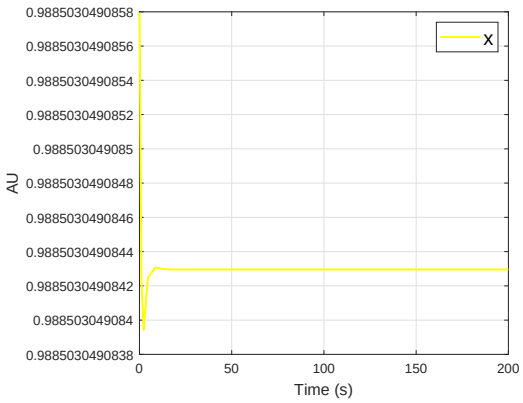

(a) X state coordinate

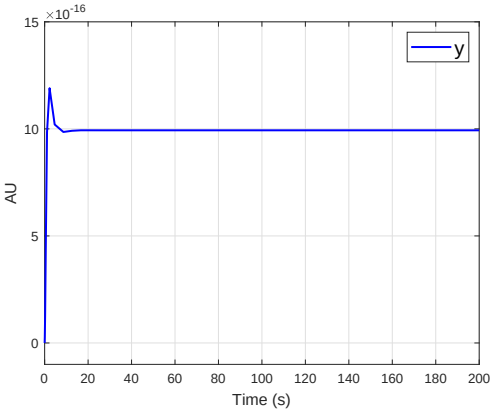

(b) Y state coordinate

Figure 5.5: X and Y state coordinates controlled by ideal external control

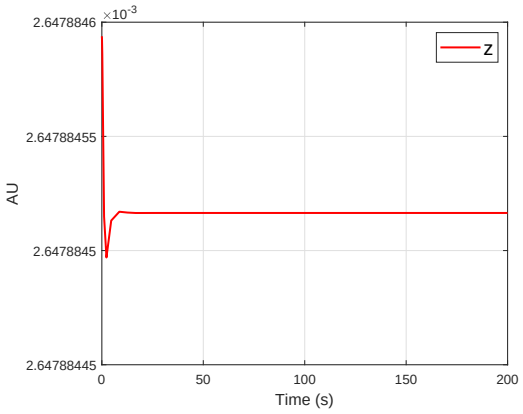

(a) Z state coordinate

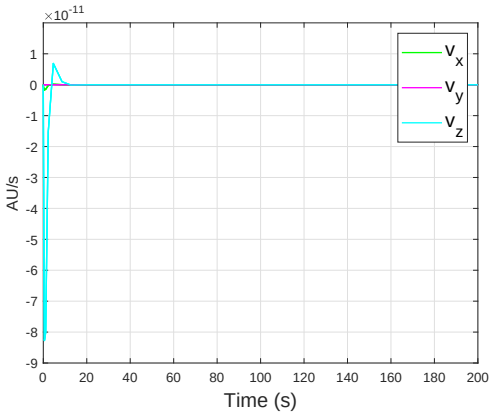

(b) V_x, V_y, V_z state velocities

Figure 5.6: Z state and velocities controlled by ideal external control

Parameter	Results
Steady state error	$0.223\,m$
Convergence rate	$0.05259 m/s$
Angles rate of change	$4\ 10^{-8} rad/s$

Table 5.3: Results of Solar Sail dynamics simulation controlled by mapping model, starting from equilibrium point.

parallel one involving linear control, it can be asserted that the new model leads to better outcomes.
Analysing the steady-state error, it drops sharply from $28m$ to $0.233m$, which proves that this new control allows for higher accuracy in achieving the desired state.
Furthermore, the minimum rate of variation of attitude angles can be set to $4\ 10^{-8}$ (compared to $7\ 10^{-6}$) making mapping control easier to achieve and less energy-consuming for the system. In this way, it is possible to control the sail by displacing the solar sail normal vector of only $0.01^{\circ}/hour$.

5.3.2 With maximum injection error

The second simulation is obtained from solar sail dynamics, augmented with the new control model, with initial condition of integration at maximum injection error: $6\ 10^{-7} AU$ or $90\ km$. Tab. 5.4 shows the parameters established for this integration. After carrying out a series of tests, it is found that better results are obtained by increasing tolerance values.

Parameter	Values
Initial condition	$[0,988502449085796; 6\ 10^{-7};$ $0,00264728459384856; 0; 0; 0]\ AU$
Integration time	$1\ 10^{3}\,s$
Tolerance (Relative and Absolute)	10^{-8}

Table 5.4: Integration parameters of Solar Sail dynamics simulation controlled by mapping model, starting from maximum injection error.

In Figs. 5.7 and 5.8 the dynamics of a controlled solar sail, from the injection point to maximum equilibrium. From these, new interesting results can be obtained, as summarised in Tab. 5.5.
The steady-state error remains very small, even in the case of the solar sail injected far from equilibrium, and convergence rate higher than the first simulation, i.e. from $0.05259 km/s$ to $0.8509 km/s$, following the same trend experienced with ideal controls.
In Fig. 5.9 it is possible to see state dynamics in the classical 3-D plot, representing the space near equilibrium point in Astronomic Units. It shows how the solar sail goes easily from maximum injection point to the equilibrium, thanks to control action.

Parameter	Results
Steady state error	$0.223\,m$
Convergence rate	$0.8509\ m/s$
Angles rate of change	$4\ 10^{-8} rad/s$

Table 5.5: Results of Solar Sail dynamics simulation controlled by mapping model, starting from maximum injection error.

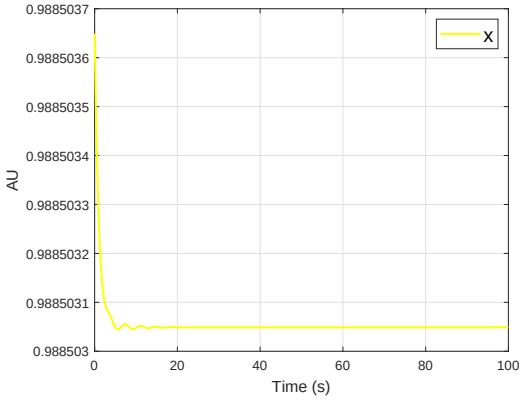

(a) X state coordinate

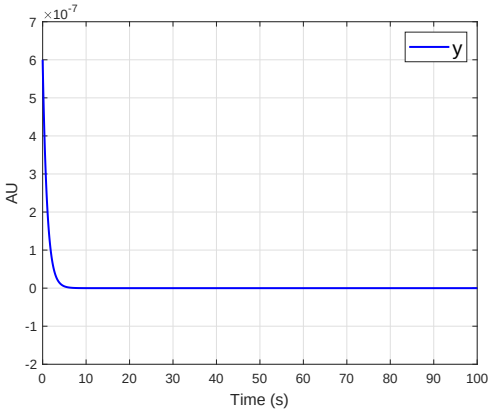

(b) Y state coordinate

Figure 5.7: X and Y state coordinates controlled by ideal external control

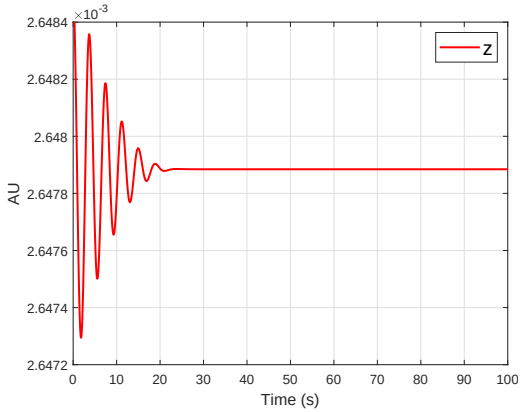

(a) Z state coordinate

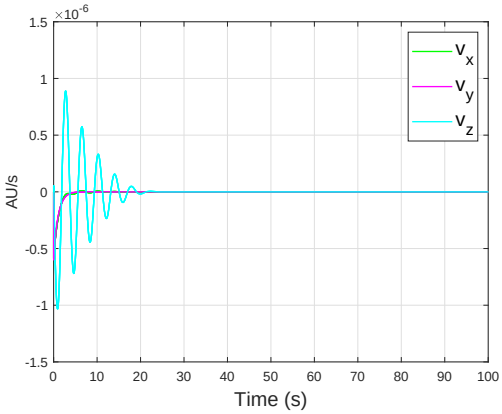

(b) V_x, V_y, V_z state velocities

Figure 5.8: Z state and velocities controlled by ideal external control

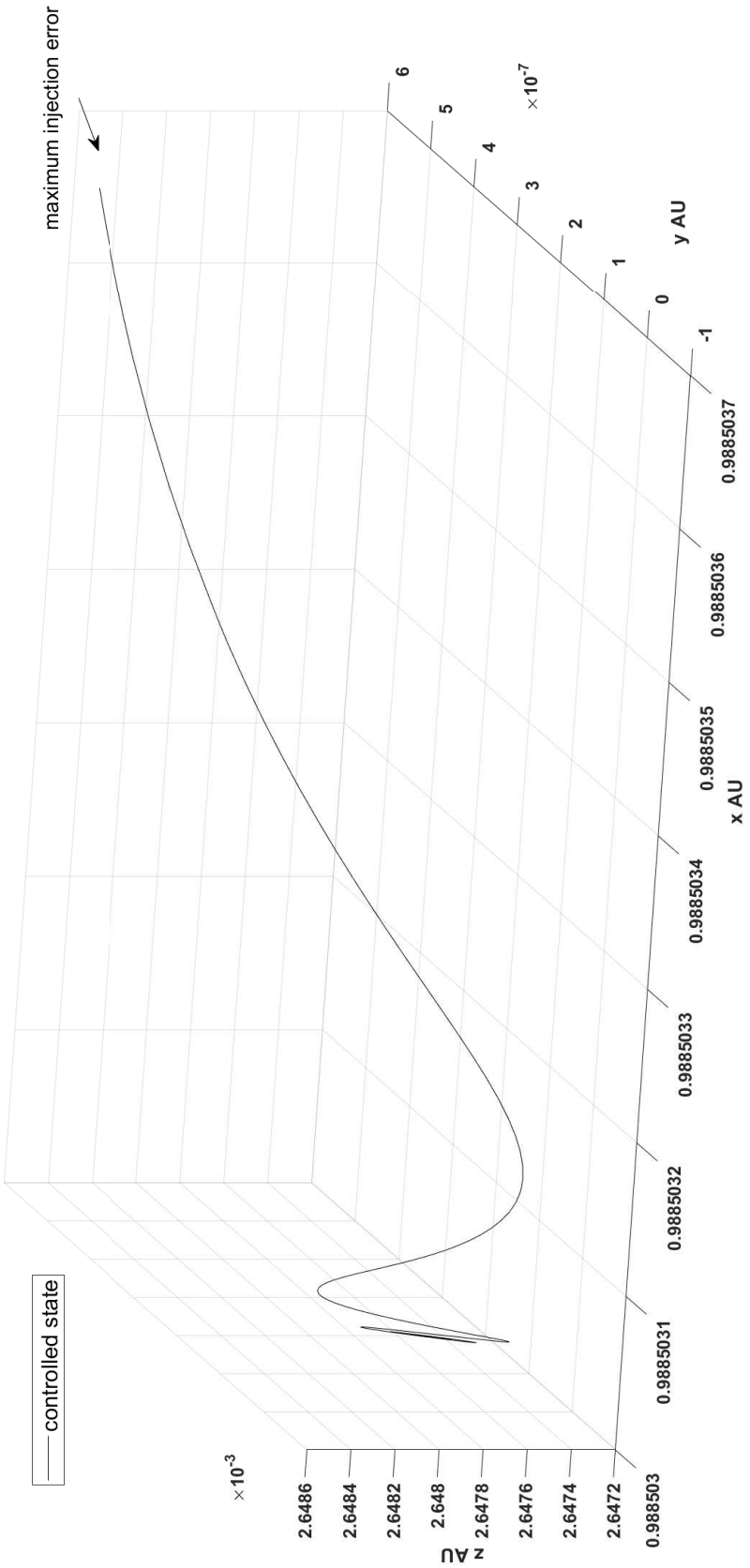

Figure 5.9: Solar sail dynamics controlled by mapping control

Attraction Area

In this section, the *Attraction area* is reported in case of solar sail dynamics subjected to the mapping control (see Fig. 5.10). Comparing it with the Attraction area in Fig. 4.8 (associated with linear control) it can be appreciated how the controllable range, around the equilibrium point, increases with respect to the linear controlled system, while the maximum injection speed range is similar. It means that the solar sail could be injected further (but still below a radius of 90km) than the case of a linear-controlled system and still be controlled thanks to the new control model.

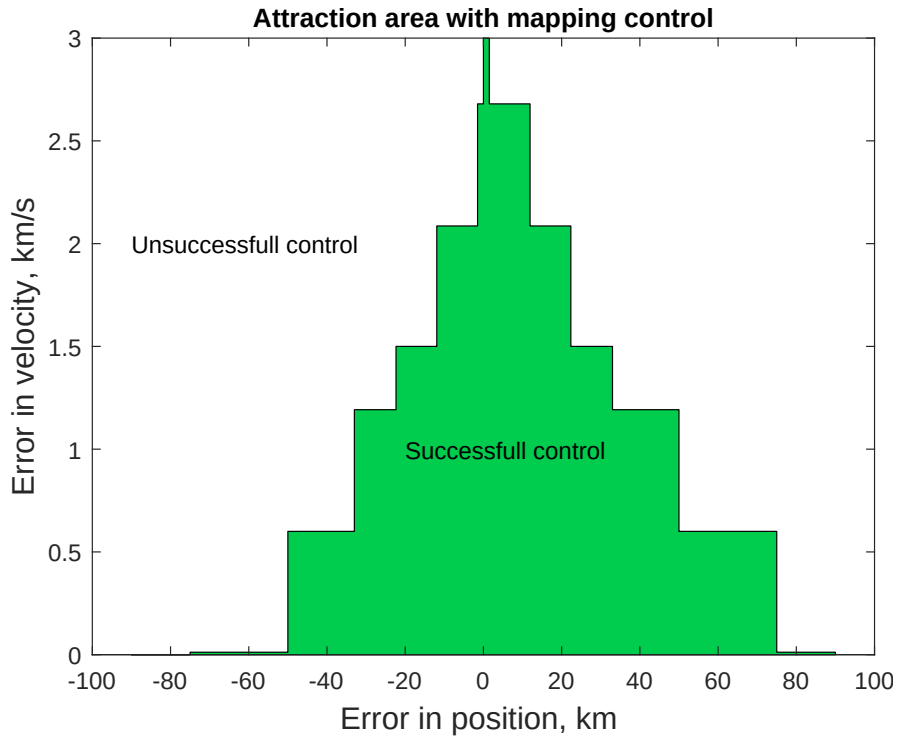

Figure 5.10: Attraction area for system dynamics subjected to mapping control

A comparative table, similar to the one compiled in previous section, has been implemented (see Tab. 5.6) including this time the linear control with attitude angles orientation and the mapping control with the same actuation mechanism. It is reminded that both the models have been implemented from *ideal Solar Sail dynamics*.

5.3.3 Control comparison

By analysing the table it can be appreciated that the *Attraction area radius* increases significantly if mapping control is adopted (almost an order of magnitude bigger than the parallel linear control). Furthermore, the SSE is different between the two cases, it undergoes a considerable decrease in the simulations carried out with the mapping control,

	Attitude linear	Attitude mapping
Attraction area radius	2.5 km	89.4 km
Steady state error (equilibrium)	28 m	0.223 m
Attitude angles rate of change limit (equilibrium)	$7\,10^{-6}$ rad/s	$4\,10^{-8}$ rad/s
Attitude angles rate of change limit (injection error)	$7\,10^{-6}$ rad/s	$4\,10^{-8}$ rad/s
Convergence rate (equilibrium)	0.628 m/s	0.05259 m/s
Convergence rate (injection error)	22.2 m/s	0.8509 m/s

Table 5.6: Comparison between linear control and mapping control involving attitude angles as actuation mechanism

confirming that this last one is better. One major outcome is observed for the limits of the attitude angles rate of change. It is reminded that a limit on attitude deflection of $1deg/h$ has been imposed. This limit was not respected by linear control with attitude angles orientation, which needed a rate of $1.5deg/h$ to be feasible and able to lead the system to the desired state. On the contrary, mapping control could handle a limit on the attitude rate of change of $0.063deg/h$. The Solar Sail large flexible structure leads to some difficulty in attitude control. Therefore, a system able to control it with very slow displacing is more feasible than others.

In conclusion, simulations demonstrate that mapping control if compared with linear, leads to better dynamics performances.

Chapter 6

Conclusions

This research intends to analyse different typologies of control methods, aimed at the Solar Sail parking in the restricted three-body problem. For this purpose, the artificial stationary solutions of SSCRTPB have been computed, and their instability (as demonstrated in past research [41]) has been proven numerically. However, asymptotic stability may be ensured through the use of feedback controls to the sail attitude, the analysis and implementation of these control schemes that are the centre of the research.
The first two models are addressed to ideal Solar Sail dynamics control, involving as actuation mechanisms the attitude angles orientation and the heliogyro configuration, which means variable β. Both have been tested on a random station point, and the simulations results confirm that involving β as control parameters leads to better state performances. Concerning the maximum injection error, heliogyro configuration model admits an injection distance from a stationary point of 1490 km, against just 2.5 km allowed by the model which is based only on attitude angles orientation. The steady-state error, reached after the state convergence, is smaller in the case controlled by the heliogyro-attitude couple mechanism, i.e. 17.4 m compared to 28 m. Furthermore, this coupled mechanism leads the state to a faster convergence, 0.165 km/s compared to 0.657 m/s in case of injection at the stationary point, and 22.2 m/s compared to 1.16523 m/s in case of sail injected at maximum distance from equilibrium point.
The last two linear control models are instead designed adopting the non-ideal Solar Sail dynamics, which show a reflectivity coefficient ρ different from 1. The inclusion of the reflectivity coefficient as a variable expected the employing of a Reflectivity Control Device, which in these models is presupposed continuous. This time, to simulate the control models' efficacy, a random point is chosen from the set of *non-ideal* dynamics equilibrium points. The two systems augmented with RCD show better outcomes than previous tests. Particular attention is paid to the latest model which includes an RCD on heliogyro configuration, as it represents a novelty among the control methods. Starting with the analysis of the steady-state error, it reaches values lower than 1 m, i.e. 0.03 m for the model that includes attitude angle orientation and RCD, and the lowest value $(0.00935\,m)$

is reached with the new model. It is worthwhile to examine also the results regarding *attitude angle rate of change limit*, indeed the third controls is feasible with a limit on the rate of change lower than the previous ones (0.010 deg/h compare to 1 deg/h), thus confirming to be easier to apply.
The second part of the research intends to design a new control model, capable of mapping a ideal feed-back control based on LQR theory. This new control method is comparable with the first linear system implemented, because both of them harness attitude angles orientation as actuation mechanism, and the *mapping control* gives significantly better results considering the controlled dynamics performances. The steady-state error decreases from 28 m in linear control case, to 0.223 m in the mapping control case. But the most meaningful difference regards the *attitude angle rate of change limit*, which for linear case results in a non-feasible value, exceeding the imposed limit of 1 deg/h, and on the contrary, the mapping control allows to adopt a minimum rate of $0,008$ deg/h. The realization of the attraction area radius, has established another difference between the three controls that use attitude angles, proving that the mapping model allows a very large injection error (90 km), followed by the linear model that includes the RCD (45 km) and finally the linear control with only attitude displacement as actuation mechanism (3 km).
It is also necessary to note the non-positive results of the last model, which shows a convergence speed not higher than the others, and since this last model has been developed more accurately, without the linearisation of the control, it requires a greater computational effort.
In conclusion, attention has been focused in designing and comparing new control solutions for stationary points of solar sails in CRTBP, because these have interesting potential applications for space science missions, such as planetary sample return, interplanetary mission, multiple small-body rendezvous and fast missions to the outer Solar System.

Appendices

A Second Partial Derivatives of the Three-Body Pseudo-Potential

The following are general expressions for the second partial derivatives of U, the pseudo-potential. Each derivative is denoted as $U_{jk} = \frac{\partial U}{\partial j \partial k}$, where $j,k \in (x,y,z)$.

$$U_{xx} = 1 - \frac{(1-\mu)}{r_1^3} - \frac{\mu}{r_2^3} + \frac{3(1-\mu)(x+\mu)^2}{r_1^5} + \frac{3\mu(x-(1-\mu))^2}{r_2^5} \tag{A.1}$$

$$U_{xy} = \frac{3(1-\mu)(x+\mu)y)}{r_1^5} + \frac{3\mu(x-(1-\mu))y}{r_2^5} \tag{A.2}$$

$$U_{xz} = \frac{3(1-\mu)(x+\mu)z)}{r_1^5} + \frac{3\mu(x-(1-\mu))z}{r_2^5} \tag{A.3}$$

$$U_{yx} = \frac{3(1-\mu)(x+\mu)y)}{r_1^5} + \frac{3\mu(x-(1-\mu))y}{r_2^5} \tag{A.4}$$

$$U_{yy} = 1 - \frac{(1-\mu)}{r_1^3} - \frac{\mu}{r_2^3} + \frac{3(1-\mu)y^2}{r_1^5} + \frac{3\mu y^2}{r_2^5} \tag{A.5}$$

$$U_{yz} = \frac{3(1-\mu)yz}{r_1^5} + \frac{3\mu y^2}{r_2^5} \tag{A.6}$$

$$U_{zx} = \frac{3(1-\mu)(x+\mu)z)}{r_1^5} + \frac{3\mu(x-(1-\mu))z}{r_2^5} \tag{A.7}$$

$$U_{zy} = \frac{3(1-\mu)yz}{r_1^5} + \frac{3\mu yz}{r_2^5} \tag{A.8}$$

$$U_{zz} = 1 - \frac{(1-\mu)}{r_1^3} - \frac{\mu}{r_2^3} + \frac{3(1-\mu)z^2}{r_1^5} + \frac{3\mu z^2}{r_2^5} \tag{A.9}$$

B Partial Derivatives of the Solar Sail Acceleration Terms Relative to Position

The expressions below are the partial derivatives of the scalar solar sail acceleration components with respect to the sail position coordinates. The notation is consistent, $a_{jk} = \frac{\partial U a_j}{\partial k}$, where $j,k \in (x,y,z)$. It is assumed that the sail attitude angles, γ and δ, are independent of position.

B.1 Ideal Solar Sail acceleration Jacobian

Here after, we will show only the element different from zero.

$$a_{xz} = \frac{2\beta(1-\mu)\cos\gamma\cos\delta}{r_1^4}\left(-\frac{(\mu+x)^2\cos\gamma\cos\delta+(\mu+x)z\sin\gamma+y(\mu+x)\cos\gamma\sin\delta}{r_1^3}+\frac{\cos\gamma\cos\delta}{r_1}\right)\left(\frac{(\mu+x)\cos\gamma\cos\delta+z\sin\gamma+y\cos\gamma\sin\delta}{r_1}\right)-2\beta(1-\mu)(\mu+x)\cos\gamma\cos\delta\frac{\left(-\frac{(\mu+x)\cos\gamma\cos\delta+z\sin\gamma+y\cos\gamma\sin\delta}{r_1}\right)^2}{r_1^4} \tag{B.1a}$$

$$a_{xy} = \frac{2\beta(1-\mu)\cos\gamma\cos\delta}{r_1^4}\left(-\frac{(\mu+x)y\cos\gamma\cos\delta+yz\sin\delta+y^2\cos\gamma\sin\delta}{r_1^3}+\frac{\cos\gamma\sin\delta}{r_1}\right)\left(\frac{(\mu+x)\cos\gamma\cos\delta+z\sin\gamma+y\cos\gamma\sin\delta}{r_1}\right)-2\beta(1-\mu)y\cos\gamma\cos\delta\frac{\left(\frac{(\mu+x)\cos\gamma\cos\delta+z\sin\gamma+y\cos\gamma\sin\delta}{r_1}\right)^2}{r_1^4} \tag{B.1b}$$

$$a_{xz} = \frac{2\beta(1-\mu)\sin\gamma}{r_1^4}\left(-\frac{(\mu+x)^2\cos\gamma\cos\delta+(\mu+x)z\sin\gamma+y(\mu+x)\cos\gamma\sin\delta}{r_1^3}+\frac{\cos\gamma\sin\delta}{r_1}\right)\left(\frac{(\mu+x)\cos\gamma\cos\delta+z\sin\gamma+y\cos\gamma\sin\delta}{r_1}\right)-2\beta(1-\mu)(\mu+x)\sin\gamma\frac{\left(\frac{(\mu+x)\cos\gamma\cos\delta+z\sin\gamma+y\cos\gamma\sin\delta}{r_1}\right)^2}{r_1^4} \tag{B.1c}$$

$$a_{yx} = \frac{2\beta(1-\mu)\cos\gamma\sin\delta}{r_1^4}\left(-\frac{(\mu+x)^2\cos\gamma\cos\delta+(\mu+x)z\sin\delta+(\mu+x)y\cos\gamma\sin\delta}{r_1^3}+\right.$$
$$\left.\frac{\cos\gamma\cos\delta}{r_1}\right)\left(\frac{(\mu+x)\cos\gamma\cos\delta+z\sin\gamma+y\cos\gamma\sin\delta}{r_1}\right)-2\beta(1-\mu)(\mu+x)$$
$$\cos\gamma\sin\delta\frac{\left(\frac{(\mu+x)\cos\gamma\cos\delta+z\sin\gamma+y\cos\gamma\sin\delta}{r_1}\right)^2}{r_1^4}$$

(B.1d)

$$a_{yy} = \frac{2\beta(1-\mu)\cos\gamma\sin\delta}{r_1^4}\left(-\frac{(\mu+x)y\cos\gamma\cos\delta+zy\sin\delta+y^2\cos\gamma\sin\delta}{r_1^3}+\right.$$
$$\left.\frac{\cos\gamma\sin\delta}{r_1}\right)\left(\frac{(\mu+x)\cos\gamma\cos\delta+z\sin\gamma+y\cos\gamma\sin\delta}{r_1}\right)-2\beta(1-\mu)(\mu+x)$$
$$y\cos\gamma\sin\delta\frac{\left(\frac{(\mu+x)\cos\gamma\cos\delta+z\sin\gamma+y\cos\gamma\sin\delta}{r_1}\right)^2}{r_1^4}$$

(B.1e)

$$a_{yz} = \frac{2\beta(1-\mu)\cos\gamma\cos\delta}{r_1^4}\left(-\frac{(\mu+x)z\cos\gamma\cos\delta-z^2\sin\gamma-yz\cos\gamma\sin\delta}{r_1^3}--+\frac{\sin\gamma}{r_1}\right)$$
$$\left(\frac{(\mu+x)\cos\gamma\cos\delta+z\sin\gamma+y\cos\gamma\sin\delta}{r_1}\right)-2\beta(1-\mu)z\cos\gamma\cos\delta$$
$$\frac{\left(\frac{(\mu+x)\cos\gamma\cos\delta+z\sin\gamma+y\cos\gamma\sin\delta}{r_1}\right)^2}{r_1^4}$$

(B.1f)

$$a_{zx} = 2\beta(1-\mu)\sin\delta\left(\frac{\frac{-(mu+x)^2\cos\gamma\cos\delta}{r_1^3}+\frac{\cos\gamma\cos\delta}{r_1}-\frac{z(\mu+x)\sin\gamma}{r_1^3}-\frac{(\mu+x)y\cos\gamma\sin\delta}{r_1^3}}{r_1^2}\right.$$
$$\left.\frac{\frac{(\mu+x)\cos\gamma\cos\delta+z\sin\gamma+y\cos\gamma\sin\delta}{r_1}}{r_1^2}\right)-2\beta(1-mu)(\mu+x)\sin\gamma\left(\frac{\left(\frac{(mu+x)\cos\gamma\cos\delta}{r_1}\right)^2}{r_1^4}\right.$$
$$\left.\frac{\left(\frac{+z\sin\gamma+y\cos\gamma\sin\delta}{r_1}\right)^2}{r_1^4}\right)$$

(B.1g)

$$a_{zy} = \frac{2\beta(1-\mu)\sin\gamma}{r_1^4}\left(-\frac{(\mu+x)y\cos\gamma\cos\delta + zy\sin\delta + y^2\cos\gamma\sin\delta}{r_1^3} + \frac{\cos\gamma\sin\delta}{r_1}\right)$$
$$\left(\frac{(\mu+x)\cos\gamma\cos\delta + z\sin\gamma + y\cos\gamma\sin\delta}{r_1}\right) - 2\beta(1-\mu)(\mu+x)$$
$$y\sin\delta\frac{\left(\frac{(\mu+x)\cos\gamma\cos\delta+z\sin\gamma+y\cos\gamma\sin\delta}{r_1}\right)^2}{r_1^4} \tag{B.1h}$$

$$a_{zz} = \frac{2\beta(1-\mu)\sin\gamma}{r_1^4}\left(-\frac{(\mu+x)z\cos\gamma\cos\delta + z^2\sin\delta + yz\cos\gamma\sin\delta}{r_1^3} + \frac{\sin\gamma}{r_1}\right)$$
$$\left(\frac{(\mu+x)\cos\gamma\cos\delta + z\sin\gamma + y\cos\gamma\sin\delta}{r_1}\right) - 2\beta(1-\mu)(\mu+x) \tag{B.1i}$$
$$z\sin\gamma\frac{\left(\frac{(\mu+x)\cos\gamma\cos\delta+z\sin\gamma+y\cos\gamma\sin\delta}{r_1}\right)^2}{r_1^4}$$

B.2 Non-ideal Solar Sail acceleration Jacobian

Concerning the partial derivatives of non-ideal scalar solar sail acceleration, the computation has been done using ®Mathematica, because the calculation was too complex and long to be done by hand.

Bibliography

[1] G Aliasi, G Mengali, and A A Quarta. "Artificial Lagrange points for solar sail with electrochromic material panels". In: *Journal of Guidance, Control, and Dynamics* 36.5 (2013), pp. 1544–1550.

[2] K J Aström and R M Murray. *Feedback systems: an introduction for scientists and engineers*. Princeton university press, 2010.

[3] H Baoyin and C McInnes. "Solar sail orbits at artificial Sun-Earth libration points". In: *Journal of Guidance, control, and dynamics* 28.6 (2005), pp. 1328–1331.

[4] H Baoyin and C R McInnes. "Solar sail equilibria in the elliptical restricted three-body problem". In: *Journal of Guidance, Control, and Dynamics* 29.3 (2006), pp. 538–543.

[5] S P Bhattacharyya, L H Keel, and A Datta. *Linear control theory: structure, robustness, and optimization*. CRC press, 2009.

[6] J D Biggs and E Ciccarelli. "In-situ tracking of a solar sail's characteristic acceleration using a robust active disturbance estimator". In: (2019), pp. 1–7.

[7] J D Biggs, C R McInnes, and T Waters. "Control of solar sail periodic orbits in the elliptic three-body problem". In: *Journal of Guidance, Control, and Dynamics* 32.1 (2009), pp. 318–320.

[8] J D Biggs and A Negri. "Orbit-Attitude Control in a Circular Restricted Three-Body Problem Using Distributed Reflectivity Devices". In: *Journal of Guidance, Control, and Dynamics* (2019), pp. 1–10.

[9] R S Blomquist. "Design study of a solid-state heliogyro solar sail". PhD thesis. Massachusetts Institute of Technology, 1990.

[10] R S Blomquist. "Heliogyro control". PhD thesis. Carnegie Mellon University, The Robotics Institute, 2009.

[11] C Bombardelli and J Peláez. "On the stability of artificial equilibrium points in the circular restricted three-body problem". In: *Celestial Mechanics and Dynamical Astronomy* 109.1 (2011), pp. 13–26.

[12] J Bookless and C McInnes. “Dynamics and control of displaced periodic orbits using solar-sail propulsion”. In: *Journal of Guidance, Control, and Dynamics* 29.3 (2006), pp. 527–537.

[13] A Borggräfe, J Heiligers, M Ceriotti, and C McInnes. “Optical control of solar sails using distributed reflectivity”. In: *Spacecraft Structures Conference*. 2014, p. 0833.

[14] J V Breakwell and J V Brown. “The ‘halo’family of 3-dimensional periodic orbits in the Earth-Moon restricted 3-body problem”. In: *Celestial mechanics* 20.4 (1979), pp. 389–404.

[15] M Ceriotti and C R McInnes. “Hybrid solar sail and SEP propulsion for novel Earth observation missions”. In: (2010).

[16] B Dachwald, M Macdonald, C R McInnes, G Mengali, and A A Quarta. “Impact of optical degradation on solar sail mission performance”. In: *Journal of Spacecraft and Rockets* 44.4 (2007), pp. 740–749.

[17] B Dachwald, G Mengali, and A Quarta. “Parametric model and optimal control of solar sails with optical degradation”. In: *Journal of Guidance, Control, and Dynamics* 29.5 (2006), pp. 1170–1178.

[18] B Dachwald, W Seboldt, and M Macdonald. “Potential solar sail degradation effects on trajectory and attitude control”. In: *AIAA guidance, navigation, and control conference and exhibit*. 2005, p. 6172.

[19] R W Farquhar. “The control and use of libration-point satellites”. In: (1968).

[20] R W Farquhar, D P Muhonen, C R Newman, and H S . Heubergerg. “Trajectories and orbital maneuvers for the first libration-point satellite”. In: *Journal of Guidance and Control* 3.6 (1980), pp. 549–554.

[21] G F Franklin, J D Powell, and A Emami-Naeini. *Feedback control of dynamic systems*. Vol. 3. Addison-Wesley Reading, MA, 1994.

[22] R Funase. “Small Solar Power Sail Demonstrator “IKAROS” and Its Achievements”. In: (2017).

[23] S Gong, H Baoyin, and J Li. “Solar sail formation flying around displaced solar orbits”. In: *Journal of Guidance, Control, and Dynamics* 30.4 (2007), pp. 1148–1152.

[24] S Gong and J Li. “Solar sail heliocentric elliptic displaced orbits”. In: *Journal of Guidance, Control, and Dynamics* 37.6 (2014), pp. 2021–2026.

[25] S Gong, J Li, and J Simo. “Orbital Motions of a Solar Sail Around the L 2 Earth–Moon Libration Point”. In: *Journal of Guidance, Control, and Dynamics* 37.4 (2014), pp. 1349–1356.

[26] J Heiligers, D Guerrant, and D Lawrence. “Exploring the heliogyro’s orbital control capabilities for solar sail halo orbits”. In: *Journal of Guidance, Control, and Dynamics* 40.10 (2017), pp. 2569–2586.

[27] J Heiligers, D Guerrant, and D Lawrence. “Heliogyro orbital control authority”. In: *International Symposium on Space Flight Dynamics*. 2015.

[28] J Heiligers, S Hiddink, R Noomen, and C R McInnes. “Solar sail Lyapunov and Halo orbits in the Earth–Moon three-body problem”. In: *Acta Astronautica* 116 (2015), pp. 25–35.

[29] KC Howell. “Three-dimensional, periodic,‘halo’orbits”. In: *Celestial mechanics* 32.1 (1984), pp. 53–71.

[30] KC Howell and SC Gordon. “Orbit determination error analysis and a station-keeping strategy for Sun-Earth L1 libration point orbits”. In: *Journal of the Astronautical Sciences* 42 (1994), pp. 207–228.

[31] KC Howell and H J Pernicka. “Station-keeping method for libration point trajectories”. In: *Journal of Guidance, Control, and Dynamics* 16.1 (1993), pp. 151–159.

[32] Z Jin and W Tianshu. “Coupled attitude-orbit control of flexible solar sail for displaced solar orbit”. In: *Journal of Spacecraft and Rockets* 50.3 (2013), pp. 675–685.

[33] R D Joslin and D N Miller. *Fundamentals and applications of modern flow control*. American Institute of Aeronautics and Astronautics, 2009.

[34] A B Kisabo, N C Uchenna, and F A Adebimpe. “Newton’s method for solving non-linear system of algebraic equations (NLSAEs) with MATLAB/Simulink® and MAPLE®”. In: *American Journal of Mathematical and Computer Modelling* 2.4 (2017), pp. 117–131.

[35] J Krishen and V M Becerra. “Efficient fuzzy control of a rotary inverted pendulum based on LQR mapping”. In: *2006 IEEE Conference on Computer Aided Control System Design, 2006 IEEE International Conference on Control Applications, 2006 IEEE International Symposium on Intelligent Control*. IEEE. 2006, pp. 2701–2706.

[36] D Lawrence and S Piggott. “Solar sailing trajectory control for Sub-L1 stationkeeping”. In: *AIAA Guidance, Navigation, and Control Conference and Exhibit*. 2004, p. 5014.

[37] P Lebedew. “The physical causes of the deviations from Newton’s law of gravitation”. In: *The Astrophysical Journal* 16 (1902), p. 155.

[38] J Liu, S Rong, F Shen, and N Cui. “Dynamics and control of a flexible solar sail”. In: *Mathematical Problems in Engineering* 2014 (2014).

[39] R H MacNeal. “The heliogyro-an interplanetary flying machine”. In: (1967).

[40] J C Maxwell. *A dynamical theory of the electromagnetic field*. The Society, 1856.

[41] C R McInnes. “Artificial Lagrange points for a partially reflecting flat solar sail”. In: *Journal of guidance, control, and dynamics* 22.1 (1999), pp. 185–187.

[42] C R McInnes. *Solar sailing: technology, dynamics and mission applications*. Springer Science & Business Media, 2013.

[43] C R McInnes, A JC McDonald, and J FL Simmons. “Solar sail parking in restricted three-body systems”. In: *Journal of Guidance, Control, and Dynamics* 17.2 (1994), pp. 399–406.

[44] IS McInnes. “Strategies for solar sail mission design in the circular restricted three-body problem”. In: *MSE Thesis, School of Aeronautics and Astronautics, Purdue University* (2000).

[45] R McKay, M Macdonald, J D Biggs, and C McInnes. “Survey of highly non-Keplerian orbits with low-thrust propulsion”. In: *Journal of Guidance, Control, and Dynamics* 34.3 (2011), pp. 645–666.

[46] G Mengali, A A Quarta, and C Circi. “Refined solar sail force model with mission application”. In: *Journal of Guidance, Control, and Dynamics* 30.2 (2007), pp. 512–520.

[47] Y Mimasu, T Yamaguchi, M Matsumoto, M Nakamiya, R Funase, and J Kawaguchi. “Spinning solar sail orbit steering via spin rate control”. In: *Advances in Space Research* 48.11 (2011), pp. 1810–1821.

[48] F Mincigrucci. “Un Algoritmo di controllo ottimo di un sistema di aerodinamica mobile per una vettura sportiva”. PhD thesis. University of Bologna, 2012.

[49] J Mu, S Gong, and J Li. “Coupled control of reflectivity modulated solar sail for GeoSail formation flying”. In: *Journal of Guidance, Control, and Dynamics* 38.4 (2014), pp. 740–751.

[50] J Mu, Sg Gong, and J Li. “Reflectivity-controlled solar sail formation flying for magnetosphere mission”. In: *Aerospace Science and Technology* 30.1 (2013), pp. 339–348.

[51] J B Pezent, R Sood, and A Heaton. “Near Earth Asteroid (NEA) Scout Solar Sail Contingency Trajectory Design and Analysis”. In: *2018 Space Flight Mechanics Meeting*. 2018, p. 0199.

[52] A Quarteroni and F Saleri. *Introduzione al calcolo scientifico: esercizi e problemi risolti con MATLAB*. Springer Science & Business Media, 2007.

[53] L Rios-Reyes and DJ Scheeres. “Generalized model for solar sails”. In: *Journal of Spacecraft and Rockets* 42.1 (2005), pp. 182–185.

[54] JJ E Slotine and W Li. *Applied nonlinear control*. Vol. 199. 1. Prentice hall Englewood Cliffs, NJ, 1991.

[55] S. Soldini, C. Colombo, and S.JI Walker. "Solar radiation pressure Hamiltonian feedback control for unstable libration-point orbits". In: *Journal of Guidance, Control, and Dynamics* 40.6 (2017), pp. 1374–1389.

[56] S Soldini, C Colombo, and SJI Walker. "Adaptive structures for spacecraft orbit control". In: (2013).

[57] Theodoros Theodorou. "Three-Axis Attitude Control of Solar Sails Utilising Reflectivity Control Devices". PhD thesis. University of Surrey (United Kingdom), 2016.

[58] Y Tsuda, O Mori, R Funase, H Sawada, T Yamamoto, T Saiki, T Endo, and J Kawaguchi. "Flight status of IKAROS deep space solar sail demonstrator". In: *Acta Astronautica* 69.9-10 (2011), pp. 833–840.

[59] P Verrier, T Waters, and J Sieber. "Evolution of the [FORMULA] halo family in the radial solar sail circular restricted three-body problem". In: *Celestial mechanics and dynamical astronomy* 120.4 (2014), pp. 373–400.

[60] G G Wawrzyniak. *The dynamics and control of solar-sail spacecraft in displaced lunar orbits*. Purdue University, 2011.

[61] B Wie. "Solar sail attitude control and dynamics, part 1". In: *Journal of Guidance, Control, and Dynamics* 27.4 (2004), pp. 526–535.

[62] B Wie. *Space vehicle dynamics and control*. American Institute of Aeronautics and Astronautics, 2008.

[63] C Wiley. "Clipper ships of space". In: *Astounding Science Fiction* 5 (1951), p. 135.

[64] W K Wilkie, J E Warren, L G Horta, K H Lyle, J Juang, J D Littell, R G Bryant, M W Thomson, P E Walkemeyer, and V Guerrant. "Heliogyro solar sail research at NASA". In: *Advances in Solar Sailing*. Springer, 2014, pp. 631–650.

[65] L Xuqiang, L Luhua, and T Guojian. "Research on solar sail halo orbits around artificial lagrange point". In: *2010 3rd International Symposium on Systems and Control in Aeronautics and Astronautics*. IEEE. 2010, pp. 347–352.